https://doi.org/10.1142/9789811264153_0025

The Symmetry Principle in Condensed Matter Physics (I)

Congjun Wu (吴从军)
Department of Physics, School of Science, Westlake University, Hangzhou 310024, Zhejiang, China
Institute for Theoretical Sciences, Westlake University, Hangzhou 310024, Zhejiang, China
Key Laboratory for Quantum Materials of Zhejiang Province, School of Science, Westlake University, Hangzhou 310024, China
Institute of Natural Sciences, Westlake Institute for Advanced Study, Hangzhou 310024, Zhejiang, China
wucongjun@westlake.edu.cn

Symmetry distills the simplicity of natural laws from the complexity of physical phenomena. The symmetry principle is of vital importance in various aspects of modern physics, including analyzing atomic spectra, determining fundamental interactions in the Standard Model, and unifying physics at different energy scales. In this chapter, novel applications of this principle are reviewed in condensed matter physics and cold atom physics for exploring new states of matter.

First, the concept of *space-time group* generalizes crystalline space group symmetries to their dynamic counterparts, including nonsymmorphic space-time symmetries (e.g. *time-screw* rotation, *time-glide* reflection, and *time-shift* rotary reflection). It includes and goes beyond the Floquet theory framework, and applies to a large class of dynamic systems such as laser-driven solid crystals, dynamic photonic crystals, and optical lattices, etc. Second, the perspective of high symmetries (e.g. SU(N) and Sp(N)) bridges large-spin cold fermion systems with high energy physics. For example, a generic SO(5), or, isomorphically Sp(4) symmetry is proved in spin-$\frac{3}{2}$ systems. Moreover, an exact SO(7) symmetry is identified, which exhibits an extraordinarily unifying power. Its χ-pairing operator extends Yang's η-pairing to a high-rank Lie algebra, integrating 21 orders in both particle-hole and particle-particle channels into a unified framework. Such systems also exhibit multi-fermion orderings, including quartetting superfluidity (charge $4e$) and quartet density wave, which are α-particle-like, or, baryon-like orderings. The resonant quantum plaquette states of SU(4) antiferromagnetism are described by a high-order gauge theory. A quantum phase transition occurs from the Slater region to the Mott region in the SU(6) Hubbard model. A tendency of convergence of itineracy and locality is revealed in 1D SU(N) systems as N goes large. Third, a new mechanism is presented to generate spin-orbit coupling based on "spin-from-isospin" via many-body Fermi

surface instabilities of the Pomeranchuk type. In contrast, the conventional wisdom views spin-orbit coupling as a single-body relativistic effect. This mechanism generalizes itinerant ferromagnetism to the unconventional symmetry versions (e.g. p-wave), which can also be viewed as magnetic multipolar orderings in momentum space.

1. Introduction

I feel honored to contribute to this Festschrift for *the Yang Centenary*. Professor C. N. Yang is the role model for Chinese physicists of my generation. Throughout our careers, we have been inspired by his milestone contributions to theoretical physics, including parity violation in the weak interaction,[1] Yang-Mills gauge theory,[2] Yang-Baxter equation,[3] and monopole gauge theories,[4,5] etc. Among these masterpieces, the symmetry principle is a threading theme, which is also a distinct style of his research.

I learned to appreciate the symmetry principle under the guidance of my Ph.D. advisor Professor Shoucheng Zhang, who himself was deeply influenced by Professor Yang. Symmetries and their applications in condensed matter physics and cold atom physics are my major research directions. Hence, I shall review progresses along this line for this Festschrift.

1.1. *General backgrounds*

The appreciation of symmetry at a fundamental level has a long history. The ancient Greeks proved the existence of only five types of convex regular polyhedra (the Platonic solids): tetrahedron, cube, octahedron, dodecahedron, and icosahedron. They hypothesized that these regular polyhedra correspond to the classic elements of water, earth, fire, air, and ether, respectively.[6] Galileo's relativity principle implies the homogeneity of space and time (translational symmetry), the isotropy of space (rotational symmetry), and the equivalence of all the inertial reference frames.[7] Einstein's relativity is a profound victory of the symmetry principle: The Lorentz symmetry is viewed as a fundamental symmetry of space-time, which is not only a property of Maxwell's equations but also the primary constraint to all physical laws.[7] In high energy physics, Yang stated, *"Symmetry dictates interaction"*, i.e., interactions among fundamental particles in the Standard Model are determined by their fundamental gauge symmetries.[8]

The first application of the symmetry principle in physics actually started in the field of condensed matter. Soon after the establishment of group theory by Galois and Cauchy in the 1830s–1840s, it was applied to analyze crystalline symmetries. In the 1890s, Schönflies and Fedorov completed the construction of the 230 space groups.[9] Each space group corresponds to one type of crystalline structure in three dimensions (3D), which is a subgroup symmetry of 3D flat space containing a discrete translational group as its normal subgroup.

In the 1880s, the concept of group was generalized to continuous groups, i.e., Lie groups, by Sophus Lie, and then calculus and differential equations entered the study of symmetry.[10] Lie group and its generators Lie algebra became the main tools to analyze symmetries. Noether proved that each continuous symmetry gives rise to a local conservation law: Momentum conservation arises from the translational symmetry; angular momentum conservation arises from the rotational symmetry,[11] etc.

The application of group theory in quantum physics was pioneered by Wigner[12] and Weyl.[13] Because of the linear nature of quantum mechanics, the eigenstates of a time-independent Hamiltonian form irreducible representations of its symmetry group G. Its generators commute with the Hamiltonian, and thus are conserved quantities. This principle is extremely successful in classifying the atomic and molecular optical spectra and explaining selection rules for optical transitions.

Two remarkable examples of hidden symmetries of simple systems are the hydrogen atom[14] and the harmonic oscillator.[15] The N-dimensional hydrogen atom possesses the $\mathrm{SO}(N+1)$ symmetry due to the conserved Runge-Lentz vectors. Classically, the Runge-Lentz vector specifies the orientation of the elliptical orbit. The N-dimensional harmonic oscillator possesses the $\mathrm{SU}(N)$ symmetry which transforms among the complex space spanned by the complex combination of coordinate and momentum $a_i = \frac{1}{\sqrt{2}}(x_i + ip_i)$.

One central theme in modern physics is the unification by the symmetry principle. Electricity and magnetism are unified by the Lorentz group. The interaction between matter and the electromagnetic field is described by the U(1) gauge theory. In particle physics, the electromagnetic and weak interactions are unified by the $\mathrm{SU}_L(2) \otimes \mathrm{U}(1)$ gauge theory as the electroweak interaction, where L refers to left-handed leptons and quarks.[16–18] The quantum chromodynamics is described by the SU(3) color gauge theory, and quarks of three colors (R, G, B) form the fundamental representation of the SU(3) group. Mesons are quark-antiquark bound states and baryons are three-quark bound states, both of which are color singlets. In addition, baryons and mesons can be classified as multiplets of the approximate SU(3) flavor symmetry.[19]

Spontaneous symmetry breaking is a crucially important concept, which was first proposed by L. Landau for constructing a general framework of phase transitions.[20–22] Most second-order phase transitions are related to certain kinds of symmetry breaking of order parameters (the matter fields). For instance, the magnetic phase transition breaks time-reversal and rotational symmetries; the charge-density-wave breaks translational symmetry; superfluidity breaks the U(1) symmetry. If a continuous global symmetry G is spontaneously broken, the transverse fluctuations of order parameters are gapless, which are the Goldstone modes as reminiscences of the original symmetry before its breaking.[23] The Goldstone manifold is represented as the coset of G/H, where H represents the residual subgroup symmetry after symmetry breaking.

Even more profound physics occurs when a gauge symmetry is spontaneously broken. For example, superconductivity is a consequence of the U(1) gauge symmetry breaking.[24,25] The electromagnetic properties of superconductors are characterized by the London equation $\mathbf{j} = -\rho_s \mathbf{A}$, where ρ_s is the superfluid density, giving rise to the celebrated Meissner effect. This is is due to the Anderson-Higgs mechanism that the gauge boson (photon) becomes massive and acquires its longitudinal component by absorbing the Goldstone mode of phase fluctuations. Consequently, the electromagnetic field can only enter the superconductor surface at the penetration depth λ with the relation of $\rho_s = c/(4\pi\lambda^2)$.

The Anderson-Higgs mechanism is essential in high energy physics.[19] The gauge bosons become massive, once the corresponding gauge symmetries are broken. This cures the apparent discrepancy between the short-range weak and strong interactions and the massless Yang-Mills gauge fields.[2] This was the major obstacle to applying the Yang-Mills theory as the paradigm for formulating fundamental interactions. Furthermore, the Higgs field generates masses for fermions of quarks and leptons as shown in the Glashow-Weinberg-Salam theory, which unifies the weak and electromagnetic interactions into the electroweak interaction.[16–18]

In the context of condensed matter physics, the symmetry principle is employed to unify seemingly unrelated phenomena. For example, Yang's pseudo-spin SU(2) symmetry based on the η-pairing unifies the charge-density-wave ordering and superconductivity.[26–28] Its extension to the SO(5) theory of high T_c superconductivity by Zhang views antiferromagnetism and d-wave superconductivity on the equal footing as different components of a 5-vector.[29,30] The sharp resonance modes of neutron scattering spectroscopy could be interpreted as the pseudo-Goldstone excitations in the superconducting ground state towards the direction of antiferromagnetism.[29,31]

Some new applications of the symmetry principle in condensed matter and ultracold atom physics will be reviewed below focusing on exploring novel states of matter. The motivation and outline of the main results for each topic are briefly explained below.

1.2. *Space-time group for dynamic systems*

A solid state physics textbook typically starts with crystalline symmetries, which are classified according to the 230 space groups, and then proceeds with the Bloch theorem setting up the framework of electron's quantum behavior in solids.[32] Space group symmetries include the discrete translational symmetry of the underlying Bravais lattice, and point group symmetries (e.g. *rotation, reflection*, and *rotary reflection*). Space group possesses nonsymmorphic symmetries, which means that under such operations there are no fixed points, including *screw rotation* and *glide reflection*. Screw rotation is the symmetry of a screw: A rotation is insufficient to maintain a screw invariant which needs to be followed by a certain translation

along the rotation axis. Glide reflection is a symmetry of a row of footprints, i.e., a reflection followed by a translation of half a period.[9]

Symmetry literally means "balanced proportions", and thus is commonly viewed as a static concept. However, time dynamics is an important topic in various subjects of physics. The recent experimental progresses, such as the pump-prob measurements[33,34] and shaken cold-atom optical lattice experiments,[35,36] have stimulated the study of dynamically driven systems.

A natural question is how to analyze symmetries of dynamic systems? Systems under periodical driving are often denoted as the Floquet ones. In such systems, time translational symmetry is violated while a discrete version still exists, which is the counterpart of the discrete spatial translational symmetry in crystals. However, within the Floquet framework, temporal symmetry is decoupled from the spatial one.[37–48]

Just like that a 3D crystal is typically not the direct-product between a 2D crystal in the *ab*-plane with a 1D crystal along the *c*-axis, a dynamic crystalline system is *not* just the direct-product between a static crystal with a Floquet periodicity. We construct the symmetry group of dynamic systems and dub it *space-time group*, which is a dynamic extension of the crystalline space group.[49] The Bloch theorem is also generalized accordingly. This concept applies to a large class of dynamic systems beyond the Floquet framework, including laser-driven solid crystals, dynamic photonic crystals, and optical lattices, etc.

There exist nonsymmorphic versions of space-time symmetries as depicted in Fig. 1.[49] (Please do not confuse them with Lorentz symmetries.) For example, a see-saw is invariant by a reflection followed by a time-shift of half a period, and this symmetry is dubbed *time-glide reflection* (Fig. 1(a)). A clock does not exhibit the rotation symmetry but a rotation combined with a suitable time-translation leaves it invariant, and this symmetry is dubbed *time-screw rotation* (Fig. 1(b)). These are actually symmetries of their world lines in analogy to screw rotation and glide reflection of space group. Another space-time nonsymmorphic symmetry, 3D rotary-reflection followed by a time-translation, does not have a space group counterpart (Fig. 1(c)).

A complete classification in 1+1D gives rise to 13 space-time groups in contrast to the 17 wallpaper space groups for the 2D static crystals, and in 2+1D we have found 275 space-time groups.[49] Space-time group symmetries also protect spectral degeneracies.

Time-screw rotation and time-glide reflection symmetries were also proposed by Morimote *et al.* independently for studying novel topological band structures in driven systems,[50] but the concept of "space-time group" was not proposed there.

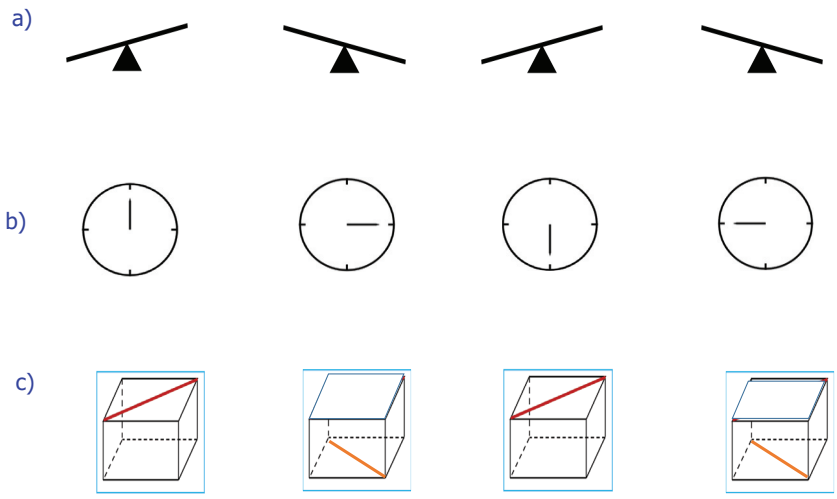

Fig. 1. Time sequence configurations for three representative space-time nonsymmorphic symmetries. (a) *Time-glide* reflection symmetry. A see-saw is invariant by a reflection followed by a time-shift of half a period. (b) *Time-screw* rotation symmetry. A clock is invariant by a rotation followed by a fractional time translation. (c) *Time-shift* rotary reflection symmetry, i.e., rotary reflection followed by a fractional time translation. Time-glide reflection and time-screw rotation are analogies of glide reflection and screw rotation of space group symmetries, respectively, while time-shift rotary reflection has no counterpart in 3D space group operations.

1.3. *High symmetry perspective to large-spin cold fermion systems*

High symmetries (e.g. SU(N) and Sp(N)) are essential in high energy physics, nevertheless, their applications in condensed matter physics are often to provide the mathematical tool of the large-N expansion to handle strong correlations.[52–55] On the other hand, cold atom physics has become a new frontier of condensed matter physics for creating novel quantum states of matter, particularly those uneasy to access in solids.

Many fermionic atoms possess large-hyperfine-spins. We have been working on exploring new states of large-spin fermions from the new perspective of high symmetries of SU(N) and Sp(N) since 2003.[56–63] It works as a guiding principle to explore beautiful many-body physics, providing a natural connection between cold atom physics and high energy physics. It is amazing to see that physics at dramatically different energy scales is deeply related. Systematic studies have been performed in exploring high symmetry effects, including the unification of competing orders,[56,58] novel quantum magnetism,[60,62] and non-Abelian topological defects.[61]

High-symmetry cold fermions have attracted considerable attentions from various research groups in the cold atom community.[64–76] This direction has also become an active experiment focus: Takahashi's group realized the SU(6) symmetric alkaline-earth fermions of ^{173}Yb.[77–80] Fallani's group studied the 1D systems of ^{173}Yb with

tunable component numbers.[81] The 10-component ^{87}Sr systems ($F = I = \frac{9}{2}$) have been studied by Killian's group,[82,83] Sengstock's group,[84,85] and Ye's group,[86–88] etc. For non-technical introductions to the experimental progress, please refer to Refs. 89 and 90.

A fundamental difference exists between large-spin cold fermion systems and large-spin solid state systems as shown in Fig. 2.[89] In solids, quantum magnetic fluctuations are suppressed in the large-S limit: Hund's rule coupling aligns spins of several electrons into a large spin, however, the intersite coupling is dominated by the exchange of a single pair of electrons, hence, spin fluctuations scale as $1/S$ as S goes large. In contrast, this restriction does not occur in cold atom systems because each large-hyperfine-spin fermion moves as an entire object. The exchange of a single pair of atoms completely flips the spin configuration. The large number of spin components actually enhanced quantum fluctuations. and they are actually even stronger than the spin-$\frac{1}{2}$ case. Hence, the large-spin physics of ultracold atoms is governed by the large-N physics of a high symmetry group where $N = 2S + 1$.

An exact and generic hidden Sp(4), isomorphically SO(5), symmetry is proved for hyperfine-spin-$\frac{3}{2}$ alkali and alkaline fermions without fine-tuning.[56,58,59,61] The candidate atoms for realizations include ^{132}Cs, ^{9}Be,^{135}Ba, ^{137}Ba, and ^{201}Hg. Yang's η-pairing pseudospin SU(2) symmetry can be generalized to the spin-3/2 Hubbard model defined on a bipartite lattice.[56,59] Such a system could exhibit an SO(7)

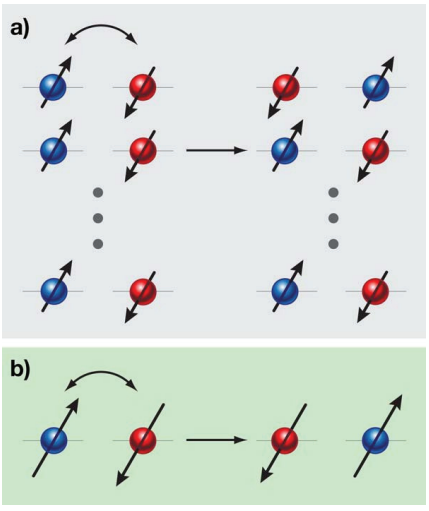

Fig. 2. Superexchange processes in (a) large-spin solid state systems and (b) large hyperfinespin cold fermion systems. In solids, quantum magnetic fluctuations are suppressed by the large-S effect; while quantum fluctuations are enhanced by the large number of spin components $N = 2S+1$. Hence, the appropriate viewpoint for large-spin fermions is the large-N physics of a high symmetry group rather than the large-S physics of the SU(2) group. This feature bridges high energy physics and ultracold atom physics in spite of hugely different energy scales. From Ref. 51.

symmetry which unifies the singlet superconductivity and the spin-quadruple density-wave order with the 7-vector representation. The adjoint representation of SO(7) can unify the quintet superconductivity, spin and spin-octupole density-wave order, and charge-density-wave, which are in total 21-dimensional.

The large-spin fermions also exhibit similar physics to that in quantum chromodynamics — the multi-particle clustering orderings. With attractive interactions, Pauli's exclusion principle allows N-fermions to form an SU(N) singlet state, a "baryon-like" multiple-fermion instability.[58,69,91,92] For the super-exchange physics in the Mott-insulating states, if each site is in the fundamental representation, it also needs N sites to form an SU(N) singlet.[57,60]

How interaction effects scale with the component number N is also an interesting question. For the SU(N) Hubbard models, systematic quantum Monte Carlo (QMC) simulations free of the sign problem have been performed for the 2D square lattice,[93,94] the square lattice with flux,[95] and the honeycomb lattice,[96] and also in 1D.[97]

1.4. *Unconventional magnetism and spontaneous spin-orbit ordering*

Spin-orbit coupling plays an important role in the research focus of topological states of matter. Conventionally, it is viewed as a single-particle property inherited from the relativistic Dirac equation, not directly related to many-body physics.[32] We have explored another possibility — the spontaneous generation of spin-orbit coupling as a many-body effect based on Fermi surface instabilities of the Pomeranchuk type.[98] This mechanism is essentially itinerant magnetic phase transitions with unconventional symmetries (e.g. p-wave), which is also magnetic multipolar orderings in momentum space.[99,100]

In ferromagnetic metals, the rotational symmetry is broken in the spin channel. However, spin polarizes along the same direction around Fermi surfaces independent of the direction of momentum, hence, the orbital rotational symmetry is unbroken as shown in Fig. 3(A). This is similar to conventional s-wave superconductors whose gap function phase keeps constant over the Fermi surface. Therefore ferromagnetism can be viewed as the "s-wave" magnetism.

As for superconductivity (fermion pairing superfluidity), there exist unconventional pairing structures, including the d-wave high T_c cuprates[101] and the p-wave superfluid ^{3}He.[102] In analogy to unconventional superconductivity, we have generalized ferromagnetism to cases of unconventional symmetries, in which spin no longer polarizes along a unique direction but varies with momentum. These unconventional magnetic states have close connections to many directions in condensed matter physics, including unconventional superconductivity,[103] spin-orbit coupling and spintronics, and electron liquid crystal states in strongly correlated systems.[104]

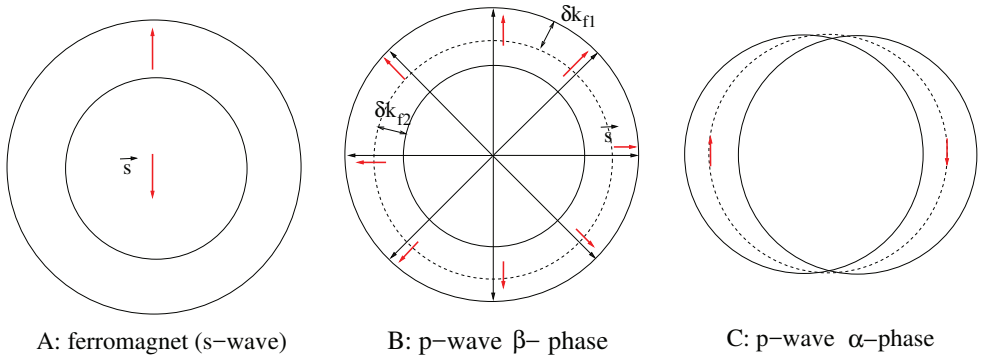

Fig. 3. Fermi surface configurations of the ferromagnetic phase (A) and the unconventional magnetic phases in the p-wave channel (the isotropic β-phase (B) and the anisotropic α-phase (C)). The ferromagnetic state can be viewed as an s-wave type magnetism since it does not break the orbital rotational symmetry. The p-wave itinerant magnetism exhibits dipolar magnetic ordering over the Fermi surface. The β-phase breaks the relative spin-orbit symmetry spontaneously, which is a particle-hole analogy to the superfluid ^{3}He-B phase. The anisotropic α-phase is the analogy of the superfluid ^{3}He-A phase. From Ref. 100.

The unconventional magnetism includes both isotropic and anisotropic cases, as shown in Figs. 3(B) and 3(C), respectively. They are dubbed the β and α-phases analogues to the superfluid ^{3}He B and A-phases, respectively. The isotropic β-phases still exhibit circular, or, spherical Fermi surfaces developing nontrivial spin-texture configurations in momentum space, providing a mechanism for dynamic generation of spin-orbit coupling independent of relativity. The anisotropic α-phases are electron liquid crystal states with spin degree of freedom, exhibiting anisotropic Fermi surface distortions. Both types of phases arise from the Pomeranchuk instability of Fermi surfaces in the spin channel, which include ferromagnetism as a special example.

The symmetry breaking pattern of the isotropic β-phase is subtle, which breaks the relative spin-orbit symmetry.[102] In non-relativistic physics, spin is an internal degree of freedom, i.e., the spin rotational symmetry $SO_S(3)$ is independent of the orbital $SO_L(3)$. The β-phase is invariant only if rotations in the two channels are performed exactly in the same way. In contrast, if there exists a difference between two rotations, i.e., the relative spin-orbit rotation, the system indeed changes. This symmetry breaking pattern is denoted as $[SO_L(3) \otimes SO_S(3)]/SO_{L+S}(3)$. In other words, the total angular momentum $J = L + S$ in the β-phase is conserved, but $L - S$ is not.

The concept of relative spin-orbit symmetry breaking was first introduced by Leggett[102] in the context of superfluid ^{3}He-B phase, whose Cooper pairing has a p-wave and spin-triplet like structure, i.e. $L = S = 1$. The pair wavefunction in the

B-phase is

$$\Psi_{pair}(\mathbf{r}_{12}) = \sum_{i=x,y,z} f_{p_i}(\mathbf{r}_{12})\chi_i, \tag{1}$$

where $f_{p_i}(\mathbf{r}_{12})$ describes the radial wavefunction with the orbital symmetry of $p_i (i = x, y, z)$, and $\chi_x = \frac{1}{\sqrt{2}}(|\uparrow\uparrow\rangle + |\downarrow\downarrow\rangle)$, $\chi_y = \frac{1}{\sqrt{2}i}(|\uparrow\uparrow\rangle - |\downarrow\downarrow\rangle)$, and $\chi_z = \frac{1}{\sqrt{2}}(|\uparrow\downarrow\rangle + |\downarrow\uparrow\rangle)$. The total angular momentum $J = L + S$ of Cooper pairs is zero, and thus the pairing is isotropic. Hence, the β-phase is the particle-hole channel analogy to the ^{3}He-B phase.

In Sec. 4, we shall review how spin-orbit coupling can be dynamically generated without relativity but from phase transitions, in a similar way to ferromagnetism. We have also extended the Fermi-liquid theory to systems with spin-orbit coupling.

1.5. *Outline*

The remaining part of this chapter is organized as follows: The concept of space-time group for dynamic systems is reviewed in Sec. 2; the high symmetry perspective of ultracold fermion physics is reviewed in Sec. 3; unconventional magnetism and spontaneous spin-orbit symmetry breaking is reviewed in Sec. 4. Conclusions are presented in Sec. 5.

2. Space-time Group for Dynamic Systems

The fundamental concept of crystal and band theory based on the Bloch theorem lay the foundation of condensed matter physics.[32] In recent years, the study of dynamic systems such as the "pump-prob" systems becomes a new focus direction.[33,34] The simplest dynamic systems exhibit space-time periodicity, and a natural question is how to classify their symmetries by extending the static crystalline symmetries. There existed previously the framework of Floquet systems, i.e., systems under periodical driving. However, in such a framework, the spatial and temporal symmetries are decoupled, hence, it cannot be the generic case.[37–48]

We construct a new framework, dubbed *space-time group*, to describe the general intertwined space-time periodicities in $D+1$ dimensions, which include both the static crystal and the Floquet crystal as special cases.[49] Compared to previously known space- and magnetic groups, space-time group is augmented by "time-screw" rotation, "time-glide" reflection, and "time-shift" rotary-reflection, involving fractional translations along the time direction. We have classified that there are 13 space-time groups in 1+1D and 275 space-time groups in 2+1D.

2.1. *Space-time unit cell and momentum-frequency Brillouin zone*

Let us begin with a simplest example of space-time crystalline symmetry. Consider a $1+1$ D system, whose time-dependent potential is the superposition of two plane

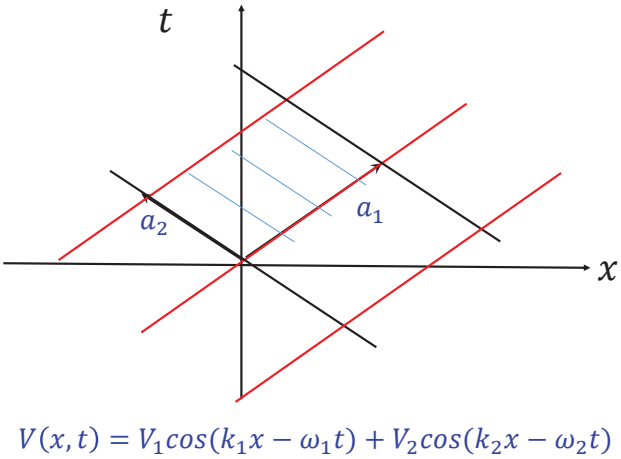

Fig. 4. The simplest space-time crystal in 1+1 D. In the general case, the space-time unit cell is a parallelogram which cannot be decomposed into a direct product between space and time domains. It exhibits neither translational nor time-translational symmetries, but does possess the combined space-time translation symmetries.

waves as plotted in Fig. 4,

$$V(x,t) = V_1 \cos(k_1 x - \omega_1 t) + V_2 \cos(k_2 x - \omega_2 t). \tag{2}$$

The wavevectors $k_{1,2}$ and frequencies $\omega_{1,2}$ are supposed to be incommensurate. If we fix a spatial position, say $x = 0$, and look at the time-dependence of $V(0,t)$, there is no temporal periodicity. For Floquet problems, the time-evolution operator $U(T)$ of one period is often used to map them into time-independent problems. Clearly, here this method generally does not apply. Similarly, if we take a snapshot at a fixed time, say $t = 0$, $V(x,0)$ has no spatial periodicity either. Hence, the ordinary Bloch theorem cannot straightforwardly be applied here.

The periodicity only appears when we extend to space-time. The unit cell is a space-time parallelogram, *not* a direct product between space and time domains. The unit vectors $\mathbf{a}_1$, $\mathbf{a}_2$ are space-time coupled,

$$\mathbf{a}_1 = \begin{pmatrix} \frac{2\pi\omega_2}{k_1\omega_2 - k_2\omega_1} \\ \frac{2\pi k_2}{k_1\omega_2 - k_2\omega_1} \end{pmatrix}, \quad \mathbf{a}_2 = \begin{pmatrix} \frac{2\pi\omega_1}{k_1\omega_2 - k_2\omega_1} \\ \frac{2\pi k_1}{k_1\omega_2 - k_2\omega_1} \end{pmatrix}, \tag{3}$$

which define space-time coupled translation symmetries. For the general case, a potential $V(\mathbf{r},t)$ exhibiting the intertwined discrete $D+1$ dimensional space-time translational symmetry satisfies

$$V(\mathbf{r},t) = V(\mathbf{r} + \mathbf{u}^i, t + \tau^i), \quad i = 1, 2, ..., D+1, \tag{4}$$

where $(\mathbf{u}^i, \tau^i) = a^i$ is the primitive basis vector of the space-time lattice.

We move to the reciprocal space and define reciprocal lattice vectors, which can be done in a similar way to solid state physics. The reciprocal lattice is spanned by

the momentum-energy basis vectors $b^i = (\mathbf{G^i}, \Omega^i)$ defined through

$$b^i \cdot a^j = \sum_{m=1}^{D} G^i_m u^j_m - \Omega^i \tau^j = 2\pi\delta^{ij}. \tag{5}$$

This minus sign is due to quantum mechanics phase convention. The $D+1$ dimensional momentum-energy Brillouin zone may not be a direct product between a momentum volume and frequency domain either. The reciprocal lattice vectors contain both momentum and frequency components.

We emphasize that the above framework is already beyond that of Floquet. Floquet systems only have one fundamental frequency, while, in our case each reciprocal lattice vector has an independent frequency. The $D+1$ dimensional space-time crystals can exhibit at most $D+1$ incommensurate frequencies. Hence, they are related to certain types of quasi-crystals.

2.2. *The generalized Bloch-Floquet theorem*

For dynamic crystal systems with space-time periodicity, the Bloch and Floquet theorems should be treated at equal footing. Below they are combined and generalized.

Consider the time-dependent Schrödinger equation $i\hbar\partial_t\psi(\mathbf{r},t) = H(\mathbf{r},t)\psi(\mathbf{r},t)$. Its solutions are denoted by the good quantum number of the (lattice) momentum-energy vector $\kappa = (\mathbf{k}, \omega)$, which is defined modulate the reciprocal lattice vectors. The Floquet-Bloch state labeled by κ takes the form of

$$\psi_{\kappa,m}(\mathbf{r},t) = e^{i(\mathbf{k}\cdot\mathbf{r}-\omega t)} u_m(\mathbf{r},t), \tag{6}$$

where m marks different states sharing the common κ. $u_m(\mathbf{r},t)$ is periodical in the space-time unit cell, which is expanded as Fourier series only involving momentum-energy reciprocal lattice vector as

$$u_m(\mathbf{r},t) = \sum_b c_{m,b} e^{i(\mathbf{G}\cdot\mathbf{r}-\Omega t)} \tag{7}$$

with $b = (\mathbf{G}, \Omega)$ taking all the momentum-energy reciprocal lattice vectors. The spectra ω_m can be solved through the secular equation,

$$\sum_{b'} \{[\varepsilon_0(\mathbf{k}+\mathbf{G}) - \Omega]\delta_{b,b'} + V_{b-b'}\} c_{m,b'} = \omega_m c_{m,b}, \tag{8}$$

where $\varepsilon_0(\mathbf{k})$ is the free dispersion, and V_b is the momentum-energy Fourier component of the space-time lattice potential $V(\mathbf{r},t)$.

The above procedure is very similar to the plane-wave expansion method of the band theory in D-dimensions, in which the static lattice potential only has Fourier components in momentum space. The difference is that the effective dimensions become $D+1$, since the reciprocal lattice vectors lie in the momentum-energy space for space-time crystals. Nevertheless, the Hilbert space of physical states remains the

same regardless of whether the potential is time-independent or not. To reconcile this discrepancy, we notice the gauge-like redundancy in the formalism based on and Eqs. (6) and (8). The solutions in the sector labeled by κ and those by $\kappa + b$ are redundant since the same state in Eq. (6) can also be expressed as $\psi_{\kappa,m}(\mathbf{r},t) = e^{i[(\mathbf{k}+\mathbf{G})\cdot\mathbf{r}-(\omega+\Omega)t]}u_{m'}(\mathbf{r},t)$ with $u_{m'}(\mathbf{r},t) = u_m(\mathbf{r},t)e^{-i(\mathbf{G}\cdot\mathbf{r}-\Omega t)}$.

The dispersion based on Eq. (8) is generally multiple-valued, represented by a D-dimensional surface in the momentum-energy Brillouin zone which is a $D+1$ dimensional torus. In the static case, the band dispersion only winds around the momentum direction. In space-time crystals, the winding patterns are richer.

Let us take the 1+1D case as a simple example. The dispersion relation $\omega(k)$ forms closed loops in the 2D toroidal momentum-energy Brillouin zone, each of which is characterized by a pair of winding numbers $\mathbf{w} = (w_1, w_2)$ with $w_{1,2}$ integers. In general, nearly all patterns $\mathbf{w} = (w_1, w_2)$ are possible except for one constraint explained as follows. Consider a weak lattice potential such that it can be treated as a perturbation. The free dispersion curve $\varepsilon(k)$ is folded into the momentum-energy Brillouin zone with crossings. Two states at a crossing point are connected by a reciprocal vector b before folding. The crossing is lifted if the momentum-energy Fourier component of V_b is nonzero. The total number of states at each k is independent of the potential strength, hence crossing can only be split along the ω-direction by opening a gap of $2|V_b|$, and $d\omega/dk$ is always finite. Hence, the contractible loops with the winding numbers $(0, 0)$ are unallowed.

Nevertheless, the winding number pattern could be constrained by spectral degeneracies protected by symmetries. For example, consider a magnetic group transformation applied to a 1+1 D space-time crystal, whose unit cell is a direct product between spatial and temporal periods a and T, respectively. Define the glide time-reversal operation $g_t(x,t) = (x + \frac{a}{2}, -t)$. It operates on the Hamiltonian as

$$g_t^{-1}H(x,t)g_t = H^*\left(x + \frac{a}{2}, -t\right). \tag{9}$$

The corresponding transformation M_{g_t} on the Bloch-Floquet wavefunction $\psi_\kappa(x,t)$ of Eq. (6) is anti-unitary defined as

$$M_{g_t}\psi_\kappa = \psi_\kappa^*\left(g_t^{-1}(x,t)\right). \tag{10}$$

Consider two special lines of the momentum-energy Brillouin zone with $\kappa_x = 0$ and $\kappa_x = \pi/a$. $M_{g_t}^2 = 1$ for states with $\kappa_x = 0$, but it becomes a Kramers symmetry $M_{g_t}^2 = -1$ for those of $\kappa_x = \pi/a$,

$$M_{g_t}^2\psi_\kappa = \psi_\kappa(x-a,t) = e^{-i\kappa_x a}\psi_\kappa = -\psi_\kappa. \tag{11}$$

Then the crossing at $\kappa_x = \pi/a$ cannot be avoided. Hence, the dispersion curve must wind along the momentum direction even times, while its windings along the energy direction cancel. The winding number is constrained to $\mathbf{w} = (2n, 0)$.

2.3. *Definition of space-time group*

Now we are ready to formally define *space-time* group in analogous to space group describing the static crystalline symmetry. It is the discrete subgroup between the direct product of the Euclidean group of D spatial dimensions and that along the time-direction $E_D \otimes E_1$. In general, space-time group *cannot* be factorized as a direct product between space and temporal subgroup groups.

In terms of coordinates, a space-time group operation Γ is defined as

$$\Gamma(\mathbf{r}, t) = (R\mathbf{r} + \mathbf{u}, st + \tau), \tag{12}$$

where R here is a point-group operation, including rotation, reflection, rotary reflection. $\mathbf{u}$ is a translation. If $\mathbf{u}$ is not a symmetry by itself, then it is non-symmorphic. Combining R and $\mathbf{u}$, they span space-groups. Further including $s = -1$, they span magnetic space-groups, which are used to describe the symmetry properties of magnetic systems. The last term of τ is time translation. Combining all the point group operations, time-reversal, spatial and temporal translations, the algebra is closed. This new symmetry group is dubbed *space-time* group.

If the time translation τ itself is not a symmetry, it should be combined with spatial transformations to form space-time nonsymmorphic symmetries as shown in Fig. 1. In 1+1 D, the only available operation to combine is spatial reflection. This is the dynamic symmetry of a see-saw [Fig. 1(a)]. A see-saw does not possess a static reflection symmetry, but it is invariant by performing reflection and time translation at half a period. This symmetry is the analogy of the glide-reflection symmetry of space group, dubbed *time-glide* reflection symmetry. In 2+1D, a new possibility is to combine τ with spatial rotation to form *time-screw* rotation, which can be intuitively understood as the dynamic symmetry of a clock [Fig. 1(b)]. Consider a simplified clock with only one pointer rotating. It does not exhibit the rotational symmetry due to the pointer, but a rotation combined with time translation can leave the clock invariant. This is the analogy of screw rotation of space group, dubbed "time-screw" rotation.

There also exist new possibilities that nonsymmorphic space-time symmetries have no analogies in static space groups. In 3+1D, a fractional time translation τ can be combined with the rotary reflection operation R, dubbed *time-shift rotary reflection* with an example depicted in Fig. 1(c). (Rotary reflection R is a rotation followed by a reflection whose $\det R = -1$ with eigenvalues $\{-1, e^{\pm i\theta}\}$ and $\theta \neq 0$.) Another possibility is a space-time translation $(\mathbf{u}, \tau)$ followed by a point group operation R. In other words, it is nonsymmorphic space group operation followed by a fractional time translation τ.

Naturally, quantum mechanical wavefunctions can be employed to span representations of space-time group. A special care needs to be taken is that the representation is anti-unitary when $s = -1$, i.e., time-reversal is involved. The operation

of Γ on the Hamiltonian is defined as

$$\Gamma^{-1}H(\mathbf{r},t)\Gamma = \begin{cases} H(\Gamma(\mathbf{r},t)) & \text{for} \quad s=1, \\ H^*(\Gamma(\mathbf{r},t)) & \text{for} \quad s=-1. \end{cases} \tag{13}$$

Correspondingly, the transformation M_Γ on the Bloch-Floquet wavefunctions $\psi_\kappa(\mathbf{r},t)$ is

$$M_\Gamma\psi_\kappa = \begin{cases} \psi_\kappa(\Gamma^{-1}(\mathbf{r},t)) & \text{for} \quad s=1, \\ \psi_\kappa^*(\Gamma^{-1}(\mathbf{r},t)) & \text{for} \quad s=-1. \end{cases} \tag{14}$$

2.4. *Classifications of space-time group*

The 2D space groups are particularly intuitive with a popular name of wallpaper groups. There exist 17 wallpaper groups corresponding to different types of planar patterns. Actually, all these patterns have been already used for ornaments since ancient times.[6]

We classify space-time crystals based on their space-time group symmetry structures. A natural starting point is to classify 1+1D space-time groups, which is an analogous problem to the 2D wallpaper groups. Due to the non-equivalence between spatial and temporal directions of the non-relativistic Schödinger equations, we cannot really rotate space and time into each other. Hence, only the 2-fold space-time rotation is allowed, i.e. $(x \to -x, t \to -t)$ and 3, 4, 6-fold rotations are not, which eliminates quite a few possibilities. On the other hand, the non-equivalence between space and time also brings richness. Spatial reflection m_x and time-reversal m_t are of a different nature. The former is a unitary operation, and the latter is anti-unitary. Similarly, as for two glide operations, a time-glide with a spatial reflection g_x is different from a space-glide with a time-reversal g_t.

Taking the above considerations into account, in total there are 13 types of space-time crystals as shown in Fig. 5. It is obvious that only two space-time crystal systems are allowed in 1+1D — oblique and orthorhombic. No square and hexagonal space-time crystals exist. Considering the Bravais lattices, the oblique case is monoclinic, and the orthorhombic case has two possibilities: the primitive one and the centered one. The oblique Bravais lattice generates 2 types of space-time crystals, the orthorhombic one generate 8, and the centered orthorhombic one generates 3, as shown in Figs. 5(a–c), respectively. For the centered orthorhombic lattices, actually their primitive cells are space-time rhombohedral. To explicitly demonstrate the full symmetries, two unit cells are plotted Fig. 5(c). There are 5 space-time groups that are non-symmorphic, and all of them belong to the orthorhombic Bravais lattice. And the rest 8 are symmorphic.

As a concrete example, look at a crystal configuration depicted in Fig. 5(b), the Pg_x one. This is the symmetry group of an array of see-saws, which is actually non-symmorphic. Such a system does have a Floquet period, but it is insufficient to show its complete space-time symmetries. In contrast, the space-time group goes

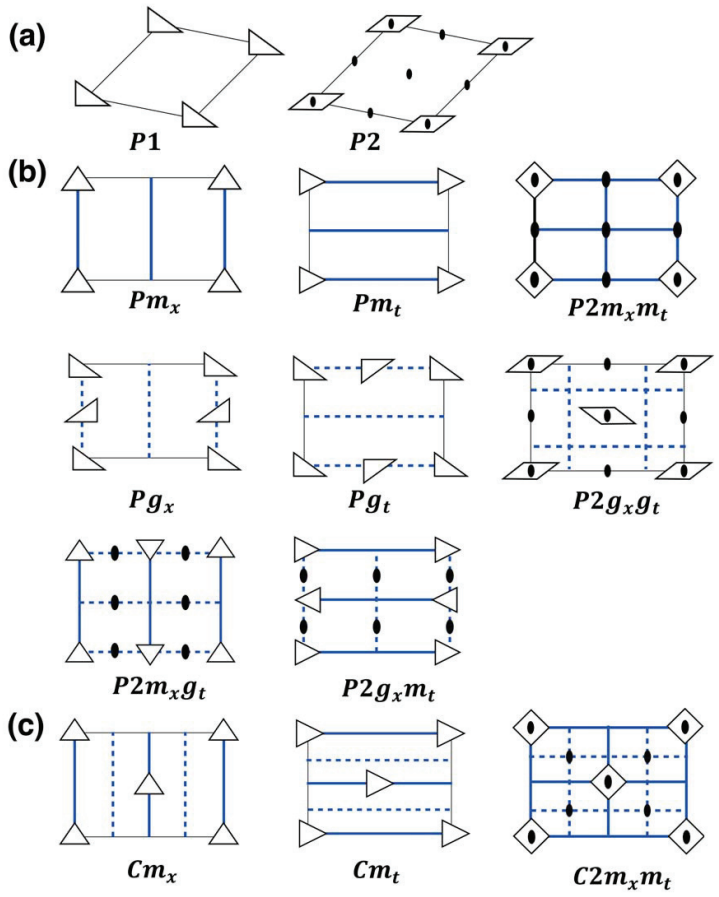

Fig. 5. Crystal configurations of 13 space-time groups in 1+1D. The solid oval marks the 2-fold space-time axis, and the parallelogram means the 2-fold axis without reflection symmetries. The thick solid and dashed lines represent reflection and glide-reflection axes, respectively. Configurations of triangles and the diamond denote the local symmetries under reflections. (a) The oblique Bravais lattice. Two space-time crystals with (P1) and without (P2) 2-fold axes in this crystal system. They generally do not possess a Floquet period, but exhibit space-time mixed translation symmetries. (b) The primitive orthorhombic Bravais lattice with 8 space-time crystals. They are denoted as Pm_x, Pm_t, $P2m_xm_t$ Pg_x, Pg_t, $P_2g_xg_t$, $P2m_xg_t$, and $P2g_xm_t$ according to their reflection and glide reflection symmetries. (c) The centered orthorhombic Bravais lattice with 2 space-time crystals denoted as Cm_x, Cm_t, $C2m_xm_t$. Two unit cells are plotted to show crystalline symmetries in this class. Among 13 space-time crystals in 1+1D, 5 of them (Pg_x, Pg_t, $P_2g_xg_t$, $P2m_xg_t$, and $P2g_xm_t$) are non-symmorphic, and the other 8 are symmorphic. From Ref. 49.

inside the Floquet period and extracts all the space-time symmetries. In the case of Pg_x, it shows the symmetry between the first and second halves of the Floquet period.

The classifications of the space-time groups in higher dimensions are generally complicated. The simple method of enumeration is cumbersome. We have classified

2+1D space-time groups based on the method of group cohomology, and the details will be presented elsewhere. This is an analogous problem to the 3D space groups. There exist 275 space-time groups with 72 of them symmorphic and the rest 203 non-symmorphic.

There are still 7 crystalline systems and 14 Bravais lattices for 2+1D space-time groups, whose numbers are the same as in the 3D case, but the situation is different. The cubic space-time crystal does not exist in 2+1D since we cannot compare the length along the time direction with that in the ab-plane, i.e., there does not exist a universal velocity like the light velocity in non-relativistic physics. Instead, there exist two different types of monoclinic space-time crystals. "Monoclinic" here means that the c-axis is perpendicular to the ab-plane, but the a and b axes are non-perpendicular to each other. The c-direction could be chosen as time, or, one of the spatial directions corresponding to the T- and R-monoclinic space-time crystals. Other crystal systems such as tetragonal, orthorhombic, trigonal, hexagonal, and triclinic ones can be similarly constructed.

2.5. *Spectral degeneracy protected by nonsymmorphic space-time symmetry*

For static crystals, it has been extensively studied that nonsymmorphic space-group symmetries can protect spectral degeneracies and enrich topological phases.[105–109] In this subsection, we show that the intertwined space-time nonsymmorhic symmetries also protect non-trivial spectral degeneracies of the driven system.

We express a general space-time group element as

$$g = T_{\mathbf{r}}(\mathbf{u})T_t(\tau)Rm_t^s, \tag{15}$$

where $T_{\mathbf{r}}(\mathbf{u})$ and $T_t(\tau)$ are spatial and temporal translations, respectively. R is a point group operator; m_t is the time-reversal operation with $s = 1$ or 0 determining whether g is anti-unitary or not, respectively. If two operations g_1 and g_2 belong to the little group of a high symmetry point $\kappa = (\mathbf{k}, \omega)$, whose point group operations commute, then

$$g_1 g_2 = T g_2 g_1 \tag{16}$$

with T a translation of integer unit vectors. T is decomposed into spatial and temporal parts as $T = T_{\mathbf{r}}(\tilde{\mathbf{u}})T_t(\tilde{t})$, where

$$\tilde{\mathbf{u}} = (\mathbf{I} - R_2)\mathbf{u_1} - (\mathbf{I} - R_1)\mathbf{u_2}, \quad \tilde{t} = 2s_2t_1 - 2s_1t_2. \tag{17}$$

Below we review degeneracies protected by this symmetry.

The representation matrices $M_{g_{1,2}}$ acting on Floquet-Bloch wavefunctions with κ satisfy

$$M_{g_1}M_{g_2} = e^{i\mathbf{k}\cdot\tilde{\mathbf{u}} - i\omega\tilde{t}} M_{g_2}M_{g_1}. \tag{18}$$

The following three cases need to be examined depending on whether $g_{1,2}$ are unitary or anti-unitary.

First, if neither g_1 nor g_2 reverses the direction of time. In this case, $\tilde{t} = 0$, and then the phase factor in Eq. (18) does not involve time. If $\mathbf{k} \cdot \mathbf{u} = 2\pi p/q$ with p and q coprime, then the Bloch-Floquet wavefunctions exhibit a q-fold degeneracy at $\kappa = (\mathbf{k}, \omega)$ proved as follows. Since g_1 belongs to the little group, a Bloch-Floquet eigenstate ψ_κ of quantum number κ can be chosen as an eigenstate of M_{g_1} satisfying $M_{g_1}\psi_\kappa = \mu\psi_\kappa$. Then consider the sequence of

$$\psi_\kappa,\ M_{g_2}\psi_\kappa,\ M_{g_2}^2\psi_\kappa, ...,\ M_{g_2}^{q-1}\psi_\kappa, \tag{19}$$

all of which share the same κ since g_2 belongs to the little group of κ. Moreover, they are also g_1's eigenstates exhibiting a set of different eigenvalues as

$$\eta, \mu\eta, \mu\eta^2, ..., \mu\eta^{q-1} \tag{20}$$

with $\eta = e^{i2\pi p/q}$. Then they are orthogonal to each other spanning a q-fold degeneracy.

Second, we consider the case that only one of $g_{1,2}$ involves time-reversal. Without loss of generality, M_{g_1} is assumed to be unitary while M_{g_2} is anti-unitary. Then the prefactor in Eq. (18) exhibits frequency dependence. Again since g_1 is in the little group, the Floquet-Bloch eigen state ψ_κ can be chosen as an M_{g_1} eigenstate, expressed as

$$M_{g_1}\psi_\kappa = e^{i\mathbf{k}\cdot\mathbf{u_1} - i\omega t_1} e^{i\theta}\psi_\kappa, \tag{21}$$

in which θ is extracted to be *only* dependent on the point group operation R_1. Based on Eq. (18), $M_{g_2}\psi_\kappa$ is also an eigenstate of g_1 as

$$M_{g_1}\left(M_{g_2}\psi_\kappa\right) = e^{i\mathbf{k}\cdot(-\mathbf{u_1}+\tilde{\mathbf{u}}) + i\omega(-\tilde{t}+t_1)} e^{-i\theta}\left(M_{g_2}\psi_\kappa\right). \tag{22}$$

Plugging in $\tilde{t} = 2t_1$, then the frequency dependence in the phase factor in Eq. (22) disappears. We conclude that if $e^{i\mathbf{k}\cdot(2\mathbf{u}_1 - \tilde{\mathbf{u}}) + 2i\theta} \neq 1$, then two phases in Eqs. (21) and (22) do not equal. Hence, the degeneracy is protected. Nevertheless, further applying high powers of M_{g2} does not bring new phases.

The last case is when both g_1 and g_2 flip the time-direction, i.e., both M_{g_1} and M_{g_2} are anti-unitary. By defining $g = g_1 g_2$ which is unitary again and combining g and g_2, we have

$$g g_2 = T_{\mathbf{r}}(\mathbf{u}) T_t(\tau) g_2 g, \tag{23}$$

which is reduced to case 2.

We emphasize that in none of the above three cases, the degeneracy condition depends on the frequency component of κ. This is expected since one can always shift the frequency of the spectrum by adding a constant to the Hamiltonian.

2.6. *Discussions*

So far the concept of *space-time group* has received considerable attentions.[110–119] We expect it would serve as a guiding principle for quantum dynamic studies, in analogy to the role of space group to static crystalline symmetries.[9] The classification of space-time group in 3+1D would be of fundamental importance if it is completed successfully, which is currently under investigation.

Actually the lattices in solids are dynamic, and the quantized lattice vibrations are phonons. However, phonons are typically thermally driven and incoherent. If a certain type of phonon mode is coherently excited, say, optically, or, by other pumping methods, it cannot be treated perturbatively.[34,120] Instead, the time-dependent motions of lattice ions should be treated at the zeroth order, i.e., we should include them in the time-dependent lattice potential of the Schrödinger equation. In artificial lattices, such as the phononic, photonic crystals, and optical lattice for ultracold atoms, lattice potentials could be manipulated on purpose.[36,110,117] In these cases, space-time group should replace space group as the symmetry guidance of quantum dynamics.

Certainly, the semi-classic transport in dynamic crystals is of importance. When the periodicity of lattice potential is weakly broken by slowly varying external fields both spatially and temporally, semi-classic equations of motion for a quantum particle could be developed.[32] We should distinguish two different types of dynamics: the fast changing periodical lattice potential which should be taken by the band structure calculation, and the slowly changing external field which should be treated in an adiabatic way. A challenging problem is how to generalize the Berry curvature formalism to the dynamic version and incorporate it into equations of motion.[121] The work in this direction would provide a general framework for further studying topological properties in dynamic systems.[122]

Another direction to explore is the connection to the research of time crystal.[43,123–132] The current study of time crystal is concentrated on the spontaneous breaking of the discrete time-translational symmetries, which is a profound interaction effect. Nevertheless, the symmetry breaking pattern typically is just the Floquet type. It would be interesting to combine these two directions together, for example, to consider how to spontaneously generate dynamic crystals with nonsymmorphic space-time symmetries. More philosophically, we could ask the problem of discrete subgroups of different types of space-time symmetries, including Galilean, Poincaré, anti-de Sitter symmetries, etc.

3. High Symmetry Perspective to Large-spin Cold Fermion Systems

The study of ultracold atom systems has become a new frontier for condensed matter physics as a way of creating novel quantum states of matter. We have proposed a

new perspective of high symmetries (e.g. SU(N) and Sp(N)) since 2003 to study the alkali and alkaline-earth fermion systems,[56–63] where N is the fermion component number and typically even. It is exciting to explore, in atomic systems, complex and beautiful many-body physics difficult to realize in usual solids.[89,90] It also significantly enriches the physics of large-N quantum magnetism by providing a realistic system.

3.1. *The generic SO(5) symmetry of spin-$\frac{3}{2}$ cold fermions*

In this subsection, we review the proof of an exact and generic hidden symmetry of Sp(4), or, isomorphically SO(5) symmetry in spin-$\frac{3}{2}$ fermion systems (e.g. ^{132}Cs, ^{9}Be, ^{135}Ba, ^{137}Ba, ^{201}Hg).[56,59,a] It plays the role of SU(2) in electron systems since its exactness is independent of dimensionality, lattice geometry, and particle filling. Such a high symmetry without fine-tuning is rare, which can be used as a guiding principle for exploring novel quantum phases.

Let us begin with the standard s-wave scattering interactions of spin-$\frac{3}{2}$ fermionic atoms.[133,134,b] Since the orbital wavefunction is symmetric in the s-wave channel, the total spin wavefunction of two fermions is constrained by Pauli's exclusion principle to be antisymmetric, which must be either singlet or quintet. The corresponding interaction parameters are denoted g_0 and g_2, respectively. The Hamiltonian reads,

$$H = \int d^d\vec{r} \left\{ \sum_{\alpha=\pm 3/2,\pm 1/2} \psi^\dagger_\alpha(\vec{r}) \left(\frac{-\hbar^2}{2m}\nabla^2 - \mu \right) \psi_\alpha(\vec{r}) + g_0 P^\dagger_{0,0}(\vec{r}) P_{0,0}(\vec{r}) + g_2 \sum_{m=\pm 2,\pm 1,0} P^\dagger_{2,m}(\vec{r}) P_{2,m}(\vec{r}) \right\}, \tag{24}$$

with d the space dimension, μ the chemical potential, and $P^\dagger_{0,0}, P^\dagger_{2,m}$ the singlet and quintet pairing operators defined through the Clebsh-Gordan coefficient for two indistinguishable particles as

$$P^\dagger_{F,m}(\vec{r}) = \sum_{\alpha\beta} \langle \frac{3}{2}\frac{3}{2}; F, m | \frac{3}{2}\frac{3}{2}\alpha\beta \rangle \psi^\dagger_\alpha(\vec{r}) \psi^\dagger_\beta(\vec{r}), \tag{25}$$

where $F = 0, 2$ and $m = -F, -F+1, ..., F$. Its lattice version is the spin-$\frac{3}{2}$ Hubbard

[a] Sp(4) and SO(5) share the same Lie algebra. Rigorously speaking, Sp(4) has spinor representations while SO(5) has not. Sp(4) is the double covering group of SO(5), and the relation between them is the same as that between SU(2) and SO(3). For simplicity, we will use Sp(4) and SO(5) interchangeably neglecting their minor difference.

[b] The total spin of an atom is often called "hyperfine spin" including contributions from the nuclear spin, electron spin and electron orbital angular momentum. Below we follow the convention of atomic physics to use F to denote an atom's hyperfine spin. For simplicity, spin and hyperfine spin are used interchangeably.

model,

$$H = -t \sum_{\langle ij\rangle,\sigma} (\psi^\dagger_{i\sigma}\psi_{j\sigma} + h.c.) - \mu \sum_{i\sigma} \psi^\dagger_{i\sigma}\psi_{i\sigma} + U_0 \sum_i P^\dagger_0(i)P_0(i) + U_2 \sum_{i,-2\le m\le 2} P^\dagger_{2m}(i)P_{2m}(i), \tag{26}$$

where t is the hopping integral, $U_{0,2}$ are the onsite Hubbard interaction parameters in the singlet and quintet channels, respectively.

So far, the perspective in Eqs. (24) and (26) is the usual spin SU(2) symmetry. The 4-component spinor, singlet and quintet channels correspond to the spin quantum numbers $\frac{3}{2}$, 0, and 2, respectively. Below we will show that this degeneracy pattern equally well fits in a high symmetry group of Sp(4), or, isomorphically, SO(5), which provides a whole new perspective in spin-$\frac{3}{2}$ fermion systems.

For this purpose, we construct the Sp(4) algebra by extending the typical charge and spin sectors. For spin-$\frac{1}{2}$ systems, charge and spin form a complete set for the particle-hole (p-h) channel observables. However, they are incomplete since there are $4^2 = 16$ bilinears in spin-$\frac{3}{2}$ systems,

$$M^I = \psi^\dagger_{i,\alpha} M^I_{\alpha\beta} \psi_{i,\beta} \quad (I = 1 \sim 16). \tag{27}$$

To systematically decompose the 16 matrix kernels of $M^I_{\alpha\beta}$, high rank spin tensors are employed,

$$\begin{aligned} &\text{particle number:} && I; && \\ &\text{spin:} && F^i, && i = 1,2,3; \\ &\text{spin quadrupole:} && \xi^a_{ij} F_i F_j, && a = 1,..,5; \\ &\text{spin octupole:} && \xi^L_{ijk} F_i F_j F_k, && L = 1,..,7, \end{aligned} \tag{28}$$

where ξ's are the typical fully symmetric, traceless tensors converting 3-vector into spherical tensors.

The five spin quadrupole matrices are denoted $\Gamma^a = \xi^a_{ij} F_i F_j$, which remarkably anticommute with each other forming a basis of the Dirac Γ matrices satisfying

$$\{\Gamma_a, \Gamma_b\} = 2\delta_{ab}. \tag{29}$$

Explicitly, they are

$$\Gamma^1 = \begin{pmatrix} 0 & -iI \\ iI & 0 \end{pmatrix}, \quad \Gamma^{2,3,4} = \begin{pmatrix} \vec{\sigma} & 0 \\ 0 & -\vec{\sigma} \end{pmatrix}, \quad \Gamma^5 = \begin{pmatrix} 0 & I \\ I & 0 \end{pmatrix}, \tag{30}$$

where I and $\vec{\sigma}$ are the 2×2 unit and Pauli matrices, respectively. They are explicitly expressed by the spin matrices as

$$\begin{aligned} &\Gamma_1 = \frac{1}{\sqrt{3}}(F_x F_y + F_y F_x), \quad \Gamma_2 = \frac{1}{\sqrt{3}}(F_z F_x + F_x F_z), \quad \Gamma_3 = \frac{1}{\sqrt{3}}(F_z F_y + F_y F_z), \\ &\Gamma_4 = F_z^2 - \frac{5}{4}, \qquad \Gamma_5 = \frac{1}{\sqrt{3}}(F_x^2 - F_y^2). \end{aligned} \tag{31}$$

Moreover, the 3 spin and 7 spin octupole matrices together can be organized into 10 commutators of Γ-matrices defined as

$$\Gamma^{ab} = -\frac{i}{2}[\Gamma^a, \Gamma^b] \quad (1 \le a, b \le 5). \tag{32}$$

Consequently, the 16 particle-hole channel bilinear operators are classified according to their properties under the Sp(4) transformations as scalar, vector, and anti-symmetric tensors (generators) as

$$\begin{aligned} n(\vec{r}) &= \psi^\dagger_\alpha(\vec{r})\psi_\alpha(\vec{r}), \quad n_a(\vec{r}) = \frac{1}{2}\psi^\dagger_\alpha(\vec{r})\Gamma^a_{\alpha\beta}\psi_\beta(\vec{r}), \\ L_{ab}(\vec{r}) &= -\frac{1}{2}\psi^\dagger_\alpha(\vec{r})\Gamma^{ab}_{\alpha\beta}\psi_\beta(\vec{r}). \end{aligned} \tag{33}$$

The SO(5) generators L_{ab} and its vectors n_a together span the SU(4) algebra. They satisfy the commutation relations as

$$\begin{aligned} &[L_{ab}, L_{cd}] = -i(\delta_{ac}L_{bd} + \delta_{bd}L_{ac} - \delta_{ad}L_{bc} - \delta_{bc}L_{ad}), \\ &[L_{ab}, n_c] = -i(\delta_{ac}n_b - \delta_{bc}n_a), \\ &[n_a, n_b] = -iL_{ab}. \end{aligned} \tag{34}$$

It is well known that the SU(4) algebra is isomorphically to SO(6), and SU(4) is the double covering group of SO(6).

In order to study pairing operators in the particle-particle channel and time-reversal transformation, we introduce the charge conjugation matrix R: The combination of R and the creation operators $R_{\alpha\beta}\psi^\dagger_\beta$ transforms the same as the annihilation operator ψ_α under the Sp(4) transformation. The existence of R is based on the pseudoreality of Sp(4) spinor representation, satisfying

$$R^2 = -1, \quad R^\dagger = R^{-1} = {}^tR = -R, \quad R\Gamma^a R = -{}^t\Gamma^a, \quad R\Gamma^{ab}R = {}^t\Gamma^{ab}, \tag{35}$$

where ${}^t\Gamma^{a,ab}$ are the transposed matrices of $\Gamma^{a,ab}$. In the representation of Eq. (30), R is expressed as $R = \Gamma_1\Gamma_3$.

Under the assistance of R, the fermion pairing operators is expressed as[61]

$$\begin{aligned} \eta^\dagger(\vec{r}) &= \mathrm{Re}\eta + i\ \mathrm{Im}\eta = \frac{1}{2}\psi^\dagger_\alpha(\vec{r})R_{\alpha\beta}\psi^\dagger_\beta(\vec{r}), \\ \chi^\dagger_a(\vec{r}) &= \mathrm{Re}\chi_a + i\ \mathrm{Im}\chi_a = -\frac{i}{2}\psi^\dagger_\alpha(\vec{r})(\Gamma^a R)_{\alpha\beta}\psi^\dagger_\beta(\vec{r}). \end{aligned} \tag{36}$$

Clearly, $\eta^\dagger(\vec{r})$ is an Sp(4) scalar, and $\chi^\dagger_a(\vec{r})$'s are a set of Sp(4) vector. They are related to the spin SU(2) representation via

$$\begin{aligned} &P^\dagger_{0,0} = -\frac{1}{\sqrt{2}}\eta^\dagger, \\ &P^\dagger_{2,0} = -i\frac{1}{\sqrt{2}}\chi^\dagger_4, \quad P^\dagger_{2,\pm1} = \frac{1}{2}(-\chi^\dagger_3 \pm i\chi^\dagger_2), \quad P^\dagger_{2,\pm2} = \frac{1}{2}(\mp\chi^\dagger_1 + i\chi^\dagger_5). \end{aligned} \tag{37}$$

The anti-unitary time-reversal transformation $T^2 = -1$ is expressed as

$$T = R\ C, \tag{38}$$

where C denotes complex conjugation. L_{ab}'s consist of spin and spin-octupole operators.[56,135] Since they are odd rank spin tensors, they are time-reversal odd. n_a's and N are time-reversal even. It is also straightforward to check that they transform differently under the T transformation

$$TnT^{-1} = n, \quad Tn_aT^{-1} = n_a, \quad TL_{ab}T^{-1} = -L_{ab}. \tag{39}$$

Now we are ready to prove the generic SO(5) symmetry of Eqs. (24) and (26). The kinetic energy part has an explicit SU(4) symmetry which is the unitary transformation among four spin components. The singlet and quintet interactions are proportional to $\eta^\dagger(\vec{r})\eta(\vec{r})$ and $\chi_a^\dagger(\vec{r})\chi_a(\vec{r})$, respectively, thus reducing the symmetry group from SU(4) to SO(5). When $g_0 = g_2$, the SU(4) symmetry is restored because $\chi_a^\dagger, \eta^\dagger$ together form the 6 dimensional antisymmetrical tensor representation of SU(4).

For the continuum model, the odd partial wave scatterings include the spin triplet and septet channels, whose interactions are denoted as g_1 and g_3, respectively. The SO(5) symmetry is broken if $g_1 \neq g_3$, and restored at $g_1 = g_3$ since the triplet and septet together could form the 10D adjoint representation of SO(5). However, to the leading order, p-wave scattering is weak for neutral atoms, and thus can be safely neglected. For the lattice model, the onsite interactions do not allow the triplet and septet interactions.

For later convenience, the lattice Hubbard model of Eq. (26) can be rewritten in another manifestly Sp(4) invariant form as

$$\begin{aligned} H_0 &= -t \sum_{\langle i,j \rangle} \left(\psi^\dagger(i)\psi(j) + h.c. \right), \\ H_I &= \sum_{i, 1\le a\le 5} \left[\frac{3U_0 + 5U_2}{16} \left(n(i) - 2\right)^2 - \frac{U_2 - U_0}{4} n_a^2(i) \right] - (\mu - \mu_0) \sum_i n(i), \end{aligned} \tag{40}$$

where the SU(4) symmetry appears at $U_0 = U_2$ as before. At half-filling, $\mu_0 = (U_0 + 5U_2)/2$ to ensure the particle-hole symmetry.[c]

3.2. *The SO(7) unification and the χ-pairing*

The spin-$\frac{1}{2}$ Hubbard model defined in a bipartite lattice in any dimensions actually possesses a pseudospin SU(2) symmetry spanned by the η-pairing operators and particle number as discovered by Yang[26] and by Yang and Zhang.[27] In this subsection, we review the extension of the pseudo-spin symmetry to the SO(7) symmetry in the spin-$\frac{3}{2}$ Hubbard model, and define the quintet χ-pairing operators. It exhibits much richer unifying power in treating a variety of competing orders at equal footing.[56]

The η-pairing operator in spin-$\frac{1}{2}$ systems sums over the onsite singlet pairing operators with opposite signs on two sublattices. The pseudospin SU(2) algebra is particularly useful for unifying competing orders in the negative-U Hubbard model.[26–28]

[c]Here half-filling means the average particle number per site equals 2, half of the component number.

The complex order parameters of superconductivity and the charge-density-wave are unified forming a 3D representation. The η-pairing generator transforms superconductivity into charge-density-wave and vice versa. At half-filling, the pseudospin SU(2) symmetry is exact, and these two types of orders are degenerate. Away from half-filling, the SU(2) symmetry is explicitly broken, and the superconducting ground state is selected. However, when applying the η-pairing operator to the ground state, it creates well-defined excitations, which are the pseudo Goldstone modes rotating superconductivity into charge-density-wave.

Before moving on, let us fully explore the symmetry structure of spin-$\frac{3}{2}$ systems. The largest algebra formed by 4-component fermions is actually SO(8),[136] including 16 p-h channel fermion bilinears and the other 12 in the p-p channel. On each site, the local SO(8) generators $M_{ab}(i)$ $(0 \le a < b \le 7)$ are organized as follows,[56,59]

$$M_{ab}(i) = \begin{pmatrix} 0 & \mathrm{Re}\chi_1(i) & \sim & \mathrm{Re}\chi_5(i) & N(i) & \mathrm{Re}\eta(i) \\ & & & & \mathrm{Im}\chi_1(i) & n_1(i) \\ & & L_{ab}(i) & & \sim & \sim \\ & & & & \mathrm{Im}\chi_5(i) & n_5(i) \\ & & & & 0 & -\mathrm{Im}\eta(i) \\ & & & & & 0 \end{pmatrix}, \tag{41}$$

with $N(i) = (n(i) - 2)/2$. For $1 \le a < b \le 5$, they are just $L_{ab}(i)$ forming its SO(5) subalgebra. The global SO(8) generators are defined as

$$M_{ab} = \sum_i M_{ab}(i), \quad \text{or,} \quad M_{ab} = \sum_i (-)^i M_{ab}(i), \quad (0 \le a < b \le 7), \tag{42}$$

depending on M_{ab} lying in the p-h or p-p channels, respectively. More explicitly, we write

$$\begin{aligned} &L_{ab} = M_{ab}, && n_a = M_{a7}, && N = M_{06}, \\ &\eta^\dagger = M_{06} - iM_{67}, && \chi_a^\dagger = M_{0a} + iM_{a6}, \end{aligned} \tag{43}$$

with $1 \le a < b \le 5$. L_{ab}, n_a and N lie in the p-h channel, and η and $\chi_a^\dagger$ lie in the p-p channel. The $\eta^\dagger$ operator is the spin-$\frac{3}{2}$ generalization of Yang's $\eta^\dagger$, both of which are spin singlet. In contrast, the $\chi_a^\dagger$ pairing operator is a non-trivial quintet generalization.

It is easy to check that the H_0 part of the Hamiltonian Eq. (40) satisfies $[H_0, M_{ab}] = 0$. However, H_{int} typically breaks the SO(8) symmetry unless it vanishes within the framework of 4-fermion interactions.

The next highest algebra is SO(7) spanned by M_{ab} with $0 \le a < b \le 6$, which is the high-rank Lie algebra generalization of Yang's pseudospin SU(2) algebra. Explicitly, they include the SO(5) generators L_{ab}, the χ-pairing operators $\mathrm{Re}\chi_a, \mathrm{Im}\chi_a$, and the particle number N. This SO(7) symmetry becomes exact at $U_0 = -3U_2$, where the interacting part of the Hamiltonian Eq. (40) is reduced to

$$H_I = \sum_{i, 0 \le a < b \le 6} \Big\{ \frac{2}{3} U_2 \ [M_{ab}(i)]^2 - (\mu - \mu_0) n(i) \Big\}. \tag{44}$$

At half-filling, $\mu = \mu_0$, then the global SO(7) symmetry becomes exact.

The SO(7) symmetric spin-$\frac{3}{2}$ Hubbard model can be further divided into two cases: $U_0 = -3U_2$ with (I) $U_2 > 0$; (II) $U_2 < 0$. The physics of case (I) lies in SO(7)'s vector representation, while that of case (II) lies in the adjoint representation.

In case (I), the system in the weak coupling regime exhibits the competition between the singlet superconductivity and density-wave of spin quadrupole orders, whose order parameters are organized as

$$V_a = \sum_i (-)^i M_{a6}, \quad \text{or,} \quad V_a = \sum_i M_{a6}, \quad (0 \le a \le 7) \tag{45}$$

depending on V_a lying in the p-h channel or the p-p channel, respectively. More explicitly, superconductivity and spin quadrupole density wave are unified as

$$V_0 = \mathrm{Re}\Delta_s, \quad V_a = \mathrm{SDW}_a \quad (1 \le a \le 5), \quad V_6 = -\mathrm{Im}\Delta_s. \tag{46}$$

They transform according to the vector representation of SO(7),

$$[M_{ab}, V_c] = i\left(\delta_{bc} V_a - \delta_{ac} V_b\right). \tag{47}$$

Hence, the Goldstone manifold is S^6. Away from half-filling, SO(7) is broken and the singlet superconductivity is selected as the ground state ordering. The χ-pairing operators remain the eigen-operators as

$$[H, \chi_a^\dagger] = -(\mu - \mu_0)\chi_a^\dagger, \quad \text{and,} \quad [H, \chi_a] = (\mu - \mu_0)\chi_a. \tag{48}$$

At $\mu < \mu_0$, applying $\chi_a^\dagger$ to the superconducting ground state $|\Omega\rangle$ creates a quintet excitation,

$$H\left(\chi_a^\dagger |\Omega\rangle\right) = (\mu_0 - \mu)\left(\chi_a^\dagger |\Omega\rangle\right), \tag{49}$$

which carries the lattice momentum $\mathbf{Q} = (\pi, \pi)$. In other words, the χ_a-pairing operator behaves like a quasi-Goldstone mode, which rotates the singlet superconductivity to the density-wave state of the a-th component of spin quadrupole density-wave.

Yang's η-pairing operators were generalized to the SO(5) theory of high T_c superconductivity, which unifies the 2-component superconductivity and 3-component antiferromagnetism into a 5-vector. Nevertheless, the SO(5) algebra is not exact.[29] The celebrated neutron resonance modes in the superconducting states were interpreted as the pseudo-Goldstone modes rotating from superconductivity to antiferromagnetism, denoted as π-modes. The χ-modes here are just analogs of the π modes SO(5) theory.[29] However, the SO(5) algebra is not exact in high T_c cuprate systems. In contrast, here the SO(7) symmetry is exact.

The SO(7) unification is even more powerful in case (II) with $U_0 > 0$, in which the 21D adjoint representation of SO(7) plays the role. The order parameter manifold includes the quintet superconductivity, the 10-fold density-wave of spin and spin octupole orders, and charge-density-wave, which are organized as

$$T_{ab} = \sum_i (-)^i M_{ab}, \quad \text{or,} \quad T_{ab} = \sum_i M_{ab}, \quad (0 \le a < b \le 6), \tag{50}$$

depending on T_{ab} lying in the p-h channel or the p-p channel, respectively. Explicitly, they are

$$\Delta_{q,a} = T_{0a} + iT_{a6}, \quad \mathrm{SDW}_{ab} = T_{ab}, \quad \mathrm{CDW} = T_{06}, \tag{51}$$

where $1 \le a < b \le 6$. They transform according to the SO(7) algebra as

$$[M_{ab}, T_{cd}] = i\left(\delta_{ac}T_{bd} + \delta_{bd}T_{ac} - \delta_{ad}T_{bc} - \delta_{bc}T_{ad}\right). \tag{52}$$

It is amazing to realize such a "grand unification" in a non-relativistic model. The Goldstone manifold is SO(7)/[SO(5)× SO(2)], which is 10-dimensional. When away from half-filling, the SO(7) symmetry is broken into SO(5), and the ground state exhibit the quintet superconductivity. Equation (49) still applies. Assuming $\langle\Omega|\Delta_{q,b}|\Omega\rangle \neq 0$, $\chi_a^\dagger|\Omega\rangle$ remains a quasi-Goldstone mode which rotates to the spin/spin octupole density-wave state SDW_{ab} if $a \neq b$, or, the charge-density-wave state if $a = b$.

The pseudo-spin SU(2) symmetry of the spin-$\frac{3}{2}$ version occurs at $U_0 = 5\ U_2$. In this case, H_I is rewritten as

$$H_I = \sum_{i,1\le a,b\le 5} \left\{-U_2\ L_{ab}^2(i) - (\mu - \mu_0)n(i)\right\}, \tag{53}$$

which only involve the SO(5) generators. Then M_{06}, M_{07}, M_{67} span an SU(2) algebra commuting with all the SO(5) generators. More explicitly, they are just the pseudo-spin SU(2) algebra spanned by the η-pairing and particle number operators. At $U_0 = 5\ U_2 < 0$, this pseudospin SU(2) symmetry unifies the singlet pairing and charge-density-wave order parameters in a similar way to the spin-$\frac{1}{2}$ negative-U Hubbard model. Again, when away from half-filling, this symmetry is broken, and the ground state is the singlet pairing state. In this case, the η-pairing operators remain eigen-operators

$$[H, \eta^\dagger] = -(\mu - \mu_0)\eta^\dagger, \quad \text{and,} \quad [H, \eta] = (\mu - \mu_0)\eta. \tag{54}$$

We emphasize that the pseudo-spin SU(2) symmetry in the spin-$\frac{3}{2}$ system is still different from that in the spin-$\frac{1}{2}$ case. In the latter case, the empty and doubly occupied states form a pseudospin-$\frac{1}{2}$ representation. In the spin-$\frac{3}{2}$ case, there are three onsite singlet states: empty, 2-particle singlet, and the 4-occupied states forming a pseudo-spin-1 representation.

Based on the above analysis and assisted by mean-field calculations, the weak-coupling phase diagram in a bipartite lattice at half-filling in two dimensions and above is shown in Fig. 6. The higher symmetries lines are as follows: The SU(4) symmetry appears along line E with $U_0 = U_2$; the SO(7) symmetry appears along lines F and H with $U_0 = -3U_2$; and the SO(5)⊗ SU(2)symmetry appears long line G with $U_0 = 5U_2$. These lines are phase boundaries separating phases A, B, C, and D. Phase A and B are regimes where repulsive interactions dominate. Hence, they are density-wave states of spin tensors. In phase A, the onsite singlet energy is smaller than the quintet energy, leading to the spin quadrupole density-wave forming the

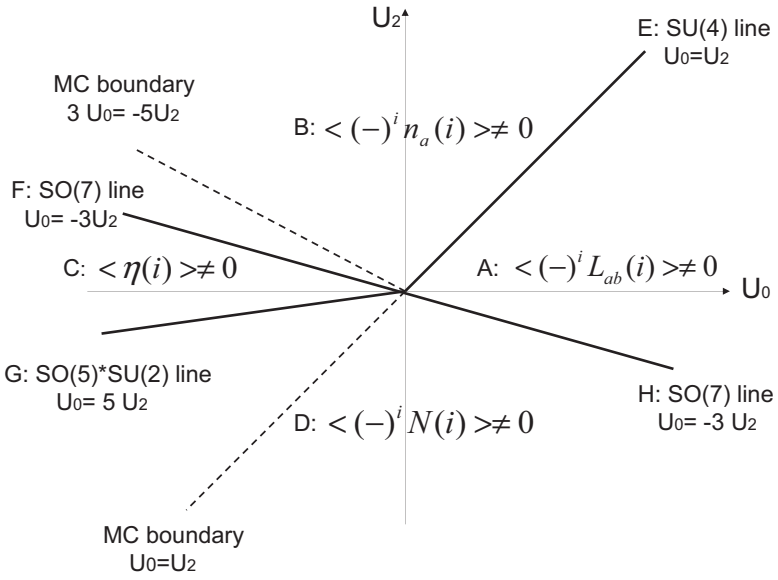

Fig. 6. Competing phases of spin-$\frac{3}{2}$ Hubbard model unified by high symmetries. (A) and (B): Antiferromagnetism in the Sp(4) adjoint and vector representations; (C): the singlet superconductivity; (D): CDW; (E), (F), (G), and (H): exact phase boundaries with higher symmetries of SU(4), SO(7), SO(5) ⊗ SU(2) and SO(7), respectively. From Ref. 56.

5-vector representation of the Sp(4) group. On the other hand, the lowest onsite states in phase B are 5-fold degenerate, leading to the spin/spin octupole density-wave forming the 10-dimensional adjoint representation of Sp(4). The Goldstone manifold in phase A is SO(5)/SO(4)=S^4, while that in phase B is SO(5)/[SO(3)⊗ SO(2)]. On line E, the SU(4) symmetry unifies the 15 dimensional density-wave orders in all the spin channels forming the SU(4) adjoint representation, whose Goldstone manifold is U(4)/[U(2)⊗ U(2)].

Phase C is the singlet pairing state, and phase D is the charge-density-wave state. Orders in phases B and C are unified along the SO(7) line F. In contrast, the SO(7) line H unifies orders in phases A, D, and the quintet pairing. Orders in phases C and D are unified along the pseudospin SU(2) symmetry line G.

At last, let us mention an interesting point that SO(7) possesses a subgroup of G_2, which is the smallest exceptional Lie group and also the automorphism group of non-associative algebra of octonions. A G_2 symmetric spin-$\frac{3}{2}$ Hubbard model is constructed which is the common subgroup of two different SO(7) algebras connected by the structure constant of octonions as shown in Ref. 63. This model exhibits various interesting symmetry breaking patterns: The G_2 symmetry can be spontaneously broken into SU(3), or, SU(2)⊗ U(1), both of which are essential in high energy physics. In quantum disordered states, quantum fluctuations generate the effective SU(3), or, SU(2)⊗ U(1) gauge theories.

3.3. *Quartet (charge-4e) superfluidity and quartet density wave*

Superconductivity arises from the coherent condensation of Cooper pairs, which is the central concept of the celebrated Bardeen-Cooper-Schrieffer (BCS) theory. Moreover, there exist multi-fermion clustering instabilities in strong correlation systems in various disciplines of modern physics. The SU(3) gauge symmetry requires three quarks to form a color singlet bound state of baryon[19]; α-particles are 4-body bound states of two protons and two neutrons, and biexcitons are bound states of two electrons and two holes. These states go beyond the framework of the BCS theory since they cannot be reduced to a 2-body problem. The competitions among the quartetting (charge $4e$) and pairing ($2e$) superfluidities, quartet and pair density wave orderings are investigated in 1D 4-component fermion systems.[58,69] In recent years, charge-$4e$ superconductivity has been proposed as a consequence of strong fluctuations of the pair-density-wave state in high T_c cuprates.[137,138] Competitions of 4-fermion orderings in the context of superconducting phase fluctuations have recently received attentions.[139–141] Excitingly experimental evidence of Little-Parks oscillations at the periods of $hc/(4e)$ and $hc/(6e)$ have been observed in the Kagome superconductor CsV_3Sb_5.[142]

Spin-$\frac{3}{2}$ systems allow the quartteting order, i.e., 4 fermions forming a clustering instability, which is also called "charge-$4e$" in condensed matter physics. A quartet in the strong coupling limit is a 4-body maximally entangled EPR state with all the spin components forming an SU(4) singlet, whose order parameter is expressed as

$$Q(x) = \psi^\dagger_{\frac{3}{2}}(x)\psi^\dagger_{\frac{1}{2}}(x)\psi^\dagger_{-\frac{1}{2}}(x)\psi^\dagger_{-\frac{3}{2}}(x). \tag{55}$$

Furthermore, spin-$\frac{3}{2}$ systems could support 6 different types of Cooper pairing states including an Sp(4) singlet and a set of Sp(4) quintet states whose order parameters are presented in Eq. (36). It would be interesting to investigate their competitions.

Assisted by the strong coupling methods for 1D problems, we are able to analyze the competition between the quartetting and pairing formations. Quartets and pairs can undergo either superfluidity or density-wave transitions depending on the charge channel interactions. Only the quartetting states are SU(4) invariant, and the 6 pairing operators presented in Eq. (36) form the rank-2 antisymmetric tensor representation of SU(4).[d] Due to the strong quantum fluctuations, non-Abelian Lie group symmetries cannot be spontaneously broken in 1D. Hence, only quartet orderings, either superfluidity or density wave, are allowed by the SU(4) symmetry. Nevertheless, if the symmetry is reduced to Sp(4), the Sp(4) singlet pairing could survive, while the quintet pairing still cannot survive. Naturally, there exist competitions between Sp(4) singlet (charge-$2e$) pairing orders and quartteting (charge-$4e$) orders. Between them it is an Ising order-disorder transition in the spin channel.

[d]In terms of SO(6), which equals $SU(4)/Z_2$, they form the 6-vector representation.

Here we briefly outline the procedure of the bosonization and renormalization group (RG) analysis, and the details were presented in Ref. 59. The Sp(4) currents include scalar (charge), vector (spin quadrupole), and tensor (spin plus spin octupole) ones,

$$J_{R,L}(z) = \psi^\dagger_{R,\alpha}(z)\psi_{R,\alpha}(z), \quad J^a_{R,L}(z) = \frac{1}{2}\psi^\dagger_{R,\alpha}(z)\Gamma^a_{\alpha\beta}\psi_{R,\beta}(z) \ (1 \le a \le 5),$$
$$J^{ab}_{R,L}(z) = \frac{1}{2}\psi^\dagger_{R,\alpha}(z)\Gamma^{ab}_{\alpha\beta}\psi_{R,\beta}(z) \ (1 \le a < b \le 5), \tag{56}$$

where R and L refer to right- and left-movers. The low energy effective Hamiltonian density $H = H_0 + H_{int}$ is written as,

$$H_0 = v_f\Big\{\frac{\pi}{4}J_R J_R + \frac{\pi}{5}(J^a_R J^a_R + J^{ab}_R J^{ab}_R) + (R \to L)\Big\},$$
$$H_{int} = \frac{g_c}{4}J_R J_L + g_v J^a_R J^a_L + g_t J^{ab}_R J^{ab}_L, \tag{57}$$

where the chiral couplings are neglected at one-loop level since it only renormalizes Fermi velocities. At the tree level, these dimensionless coupling constants are related by the pair interaction parameters g_0, g_2 defined in Eq. (24) as $g_c = (g_0 + 5g_2)/2$, $g_v = (g_0 - 3g_2)/2$, $g_t = -(g_0 + g_2)/2$. Certainly, they are renormalized significantly under the RG process. At $g_v = g_t$, or, $g_0 = g_2$, the SU(4) symmetry is restored.

The phase diagram at incommensurate fillings is presented at Fig. 7. The charge sector remains gapless and decouples with the spin sectors. In the spin sector, three phases are identified: Phase A is the gapless Luttinger liquid phase lying in the repulsive interaction region where $0 < g_2 < g_0$, which is controlled by the non-interacting fixed point. Phase B is the quartetting phase controlled by the strong coupling fixed point along the SU(4) line with $g_v = g_t \to +\infty$, or, $g_0 = g_2 \to -\infty$. It lies in the regime where attractive interactions dominate. Phase C is the spin singlet pairing phase controlled by the strong coupling point along the line of $-g_v = g_t \to +\infty$ corresponding to $g_0 \to -\infty$ and $g_2 \to 0$. The pairing phase even covers the regime with a purely repulsive interaction regime.

Within quartetting phase B, there also exist two competing orders, the quartetting superfluidity and quartet density wave. By checking the periodicity, the quartet density wave corresponds to the $2k_f$ CDW. Four fermions first form quartets, and then they either undergo superfluidity, or, density wave ordering. As for the charge sector, their bosonic expressions are

$$Q = \psi^\dagger_{\frac{3}{2}}\psi^\dagger_{\frac{1}{2}}\psi^\dagger_{-\frac{1}{2}}\psi^\dagger_{-\frac{3}{2}} \propto e^{2i\sqrt{\pi}\theta_c}, \quad O_{qdw} = \psi^\dagger_{R\alpha}\psi_{L\alpha} \propto e^{i\sqrt{\pi}\phi_c}. \tag{58}$$

The scaling dimensions for quartet superfluidity and density-wave orders are $1/K_c$ and $K_c/4$, respectively. Hence, the quartet superfluidity wins at $K_c > 2$, while the quartet density wave wins at $K_c < 2$.

Similarly in phase C, Cooper pairs can either undergo superfluidity, or, pair density wave ordering. The pair density wave corresponds to the $4k_f$ charge density

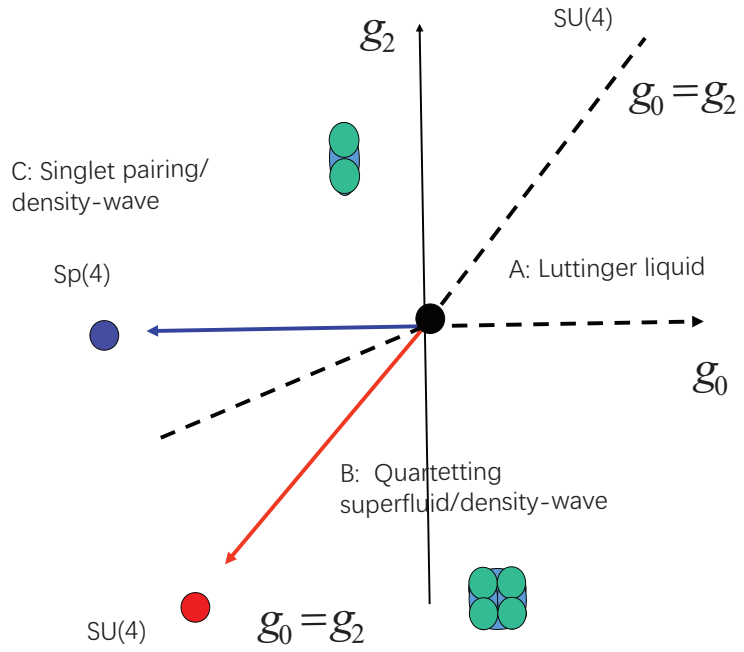

Fig. 7. Competition between quartetting (charge-4e) and singlet pairing (charge-2e) phases in 1D spin-$\frac{3}{2}$ systems at incommensurate fillings. Combined with the charge channel Luttinger parameter K_c, three phases are identified with phase boundaries marked by dashed lines. (A) The gapless Luttinger liquid phase controlled by the non-interacting fixed point (the black spot). (B) Quartetting superfluidity at $K_c > 2$ or quartet density-wave ($2k_f$) at $K_c < 2$. They are controlled by the strong coupling fixed point along the SU(4) line (the red spot); (C) singlet pairing superfluidity at $K_c > 1/2$ or pair density wave ($4k_f$) at $K_c < 1/2$. They are controlled by the strong coupling fixed point along $g_2 = 0$ (the blue spot). Phases B and C are both gapped in spin channels, and the transition between them is an Ising order-disorder transition. From Ref. 58.

wave. As for the charge sector, their bosonic expressions are

$$\Delta_s = \eta^\dagger = \psi^\dagger_{\frac{3}{2}}\psi^\dagger_{-\frac{3}{2}} - \psi^\dagger_{\frac{1}{2}}\psi^\dagger_{-\frac{1}{2}} \propto e^{i\sqrt{\pi}\theta_c}, \quad O_{pdw} = \psi^\dagger_{R\alpha}\psi^\dagger_{R\beta}\psi_{L\beta}\psi_{L\alpha} \propto e^{2i\sqrt{\pi}\phi_c}. \quad (59)$$

The scaling dimensions for the singlet pairing and pair density wave orders are $1/(4K_c)$ and K_c, respectively. Hence, the pairing superfluidity dominates over the pair-density-wave at $K_c > 1/2$. In the region of $1 > K_c > 1/2$, pairing superfluidity is the leading instability in an overall repulsive interaction environment.

The boundary between phase B quartetting (charge-4e) and phase C singlet pairing (charge-2e) is determined by the unstable fixed point $(g_v = 0, g_t \to \infty)$, which is approximately plotted in Fig. 7. The competitions between these two phases can be mapped to a phase-locking problem of two-band superconductivity. The first component is $\Delta_1 = \psi^\dagger_{\frac{3}{2}}\psi^\dagger_{-\frac{3}{2}}$, and the second one $\Delta_2 = \psi^\dagger_{\frac{1}{2}}\psi^\dagger_{-\frac{1}{2}}$, whose bosonic representations are

$$\Delta_1 \propto e^{i\sqrt{\pi}\theta_1} = e^{i\sqrt{\pi}(\theta_c+\theta_r)}, \quad \Delta_2 \propto e^{i\sqrt{\pi}\theta_2} = e^{i\sqrt{\pi}(\theta_c-\theta_r)}, \quad (60)$$

where the charge channel θ_c is the average phase and θ_r is the relative phase. In fact, θ_r and its vortex, or, dual field ϕ_r, are of the spin quadrupole channel. The bosonic expressions of the pairing and quartetting order parameters are expressed as

$$\Delta_s = \Delta_1 - \Delta_2 \propto e^{i\sqrt{\pi}\theta_c} \cos\sqrt{\pi}\theta_r, \quad Q = \Delta_1\Delta_2 = e^{i2\sqrt{\pi}\theta_c} \cos 2\sqrt{\pi}\phi_r. \tag{61}$$

θ_c is power-law fluctuating, and does not play a role in the transition between quartetting and pairing. It is the relative phase fluctuations that control the transition as described by the sine-Gordon theory,

$$H_{eff} = \frac{1}{2}\left\{(\partial_x\theta_r)^2 + (\partial_x\phi_r)^2\right\} + \frac{1}{2\pi a^2}\left(\lambda_1 \cos 2\sqrt{\pi}\theta_r + \lambda_2 \cos 2\sqrt{\pi}\phi_r\right), \tag{62}$$

which contains cosine terms of both θ_r and ϕ_r.

If $\lambda_1 > \lambda_2$, the relative phase θ_r is pinned leading to the pairing order; otherwise if $\lambda_1 < \lambda_2$, the vortex (dual) field ϕ_r is pinned giving rise to the quartetting order. The transition occurs at $\lambda_1 = \lambda_2$. Equation (62) can be mapped to two free Majorana fermions with masses $m_\pm = |\lambda_1 \pm \lambda_2|$. One channel becomes massless at the transition, which is the Ising critical point.

As a difference between the pairing and quartetting orders, there exist quartet breaking processes of $4 \to 1 + 3 \to 1 + 1 + 2$ and $4 \to 2 + 2$, which can be used to distinguish quartetting and pairing. The vortex lattice configurations are also different for quartetting superfluidity. In the quartetting superfluid, the flux quantization is $hc/(4e)$. Hence, the number of vortices should be doubled compared to those of pairing superfluidity.

3.4. *Color magnetism*

The prominent multi-particle correlations also manifest in the SU(N) quantum antiferromagnetism in the Mott insulating states at $1/N$-filling, i.e., one fermion per site. The superexchange favors the tendency that every N sites form an SU(N) singlet as dubbed "color magnetism" due to its similarity to the SU(3) gauge theory of quantum chromodynamics in which 3 quarks form a color singlet.

In the one-dimensional Sp(4) Heisenberg chain in the fundamental spinor representation, it has been found that the ground state exhibits oscillations at the period of four sites.[58,62] The plaquette tendency was investigated in the SU(4) symmetric Kugel-Khomskii model by diagonalization up to the size of 4×4 sites.[143] The Majumdar-Ghosh model was generalized to the SU(4) case in a ladder system whose ground state is solvable as a direct product state of SU(4) plaquettes.[57] The 4-site SU(4) singlet plaquette wavefunction can be written as

$$\frac{1}{\sqrt{4!}}\epsilon_{\alpha\beta\gamma\delta}\psi^\dagger_\alpha(1)\psi^\dagger_\beta(2)\psi^\dagger_\gamma(3)\psi^\dagger_\delta(4)|\Omega\rangle, \tag{63}$$

which is a 4-particle maximally entangled EPR state.

Consider the SU(4) antiferromagnetism with each site in the fundamental representation in a 3D cubic lattice. We construct the SU(4) resonating plaquette model in 3D in analogous to the Rokhsar-Kivelson quantum dimer model in 2D square lattice.[60,144] There exist three resonant configurations: the left-right, front-back, up-bottom plaquette coverings in a cube as shown in Fig. 8.

The Rokhsar-Kivelson (RK) type Hamiltonian is constructed as[145]:

$$H = -t \sum_{\text{each cube}} \{|A\rangle\langle B| + |B\rangle\langle C| + |B\rangle\langle C| + h.c.\} + V \sum_{\text{each cube}} \{|A\rangle\langle A| + |B\rangle\langle B| + |C\rangle\langle C|\}, \quad (64)$$

where t is assumed to be positive and V is the plaquette flipping amplitude. Similar to the RK point of the quantum dimer model, here at $V/t = 2$, the ground state is the equal weight superposition of all plaquette configurations connected by local flips.[144]

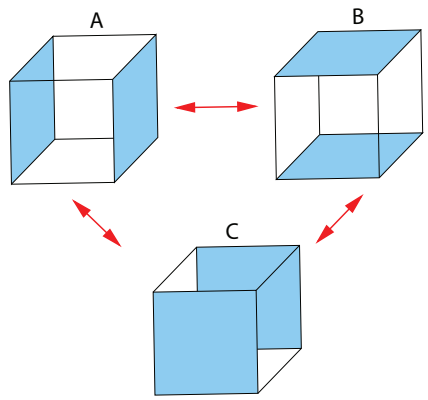

Fig. 8. In the SU(4) Mott-insulator at quarter-filling, i.e., one particle per site in the fundamental representation of SU(4). The superexchange interaction favors four sites of a plaquette form an SU(4) singlet in analogous to the dimer formation in the SU(2) antiferromagnetism. For a 3D cube, there exist three flappable plaquette configurations, based on which a quantum plaquette model can be constructed. It can be described by an effective high-rank gauge theory with conserved electric dipoles instead of charges. From Ref. 60.

The low energy physics of the quantum plaquette model can be mapped to a gauge theory model, actually, it is a high order gauge theory. We assign each face with an integer number n only taking values of 1 and 0: 1 corresponds to that the plaquette is an SU(4) singlet, and otherwise, 0. The "electric field" at site i is defined as a rank-2 symmetric traceless tensor

$$E_{i,\mu\nu} = \eta(i)\left(n_{i+\frac{1}{2}\hat{\mu}+\frac{1}{2}\hat{\nu}} - \frac{1}{2}\right), \quad (65)$$

where $\eta(i) = \pm 1$ marking the sublattice, and $i + \frac{1}{2}\hat{\mu} + \frac{1}{2}\hat{\nu}$ refers to the location of a face center. Since each site can only join one singlet, the sum of n over all the twelve

faces sharing the same site is constrained to be 1, which can be represented as

$$\nabla_x \nabla_y E_{xy} + \nabla_y \nabla_z E_{yz} + \nabla_z \nabla_x E_{zx} = 5\eta(i), \tag{66}$$

where ∇ is the lattice derivative. According to the standard electrodynamics, E is conjugate to the vector potential $A_{i,\mu\nu}$, which is also a rank-2 tensor, as

$$[E_{i,\mu\nu}, A_{j,\rho\sigma}] = i\delta_{ij}(\delta_{\mu\rho}\delta_{\nu\sigma} + \delta_{\mu\sigma}\delta_{\nu\rho}). \tag{67}$$

Since E is like angular momentum taking integer numbers, A should behave as an angular variable $A_{i,\mu\nu} = \eta(i)\,\theta_{i+\frac{1}{2}\hat{\mu}+\frac{1}{2}\hat{\nu}}$, which is compact with the period of 2π. Then

$$[E_{i,\mu\nu}, e^{iA_{j,\nu\sigma}}] = (\delta_{\mu\rho}\delta_{\nu\sigma} + \delta_{\mu\sigma}\delta_{\nu\rho})e^{iA_{j,\nu\sigma}}. \tag{68}$$

With these preparations, the plaquette flipping term in Eq. (64) is represented as

$$H_t = -\,t\left\{\cos(\nabla_z A_{xy} - \nabla_x A_{yz}) + \cos(\nabla_x A_{yz} - \nabla_y A_{zx}) + \cos(\nabla_y A_{zx} - \nabla_z A_{xy})\right\}. \tag{69}$$

The associated gauge invariant transformation is,

$$A_{\mu\nu} \to A_{\mu\nu} + \nabla_\mu \nabla_\nu f, \tag{70}$$

where f an arbitrary scalar function. The corresponding Gauss's law becomes

$$\partial_i \partial_j E_{ij} = \rho. \tag{71}$$

Its physical meaning has recently been revealed in the context of the "fracton" physics, which is a recent focus in the condensed matter community for exotic states of matter and has the potential of applications for topological quantum memory.[146]

3.5. *Half-filled SU(N) Hubbard models: Slater vs. Mott physics*

How interactions drive a partially filled band into an insulating state is an outstanding problem. There exist two basic physical pictures — the Slater physics (Fermi surface nesting) at weak coupling and the Mott physics at strong coupling. For the SU(2) case, the antiferromagnetic (AFM) order increases monotonically and smoothly. No phase transition exists between the Slater and Mott regions.[147–149]

There exist qualitative differences between the Slater and Mott regimes for the two-dimensional SU(N) Hubbard models arising from the enhanced spin and charge fluctuations at $N > 2$. Previous large-N studies in the literature mostly focus on the antiferromagnetic Heisenberg models.[55,150] In contrast, the interplay between charge and spin physics is even more challenging, which could be investigated via the sign-problem free quantum Monte-Carlo (QMC) simulations. The following fermionic SU(N) Hubbard model at half-filling is employed,

$$H = -t\sum_{\langle ij\rangle}\left\{c^\dagger_{i\alpha}c_{j\alpha} + h.c.\right\} + U\sum_i\left(n(i) - \frac{N}{2}\right)^2, \tag{72}$$

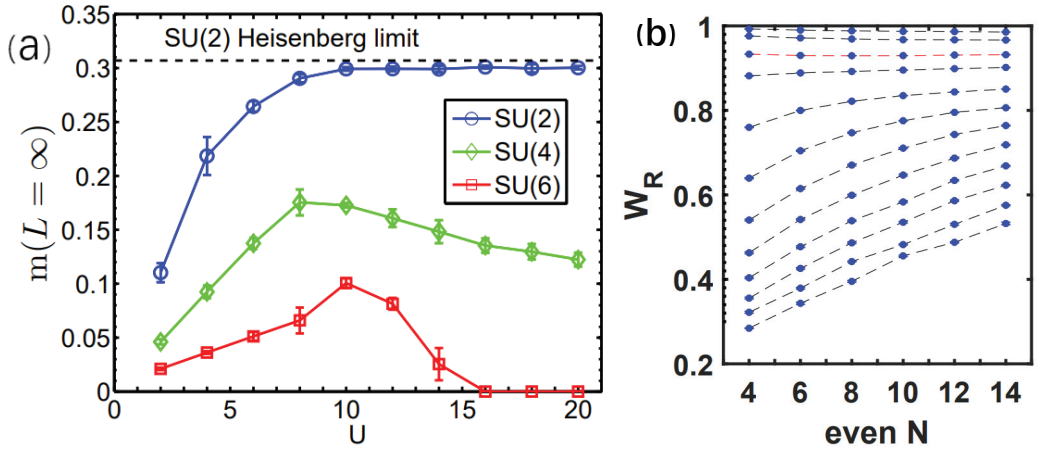

Fig. 9. QMC simulations on SU(N) Hubbard models to reveal how interaction effects scale with fermion component number N. (a) The AFM orders of the SU(N) Hubbard models in the square lattice as varying U and N. The AFM order shows a monotonically increase at $N = 2$ but behaves differently at $N = 4$ and 6. For the latter cases, the AFM orders start to grow and then drop as increasing U. In particular, it is completely suppressed in the SU(6) case at $U > U_c$ at $N = 6$, after which the VBS order appears. This shows a quantum phase transition from the Slater physics to the Mott physics region. (From Ref. 93.) (b) QMC simulations of the relative bandwidth W_R for the 1D SU(N) Hubbard model at half-filling. The results show the convergence between itineracy and locality as $N \to \infty$. The dashed lines shown as a guide from top to bottom correspond to $U/t = 0.5; 1.0; 2.0; 3.0; 5.0; 7.0; 9.0; 11.0; 13.0; 15.0; 17.0; 19.0$, respectively. The cross-over lines with $U/t = 2$ (marked red) separating the weak and strong interaction regions are nearly N-independent. (From Ref. 97.)

where N is an even number. The U-term is written in the particle-hole symmetric form, which pins the average particle number per site at $N/2$, i.e., half-filling.

QMC simulations indicate the fundamental difference between the SU(N) case and SU(2) case as shown in Fig. 9(a) for a square lattice. The AFM orders in both SU(4) and SU(6) cases start to appear at small U in agreement with the Slater physics, where the single-particle gaps are exponentially small. As U further increases, the AFM orders reach the maxima and then decrease. Meanwhile, the single-particle gaps scale linearly with U, marking the onset of Mott physics. For the SU(6) case, the AFM order is completely suppressed at a large value of $U_c \approx 13.3$. Fitting the simulation data shows that the critical exponents of the AFM order with $\nu = 0.60$ and $\eta = 0.44$.[94] At $U > U_c$, the transition to the valence-bond-solid (VBS) state is found, which can be interpreted as the transition from the Slater regime to the Mott regime where the local-moment super-exchange dominates.

How do interaction effects scale with N with fixing the filling level and the interaction U? Sign-problem free QMC simulations have been performed for the half-filled SU(N) Hubbard models in 1D to address this problem.[97] Based on simulation results, we conjecture the existence of a universal interacting state as $N \to \infty$

explained as follows: The relative bandwidth is defined to reflect the correlation strength,

$$W_R(U,N) = E_{k,N}(U)/E_K(0), \tag{73}$$

where $E_{K,N}(U)$ is the kinetic energy per component with the interaction parameter U and component number N, and $E_K(0)$ is that at $U = 0$. Hence $W_R(U = 0, N) = 1$ for the free system, and it becomes 0 in the strong coupling limit at $U = \infty$. At small values of U/t, say $U/t \sim 1$, fermions are nearly itinerant, and correlations manifest through inter-component collisions. Hence, $W_R(U,N)$ decreases monotonically as N increases which enhances the collision possibility resulting in the amplification of correlations. In contrast, at large values of U/t, say, when $U/t > 10$, increasing N softens the Mott insulating background. The kinetic energy gained from virtual hoppings scales as N^2t^2/U, hence, $W_R(U,N)$ increases linearly as increasing N. In the crossover region which lies around $U/t \approx 2$, $W_R(U,N) \approx 0.9$ nearly independent on N. Although the simulation data are still inconclusive, we conjecture that

$$\lim_{N\to\infty}[1 - W_R(U,N)] \approx 0.1, \tag{74}$$

which means an interacting large-N limit. It means that weak and strong interacting systems are driven to a crossover region as $N \to \infty$, but from opposite directions exhibiting a convergence of itinerancy and Mottness. On the other hand, $\lim_{N\to\infty}\lim_{U\to 0}[1 - W_R(U,N)] = 0$. Hence, there exists a singularity at $U \to 0$ and $N \to \infty$. Other physical quantities, including the Fermi distribution, and the spin structure factor, also exhibit nearly N-independent behavior. More analytic and numeric works are needed to further check if there exists a universal strongly interacting limit with vanishing charge gaps as $N \to \infty$, and its possible connection to non-Fermi liquid states.

3.6. *Discussions*

The perspective of high symmetries (SU(N), Sp(N)) brings much richness and novelty to studying large-spin ultracold fermions. The large numbers of spin components render the system in the quantum large-N regime instead of the semi-classical large-S regime. We have reviewed systematically the hidden Sp(4) symmetries in spin-$\frac{3}{2}$ systems, the unification based on the χ-pairing which is an SO(7) generalization of Yang's η-pairing. Quartet superfluidity, quartet density wave state, and plaquette singlet formation in the Mott insulating state exhibit similar features of multi-particle clustering correlations analogous to the color singlet in quantum chromodynamics. Interaction effects as varying the value of N are investigated, which show a tendency of convergence of itinerancy and Mottness as $N \to \infty$.

On the experimental side, there have been significant progresses in the past decade. The SU(6) symmetric ^{173}Yb[77,80] and SU(10) symmetric ^{87}Sr[82] fermion atom systems have been experimentally realized. The nuclear spin, as well as the

electron-orbital degree of freedom, leads to rich physics.[64,65] Various SU(N) symmetric quantum degenerate gases and Mott insulators in optical lattices have been realized.[64,77,78,80–82] As for spin-$\frac{3}{2}$ systems, there are a few candidate atoms ^{132}Cs, ^{9}Be, ^{135}Ba, ^{137}Ba and ^{201}Hg. Considering the rapid developments in this field, we expect that the exotic Sp(4) physics could also be experimentally investigated.

4. Unconventional Magnetism and Spontaneous Spin-Orbit Ordering

In the non-relativistic Fermi liquid theory, spin is an internal symmetry independent of orbital rotations, which rigorously speaking should be denoted as "isospin" instead of spin from the relativistic perspective. In the mechanism of unconventional magnetic transitions, "isospin" develops entanglement with momentum orientation and genuinely becomes the physical spin, hence, it shares the same spirit of "spin-from-isospin" in gauge theories.[151] The consequential states can be viewed as "non-s-wave" generalizations of ferromagnetic metals in which spin no longer polarizes along a unique direction but varies with momentum forming a non-trivial representation of the rotation group.[100,152]

In other words, effective spin-orbit coupling is generated as an order parameter through the Pomeranchuk type of Fermi surface instabilities, which is tunable by external parameters such as temperature and pressure. Furthermore, similar to magnetic fluctuations in ferromagnets, this effective spin-orbit coupling possesses its collective mode dynamics. This gives rise to a conceptually new mechanism to generate spin-orbit coupling dynamically without involving relativity.[99,100] Due to the richness of many-body physics, unconventional magnetism potentially provides a new way to engineer spin-orbit couplings and to control electron spins.

4.1. *Fermi liquid theory and Pomeranchuk instabilities*

In this subsection, we briefly review the concept of the non-relativistic Fermi liquid theory and Pomeranchuk instability.[98]

A large part of our current understanding of interacting electronic systems is based on the Landau Fermi liquid theory, which was designed originally for the normal state ^{3}He and also applies to most metals.[102,153] The central assumption is the existence of the well-defined Fermi surface and fermionic quasi-particles, which exist as long-lived states at very low energies. Interactions among quasi-particles, which are reflected by the forward scattering processes of quasi-particles near the Fermi surface, are described by the Landau interaction functions. The Landau interaction function can be classified into the density (particle-hole singlet) and spin (particle-hole triplet) channels, which are also traditionally denoted as symmetric

(s) and asymmetric (a) channels, respectively,

$$f_{\alpha\beta,\gamma\delta}(\hat{\mathbf{k}}_1,\hat{\mathbf{k}}_2) = f^s(\hat{\mathbf{k}}_1,\hat{\mathbf{k}}_2) + f^a(\hat{\mathbf{k}}_1,\hat{\mathbf{k}}_2)\vec{\sigma}_{\alpha\beta}\cdot\vec{\sigma}_{\gamma\delta}, \tag{75}$$

where $\hat{\mathbf{k}}$ is the direction of quasi-particle momentum close to the Fermi surface. Each of them can be further decomposed into different orbital partial wave channels as

$$f^{s,a}(\hat{\mathbf{k}},\hat{\mathbf{k}}') = \sum_l f_l^{s,a} P_l(\hat{\mathbf{k}}\cdot\hat{\mathbf{k}}') \tag{76}$$

where P_l is the l-th Legendre polynomial and l denotes the orbital angular momentum of the partial wave channel.

In the Landau Fermi liquid theory, the interactions among quasi-particles are captured by a few dimensionless Landau parameters

$$F_l^{s,a} = N_0 f_l^{s,a}, \tag{77}$$

where N_0 is the density of states on the Fermi surface. Physical susceptibility in each channel acquires significant renormalizations by the Landau interactions,

$$\chi_{FL,l}^{s(a)} = \chi_{0,l}\frac{1+F_1^s/3}{1+F_l^{s(a)}/(2l+1)}, \tag{78}$$

where$\chi_{0,l}$ is the susceptibility of free fermi gas. Spin susceptibility lies in the F_0^a channel, and compressibility lies in the F_0^s channel.

Pomeranchuk instabilities refer to a large class of instabilities of Fermi surface distortions in both the density and spin channels.[98] In order for the Fermi surface to be stable, Landau parameters $F_l^{s(a)}$ cannot be too negative. Otherwise, Fermi surface distortions will occur. The Fermi surface could be viewed as an elastic membrane in momentum space. Let us perturb the Fermi surface and expand the energy cost in different partial-wave channels. We arrive at

$$\frac{\Delta E}{V} = \frac{2\pi}{N_0}\sum_{lm}\left\{\left(1+\frac{F_l^{s,a}}{2l+1}\right)|\delta n_{lm}^{s,a}|^2\right\}, \tag{79}$$

where $\delta n_{lm}^{s(a)}$ are amplitudes of Fermi surface distortions in the corresponding partial-wave channels, and V the system volume. The first term is the kinetic energy cost which is always positive, while the second term is the interaction contribution, which can be either positive or negative. When $F_l^{s,a} < -(2l+1)$, the surface tension of the Fermi surface goes negative, and develops instability in the corresponding channels, which is consistent with the divergence of susceptibility in Eq. (78) at $F_l^{s,a} = -(2l+1)$.

The most familiar Pomeranchuk instabilities are found in the s-wave channel, i.e., ferromagnetism at $F_0^a < -1$ and phase separation at $F_0^s < -1$. Pomeranchuk instabilities in non-s-wave wave channels $(l \geq 1)$ have been attracting a great deal of attention.[99,100,154–166] The density channel instabilities result in uniform but

anisotropic liquid (nematic) phases,[167] which have been investigated in the context of doped Mott insulators[168] and high T_c materials.[161] Experimental evidence has also been found in ultra-high mobility two-dimensional electron gases (2DEG) in $Al_xGa_{1-x}As$-GaAs heterostructures and quantum wells in nearly half-filled high Landau levels at very low temperatures,[169,170] and near the metamagnetic transition of the ultra-clean samples of the bilayer ruthenate $Sr_3Ru_2O_7$.[171–173]

Unconventional magnetism corresponds to Pomeranchuk instabilities in the spin channel with $l \geq 1$.[99,100,154,155,163–165] In Ref. 99, these states are classified by the author and Zhang as isotropic and anisotropic phases dubbed β and α-phases, respectively. The α-phases was studied by many groups before: The p-wave phase was first studied by Hirsch[154,155] under the name of the "spin-split" state, and was also proposed by Varma *et al.*[163,164] as a candidate for the hidden order phenomenon in URu_2Si_2; the d-wave phase was studied by Oganesyan *et al.*[167] under the name of "nematic-spin-nematic" phase. Systematic studies of ground state properties and collective excitations in both the anisotropic α and isotropic β-phases have been performed.[100,152] Chubukov and Maslov found that when approaching the ferromagnetic quantum critical point, the p-wave channel spin Pomeranchuk instability develops before the ferromagnetic instability.[174]

4.2. *Unconventional magnetism as multipolar orderings*

The unconventional magnetic order parameters are defined as multipolar parameters in momentum space but not in coordinate space.[99,100] For simplicity, we first take the 2D p-wave case as an example. Its order parameters are the x and y-spatial components of spin-dipole moments defined as

$$\mathbf{n}_1 = \frac{|f_1^a|}{V}\sum_{\mathbf{k}} \mathbf{s}(\mathbf{k})\ \hat{k}_x, \quad \mathbf{n}_2 = \frac{|f_1^a|}{V}\sum_{\mathbf{k}} \mathbf{s}(\mathbf{k})\ \hat{k}_y, \tag{80}$$

where f_1^a is the Landau interaction parameter defined in Eq. (76); $\hat{k}_{x,y} = k_{x,y}/|k|$ are the p-wave angular form factors; $\mathbf{s}(\mathbf{k}) = \langle c^\dagger_{\mathbf{k}\alpha}\vec{\sigma}_{\alpha\beta}c_{\mathbf{k}\beta}\rangle$ is the spin-moment of momentum $\mathbf{k}$, and $\langle\rangle$ means ground state expectation value. Each of $\mathbf{n}_{1,2}$ is a 3-vector in spin space. This is a natural generalization of the ferromagnetic moment $\mathbf{S} = \sum_{\mathbf{k}} \mathbf{s}(\mathbf{k})$ whose s-wave angular form factor is just a constant.

In the anisotropic p-wave α-phase depicted in Fig. 3(C), the order parameter configuration is equivalent to only one of $\mathbf{n}_1$ and $\mathbf{n}_2$ is nonzero, or more generally, $\mathbf{n}_1 \parallel \mathbf{n}_2$. Their orientation in spin space is arbitrary. The order parameter configuration in the p-wave β phase depicted in Fig. 3(B) shows that $\langle n_1^x\rangle = \langle n_2^y\rangle \neq 0$. More generally, this is equivalent to both $\mathbf{n}_{1,2} \neq 0$ and their orientations are perpendicular to each other as $\mathbf{n}_1 \perp \mathbf{n}_2$. Using an optics analogy, the spin configuration over the Fermi surface in the α-phase is linearly polarized, while that in the β-phase is circularly polarized.

This order parameter definition can be easily generalized into other partial wave channels in 2D and 3D systems by using the corresponding multipolar angular form factors. For example, the 2D d-wave channel order parameters can be defined as components of spin-quadrupole moments

$$\mathbf{n}_1^d = \frac{|f_2^a|}{V}\sum_{\mathbf{k}} \mathbf{s}(\mathbf{k})\ \cos 2\phi_{\mathbf{k}}, \quad \mathbf{n}_2^d = \frac{|f_2^a|}{V}\sum_{\mathbf{k}} \mathbf{s}(\mathbf{k})\ \sin 2\phi_{\mathbf{k}}, \tag{81}$$

where ϕ_k is the azimuthal angle of $\mathbf{k}$. We could also combine them as a matrix form $n^{\mu,b}$ with each column representing a 3-vector $\mathbf{n}_b$. Below we will use the matrix and vector forms of order parameters interchangeably.

The 3D counterpart of these expressions can be written in terms of spherical harmonic functions. Hence, in 3D the Latin label b of the order parameter $n^{\mu b}$ take $2l+1$ values, while the Greek index μ still takes x, y, z.

We consider a 2D Fermi-liquid system focusing on a general partial-wave channel-l. Since there is no spin-orbit coupling, the symmetry is the direct product $SO_L(2) \otimes SO_S(3)$, where L and S refer to the orbit and spin channels, respectively. The Landau interaction function f_a^l could depend on the total momentum $\mathbf{q}$ of the particle-hole excitations with the assumption that

$$f(\mathbf{q}) = \frac{f_l^a}{1+\kappa|f_l^a|q^2}, \tag{82}$$

which gives rise to an interaction range $\xi \approx \sqrt{\kappa|f_l^a|}$. Mean-field theory is valid when $\xi \gg d \approx 1/k_F$, where d is the inter-particle distance. After the mean-field decomposition, the mean-field Hamiltonian becomes

$$H_{MF} = \sum_{\mathbf{k}} \psi_\alpha^\dagger(\mathbf{k})\left[\epsilon(\mathbf{k}) - \mu - (\mathbf{n}_1\cos(l\theta_{\mathbf{k}}) + \mathbf{n}_2\sin(l\theta_{\mathbf{k}}))\cdot\vec{\sigma}\right]\psi_\beta(\mathbf{k}) + \frac{|n_1|^2+|n_2|^2}{2|f_l^a|}. \tag{83}$$

The validity of mean-field theory at quantum criticality requires an analysis of quantum fluctuations which are not included in mean-field theory.[175,176]

To determine the ground state configuration of $\vec{n}_{1,2}$, the Ginzburg-Landau (GL) free energy is constructed as,

$$F(\mathbf{n}_1,\mathbf{n}_2) = \gamma_1\partial_a\mathbf{n}_b\cdot\partial_a\mathbf{n}_b + r(\mathbf{n}_1^2+\mathbf{n}_2^2) + v_1[\mathbf{n}_1^2+\mathbf{n}_2^2]^2 + v_2|\mathbf{n}_1\times\mathbf{n}_2|^2. \tag{84}$$

The coefficients r, $v_{1,2}$ are calculated from mean-field free energy in Ref. 100, whose expressions are omitted here.

When $l=1$, a new gradient term can appear which contains the linear order spatial derivative and the cubic order of order parameters as

$$\Delta F(\mathbf{n}_1,\mathbf{n}_2) = \gamma_2\epsilon_{\mu\nu\lambda}n^{\mu a}n^{\nu b}\partial_a n^{\lambda b} = \gamma_2\{(\partial_x\mathbf{n}_2 - \partial_y\mathbf{n}_1)\cdot(\mathbf{n}_1\times\mathbf{n}_2)\}. \tag{85}$$

Such a term is allowed because $\mathbf{n}_{1,2}$ are odd under parity transformation and even under time-reversal transformation, i.e., $P\mathbf{n}_{1,2}P^{-1} = -\mathbf{n}_{1,2}$, and $T\mathbf{n}_{1,2}T^{-1} = \mathbf{n}_{1,2}$. It

does not bring much effect in the normal phase because it is at the cubic order of the order parameter. However, we will see in Sec. 4.4.2, this term becomes important in the ordered p-wave β-phase, which drives a Lifshitz transition spontaneously developing a chiral pitch.

Both α and β-phases are driven by the negative value of r, i.e., $F_l < -2$ in 2D. Whether the ground state takes the β or α-phase depends on the sign of v_2. If $v_2 < 0$, Eq. (84) favors $\mathbf{n}_1 \perp \mathbf{n}_2$, thus gives rise to the β-phase. On the other hand, α-phase appears at $v_2 > 0$, which favors $\mathbf{n}_1 \parallel \mathbf{n}_2$.

4.3. *"Spin from isospin" in non-relativistic systems*

Spin in the relativistic theory, by definition, is part of the generators of the rotation transformation. Hence, it is always coupled to momentum as required by the Lorentz invariance. While in the non-relativistic theory, it decouples from momentum, and becomes an "isospin" type internal degree of freedom. The α and β-phases entangle spin with momentum together via order parameters. In this sense, spin genuinely changes from the status of "isospin" into spin. As we explained before, this effective spin-orbit coupling arises from many-body interaction instead of the single-particle relativistic physics.

In the isotropic β-phase with $l \geq 1$, spin winds around the Fermi surface, exhibiting a vortex-like structure in momentum space. For the 2D p-wave β-phase depicted in Fig. 10(A), its mean-field single particle Hamiltonian reads

$$H_{MF,\beta} = \sum_{\mathbf{k}} \psi^{\dagger}(\mathbf{k}) \Big[\epsilon_0(\mathbf{k}) - \mu - \bar{n}(\hat{k}_x \sigma_x + \hat{k}_y \sigma_y) \Big] \psi(\mathbf{k}), \tag{86}$$

where $|n_1| = |n_2| = \bar{n}$. It exhibits a $\vec{\sigma} \cdot \mathbf{k}$ type spin-orbit coupling, which is called the gyrotropic spin-orbit coupling.[177] The fermion spectrum is isotropic as $\epsilon(\mathbf{k}) = \epsilon_0(\mathbf{k}) \pm \bar{n}$ in the β-phase. Similarly to the ferromagnet, Fermi surfaces in the β-phase split into large and small circles. However, they are characterized by helicity, i.e., the spin projection along its momentum, not by spin polarization.

The symmetry breaking in the β-phases is particularly interesting. The normal Fermi liquid state has both spin and orbital rotational symmetries. The state depicted in Fig. 10(A) is still isotropic where the total angular momentum $\mathbf{J} = \mathbf{L} + \mathbf{S}$ remains conserved although $\mathbf{L}$ and $\mathbf{S}$ are no longer separately conserved. If we fix momentum and only rotate spin, the configuration in Fig. 10(A) changes. In other words, the relative spin-orbit symmetry is broken, a concept first proposed by Leggett in superfluid ^{3}He systems.[102]

In solid state physics, Rashba and Dresselhaus are two familiar spin-orbit couplings whose spin configurations in momentum space are depicted in Figs. 10(B) and 10(C), which corresponds to order parameter configurations of $(\mathbf{n}_1 \parallel \hat{y},\ \mathbf{n}_2 \parallel -\hat{x})$, and $(\mathbf{n}_1 \parallel \hat{x},\ \mathbf{n}_2 \parallel -\hat{y})$, respectively. These two spin-orbit couplings are equivalent to

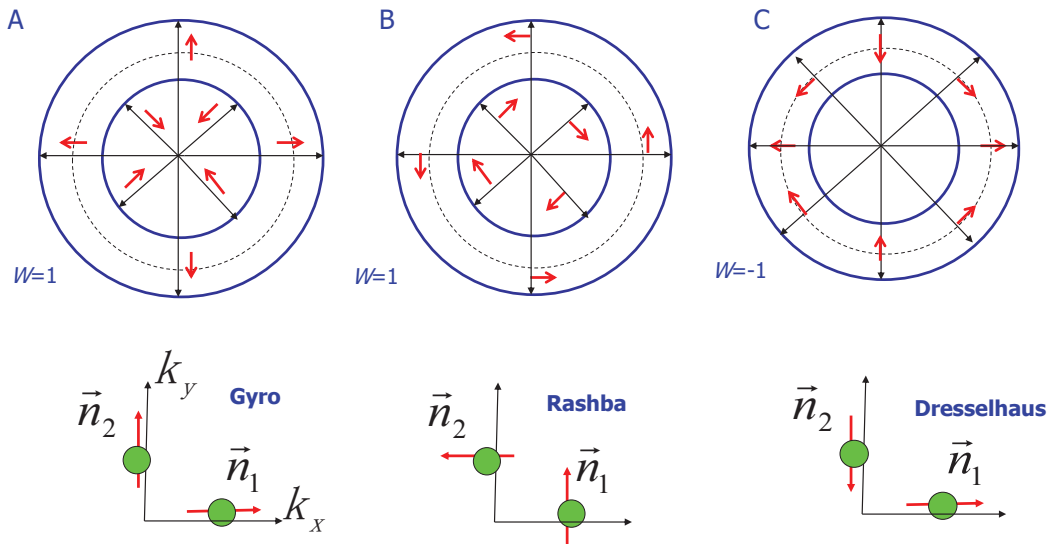

Fig. 10. Spontaneous spin-orbit orderings in the β-phases. Order parameter configurations and the momentum space vortices with the winding numbers $w = \pm 1$. (A) Gyrotropic ($w = 1$), (B) Rashba ($w = 1$), (C) Dresselhaus ($w = -1$). From Ref. 100.

the gyrotropic one in Eq. (86) up to a global spin rotation. Starting from the configuration depicted Fig. 10(A), we can arrive at the Rashba configuration by fixing $\mathbf{k}$ unchanged and rotating electron spin around the z-axis at 90° of each $\mathbf{k}$. Similarly the Dresselhaus configuration can be obtained by the rotation around the x-axis at 180°. These ground state spin configurations exhibit, in momentum space, the vortex structures with the winding numbers $w = \pm 1$. In principle, we can perform an arbitrary spin rotation to obtain all the equivalent states, thus the ground state Goldstone manifold is $[SO_L(2) \otimes SO_S(3)/SO(2)_J = SO(3)$.

This vortex picture in momentum space can be generalized into a general F_l^a channel with the winding numbers $\pm l$. In fact, the generated spin-orbit coupling pattern is beyond the relativity framework. In particular, for even values of l, the dynamic spin-orbit orders break time-reversal symmetry, while the relativistic spin-orbit coupling is time-reversal invariant. The mean-field Hamiltonian $H_{\beta,l}$ for the β-phase in angular momentum channel l can be expressed through a d-vector, defined by $\mathbf{d}(\mathbf{k}) = (\cos(l\theta_{\mathbf{k}}), \sin(l\theta_{\mathbf{k}}), 0)$, as

$$H_{\beta,l} = \sum_{\mathbf{k}} \psi^\dagger(\mathbf{k}) \Big[\epsilon(\mathbf{k}) - \mu - \bar{n}\vec{d}(\theta_{\mathbf{k}}) \cdot \vec{\sigma}) \Big] \psi(\mathbf{k}), \tag{87}$$

where $\mathbf{d}(\theta_{\mathbf{k}})$ is the spin quantization axis for the single particle state at $\mathbf{k}$. Each Fermi surface is characterized by the eigenvalues ± 1 of the helicity operators $\vec{\sigma} \cdot \mathbf{d}(\hat{\mathbf{k}})$.

The mean-field Hamiltonian in the anisotropic α-phase (Fig. 3(C)) can be written as

$$H_{MF,\alpha} = \sum_{\mathbf{k}} \psi^\dagger(\mathbf{k})\{\epsilon_0(\mathbf{k}) - \mu - \bar{n}\hat{k}_x\sigma_z\}\psi(\mathbf{k}). \tag{88}$$

The fermion spectra read $\epsilon(k) = \epsilon_0(k) \pm \bar{n}\hat{k}_x$, and the spin up and down Fermi surfaces shift to left and right, respectively. This configuration is equivalent to the combination of Rashba and Dresselhaus spin-orbit couplings with an equal strength. It is an anisotropic phase in both spin and orbit channels. Generally the Fermi surface shift can along any in-plane direction, and the spin axis can pick any 3D direction, thus the ground state Goldstone manifold is $[SO_L(2)\otimes SO_S(3)]/[SO_S(2)] = SO_L(2) \otimes S_2$.

These β and α-phases are particle-hole channel analogies to the triplet p-wave pairing superfluid ^{3}He-B and A phases, respectively. The order parameters in ^{3}He are defined as x, y and z-spatial components of the dipole-moment of the Cooper pairing amplitude over the Fermi surfaces.[102,178] They are defined as

$$\mathbf{\Delta}_i = \sum_{\mathbf{k}} \mathbf{\Delta}(\mathbf{k})\ \hat{k}_i \quad (i = x, y, z), \tag{89}$$

where $\mathbf{\Delta}(\mathbf{k}) = \langle c^\dagger_\alpha(\mathbf{k})(i\sigma_2\vec{\sigma})_{\alpha\beta}c^\dagger_\beta(-\mathbf{k})\rangle$. Each one of $\mathbf{\Delta}_x, \mathbf{\Delta}_y$ and $\mathbf{\Delta}_z$ is a 3-vector in spin space. In the B-phase, $\mathbf{\Delta}_{x,y,z}$ are perpendicular to each other forming a triad. In the A-phase only two of them are nonzero with a phase difference of $\frac{\pi}{2}$, and they are parallel to each other in spin space. As a result, the B-phase is essentially isotropic with a constant gap over the Fermi surface, while the A-phase is anisotropic with nodes.

From the symmetry point of view, the unconventional magnetic β and α phases exhibit similar properties to the ^{3}He-B and A phases under spatial rotations. The angular form factor of the gap functions in the ^{3}He-B and A phases are very similar to the Fermi surface splittings in the p-wave magnetic β and α-phases, respectively.

4.4. *Collective excitations in unconventional magnetic states*

As a result of spontaneous symmetry breaking, unconventional magnetic states exhibit low energy excitations. In this subsection, we review the Goldstone modes in both α and β-phases. Such modes are absent in the conventional spin-orbit coupling systems.

4.4.1. *Goldstone modes in the α-phase*

We first comment on the stability of the p-wave α-phase. The Ginzburg-Landau energy of Eq. (85) contains a cubic term linear in spatial derivatives. It might induce a linear derivative coupling between the massless Goldstone modes at the quadratic level, leading to a Lifshitz instability in the ground state. However, as

will be shown below, the Goldstone modes in the α-phase share the same index in either the orbital or the spin channel as the condensed mode. Hence, they cannot be coupled together by Eq. (85).

The α-phases break rotational symmetries in both orbital and spin channels, hence, the Goldstone modes can be classified into density and spin channel modes, respectively. Without loss of generality, we assume the ordered configuration as shown in Fig. 3(C),

$$\langle n_{\mu b}\rangle = \bar{n}\delta_{\mu z}\delta_{b1}, \quad \text{i.e.} \quad , \mathbf{n}_1 = \bar{n}\hat{e}_z, \mathbf{n}_2 = 0. \tag{90}$$

In other words, spin configuration is along $\pm\hat{\mathbf{z}}$, and Fermi surface distortion is along the x-axis. Three collective modes are Goldstone modes, including one branch in the density channel, and two branches in the spin channel.

The density channel Goldstone mode is the oscillation of the distorted Fermi surface. It is associated with the field n_2^z,

$$n_2^z(\mathbf{q}) = -\frac{f_1^a(\mathbf{q})}{V}\sum_{\mathbf{k}} \psi^\dagger_{\mathbf{k}+\mathbf{q}}\vec{\sigma}\psi_{\mathbf{k}}k_y, \tag{91}$$

which describes the Fermi surface oscillation in the y-direction while keeping the spin configuration unchanged. Calculations at the random-phase approximation (RPA) level show the effective Lagrangian,

$$L^\alpha_{FS}(\mathbf{q},\omega) = N_0\left[\frac{q\xi^2}{|F_l^a|} - i\frac{\omega}{2v_f q}(1+2\cos 2\phi_q)\right]. \tag{92}$$

This Goldstone mode is overdamped because of the Landau damping, and the damping is anisotropic depending on propagation directions.

The spin channel Goldstone modes $n_{sp,x\pm iy}$ describe spin oscillations while keeping the Fermi surface unchanged, which are spin-dipole precession modes. In contrast, they exhibit nearly isotropic underdamped dispersion relations at small propagating wavevectors with the dispersion relation

$$\omega^2_{x\pm iy} = \frac{\bar{n}^2}{|F_1^a|}(q\xi)^2. \tag{93}$$

Different from spin-waves in the ferromagnets, the dispersion relation here is linear with momentum, which is a consequence of time-reversal symmetry.

4.4.2. *Goldstone modes in the β-phase*

We further study the Goldstone modes in the β-phase. For simplicity, we consider the 3D β-phase with the isotropic ground state exhibiting

$$n^{\mu a} = \bar{n}\delta_{\mu a}. \tag{94}$$

In other words, $\mathbf{n_{1,2,3}}$ form an orthogonal triad. The total angular momentum $\mathbf{J}$ remains conserved, such that fluctuations of $\delta n^{\mu a}$ are classified into eigenstates of $\mathbf{J}$

as $O_{jj_z}(\mathbf{q},\omega)$. $j = 0, 1, 2$ mean the singlet, triplet and quintet channels respectively, and j_z is the SO(2) quantum number rotating around the propagation direction $\mathbf{q}$.

The Goldstone modes belong to the triplet channel ($j = 1$), which are the small relative spin-orbit rotations as

$$O_{1,0}(\mathbf{q},\omega) = \frac{1}{\sqrt{2}}\epsilon_{z\mu a}\delta n^{\mu a}(\mathbf{q},\omega), \quad O_{1,\pm1}(\mathbf{q},\omega) = \frac{1}{2}(\epsilon_{x\mu a} \pm i\epsilon_{y\mu a})\delta n^{\mu a}(\mathbf{q},\omega). \quad (95)$$

The RPA approximation gives the dispersion relations,

$$\omega^2 = 4\bar{n}^2|F_1^a|\left(\frac{\kappa q^2}{N_f} + \frac{j_z|q|x}{18k_f}\right) \qquad \left(x = \frac{\bar{n}}{v_f k_f}, j_z = 0, \pm1\right), \quad (96)$$

which is valid in the low energy regime of $\omega, v_f q \ll \bar{n} \ll v_f k_f$.

The linear dependence on q in the dispersion Eq. (96) is due to the broken parity in the ordered β phase. Consequently, ω^2 becomes negative for the branch with helicity $j_z = -1$ at small q. This means that the uniform ground state in the β-phase is unstable, instead it exhibits a Lifshitz-like instability. This behavior is a general feature in systems with broken parity such as the spiral order in helical magnets, and the cholesteric liquid crystals.[179] The true ground state configuration in the β phase is complicated with the preliminary analysis presented in Ref. 100.

4.4.3. *Resonances in inelastic neutron scattering spectroscopy*

The unconventional magnetic orders are spin-multipole moment in momentum space and cannot couple to neutron magnetic moments statically. Hence, there should be no elastic Bragg peaks. The spin-channel Goldstone modes in the α-phase do not couple to neutron moments directly, either. Nevertheless, they carry spin quantum numbers and thus couple to spin-wave modes dynamically.

Consider the following commutation relations,

$$[S_x, n_1^y] = in_1^z, \quad [S_y, n_1^x] = -in_1^z. \quad (97)$$

In the p-wave α-phase with the configuration given in Eq. (90), n_1^z can be replaced by the constants of $\pm i\bar{n}$. As a result, the Goldstone modes n_1^x and n_1^y become conjugate to spin, and the coupling to spin is developed dynamically.

More formally, we can write down the following coupling Lagrangian,

$$L = (\vec{n}_1 \times \partial_t \vec{n}_1 + \vec{n}_2 \times \partial_t \vec{n}_2) \cdot \vec{S}. \quad (98)$$

In the ordered state of Eq. (90), it is reduced to

$$L = \bar{n}\left(S_y \partial_t n_{1x} - S_x \partial_t n_{1y}\right). \quad (99)$$

The RPA approximation shows that the dynamic spin-spin correlation function behaves as

$$\chi_s(\mathbf{q},\omega) = \langle S_+(\mathbf{q},\omega) S_-(-\mathbf{q},-\omega)\rangle = \frac{N_0 \frac{\omega^2}{\bar{n}^2}}{\frac{\kappa q^2}{N_0} - \frac{2}{|F_1^a|}\frac{\omega^2}{\bar{n}^2} - i\delta}. \quad (100)$$

Hence, it induces a resonance part in the transverse spin wave-excitations. The spectral functions exhibit the δ-peak at the excitation energy of the Goldstone mode,

$$\mathrm{Im}\chi_s(\mathbf{q},\omega) = \kappa\pi v_f^2 \bar{n}^2 q^2 |F_1^a|^2 \delta(\omega^2 - \omega_q^2), \tag{101}$$

which can be detected in the inelastic neutron scattering experiments. This is very similar to the interpretation of the SO(5) theory of the neutron resonance mode: the π-mode lies in the particle-particle channel which decouples from spin in the normal state, but becomes conjugate to spin in the superconducting state giving rise to spin resonances.[29–31]

Such a resonance peak only exhibits in the ordered phase, and vanishes in the disordered phase. As shown in Eq. (99), in the anisotropic α-phases this resonance only occurs in spin-flip channels. Similar analysis can also be performed in the isotropic β-phases, in which the resonances occur in both spin-flip and non-flip channels.[100]

4.5. *Spin-orbit coupled Fermi liquid theory*

So far we have considered the dynamic generation of spin-orbit coupling in non-relativistic Fermi liquid theory. Nevertheless in materials with heavy elements, there does exist the relativistic spin-orbit coupling.

If a system does not exhibit inversion symmetry, the relativistic spin-orbit coupling leads to Fermi surface splitting, say, the Rashba type. In this case, the relativistic spin-orbit coupling behaves like an external field which would round off the unconventional phase transition and pin down a particular spin-orbit ordering configuration. This situation is similar to cooling a magnet below the transition temperature in an external magnetic field.

On the other hand, if a system Hamiltonian still preserves both parity and time-reversal symmetries, the Fermi surface should remain doubly degenerate. Spin-orbit coupling does not manifest itself in the Fermi surface splitting but should exhibit in the Landau Fermi liquid theory. Such a situation also occurs in the presence of prominent magnetic dipolar interactions, which is invariant under simultaneous rotations in both orbital and spin channels, but not under a rotation in either channel. Landau-Fermi liquid theory has been extended to this situation.[177,180]

In the inversion invariant spin-orbit coupled systems, the fermion distribution function is reorganized in the spin-orbit coupled bases as

$$\delta n_{\alpha\alpha'}(\hat{k}) = \sum_{JJ_z;LS} \delta n_{JJ_z;LS}\ Y_{JJ_z;LS}(\hat{k},\alpha\alpha'), \tag{102}$$

where $Y_{JJz;LS}(\hat{k},\alpha\alpha')$ is the spin-orbit coupled spherical harmonic functions

$$Y_{JJz;LS}(\hat{k},\alpha\alpha') = \sum_{ms_z} \langle LmSs_z|JJ_z\rangle Y_{Lm}(\hat{k})\chi_{Ss_z,\alpha\alpha'}, \tag{103}$$

and $\chi_{Ss_z,\alpha\alpha'}$ is the bases for the particle-hole singlet (density) channel and triplet (spin) channel, respectively. The Landau interaction function is generalized to the interaction matrix,

$$\frac{N_0}{4\pi} f_{\alpha\alpha';\beta\beta'}(\hat{k},\hat{k}') = \sum_{JJ_zLL'} Y_{JJz;L1}(\hat{k},\alpha\alpha') F_{JJ_zL1;JJ_zL'1} Y^{\dagger}_{JJz;L'1}(\hat{k},\beta\beta'), \quad (104)$$

where we only keep the particle-hole triplet component. The Landau matrix is diagonal with respect to the total angular momentum J and its z-component J_z, but may have off-diagonal elements with $L \neq L'$. Constrained by the inversion symmetry, $L - L' = 0, 2$.

Similar to the non-relativistic case, when an eigenvalue of the Landau interaction matrix is negatively large, i.e., $\lambda < -1$, it triggers the Pomeranchuk instability in the corresponding channel. For example, the instability in the channel with $J = 1^-$, $L = S = 1$, where " $-$ " means odd parity, generates the 3D analogy of the Rashba spin-orbit coupling,

$$H_{so,1^-} = |n| \sum_k \psi^{\dagger}(\mathbf{k})(\mathbf{k} \times \vec{\sigma}) \cdot \hat{\mathbf{l}} \psi(\mathbf{k}), \quad (105)$$

where $\hat{\mathbf{l}}$ is a 3D unit direction, $|n|$ is the magnitude of the spin-orbit order parameter. The Pomeranchuk instability promotes it to the single particle level by breaking the rotational symmetry and parity.

Let us still use the order parameter $n^{\mu b}$ defined in Sec. 4.2 to represent the order parameters in the sector $L = S = 1$ for a 3D inversion invariant spin-orbit coupled Fermi liquid theory. The 3×3 matrix of n includes three sectors of $J = 0, 1, 2$, which corresponds to pseudo-scalar (gryotropic), vector (Rashba), and tensor (Dresselhaus) type spin-orbit coupling, respectively.

The Ginzburg-Landau free energy can be constructed as $F = F_0 + \Delta F$,

$$\begin{aligned} F_0 &= r_0 \mathrm{tr}\left(n^T n\right) + \beta_1 \left(\mathrm{tr}\left(n^T n\right)\right)^2 + \beta_2 \mathrm{tr}\left(n^T n\right)^2, \\ \Delta F &= \frac{r_1}{3} \left(\mathrm{tr} n\right)^2 + \frac{r_2}{4} \mathrm{tr}\left(n^T - n\right)^2. \end{aligned} \quad (106)$$

Under $SO_L(3)$ and $SO_S(3)$ rotations, n is transformed as $n \to T_S n T_L^{\dagger}$, where $T_{L,S}$ is the rotation matrix in the orbit and spin channels, respectively. F_0 is invariant under independent T_L and T_S, and ΔF is only invariant under simultaneous spin-orbit rotations. The $r_{1,2}$ terms are an analogy to magnetic anisotropy for magnetic phase transitions, which lead to different types of universal classes. Then at the quadratic level, the eigenvalues of the pseudo-scalar, vector, tensor channels are determined by $r_0 + r_1$, $r_0 + r_2$, and r_0, respectively. The actual ordering depends on which eigenvalue is negatively most dominant. If the pseudo-scalar channel instability dominates, the phase transition only breaks parity, which is an Ising type transition without the Goldstone mode. If the vector channel instability dominates, there is also rotational symmetry breaking with the Goldstone manifold S^2. The symmetry

breaking pattern for the tensor ordering channel is more involved, the Goldstone manifold is formally denoted as $SO(3)/G$, where G is the residual symmetry group in the ordered state. The nature of G depends on in which tensor component the symmetry breaking takes place. Nevertheless, when β_2 is included, the situation is complicated, and the analysis of the phase diagram is deferred to another work.

4.6. *Discussions*

We are not aware of conclusive evidence for the existence of the unconventional magnets. Taking into account the great discoveries of the unconventional superconductivity and pairing superfluidity in high T_c cuprates and ^{3}He, respectively, we are optimistic that unconventional magnetic phases also exist in Nature. We propose to systematically search for these new phases in ^{3}He, ultracold atomic systems, semiconductors, heavy fermion materials and ruthenates, both in experiments and in numerical simulations.

Unconventional magnetic orders are natural generalizations of itinerant ferromagnetism, whose driving force is still the exchange interaction. But it needs to be in the non-local version, i.e., a non-s-wave channel. Nevertheless, interactions in the high angular momentum channels are typically weak. In Ref. 181, a heuristic argument is provided to employ the orbital hybridized band structure to promote the Landau interaction to high partial-wave channels. Consider a d_{xz}/d_{yz} hybridized orbital band. Around the Fermi surface, the Bloch wavefunction takes the orbital configuration as

$$|\Psi_\alpha(\mathbf{k})\rangle = e^{i\mathbf{kr}}\left(\cos\phi_k|d_{xz}\rangle + \sin\phi_k|d_{yz}\rangle\right)\otimes\chi_\alpha, \tag{107}$$

where χ_α is the spin eigenstate. The Landau interaction at the Hartree-Fock level is

$$\begin{aligned} f_{\uparrow\uparrow}(\mathbf{k}_1\mathbf{k}_2) &= V(\mathbf{q}=0) - \frac{1}{2}(1+\cos 2\theta_{\mathbf{k}_1\mathbf{k}_2})V(\mathbf{k}_1-\mathbf{k}_2), \\ f_{\uparrow\downarrow}(\mathbf{k}_1\mathbf{k}_2) &= V(\mathbf{q}=0). \end{aligned} \tag{108}$$

The appearance of the d-wave form factor $\cos 2\theta_{\mathbf{k}_1\mathbf{k}_2}$ is due to the orbital hybridization, i.e., even though two electrons possess the same spin, they can still be distinguished by their orbital components. Hence, although $V(\mathbf{k}_1-\mathbf{k}_2)$ could be dominated by the s-wave component, the angular form factor shifts a significant part of the spectral weight into the d-wave channel. Based on this formalism, a possible explanation of the nematic transition observed in $Sr_3Ru_2O_7$ was provided.

Below we summarize several possible directions for searching unconventional magnetism. Ferromagnetic fluctuations in the normal state of ^{3}He are strong. The values of F_{1a} of ^{3}He are measured as negative via the normal-state spin diffusion constant, spin-wave spectrum, and the temperature dependence of the specific heat.[182–185] It varies from around -0.5 to -1.2 with increasing pressures to the

melting point, reasonably close to the instability point $F_1^a = -3$. We conjecture that ^{3}He could support unconventional magnetism under certain conditions or exhibit strong fluctuations of these orders.

An important direction to search for unconventional magnetism is the so-called "hidden-order" systems. Hidden orders typically mean that thermodynamic quantity measurements exhibit a transition to a low temperature ordered state. However, the nature of the orders remains unknown since they do not exhibit themselves in typical detections. Unconventional magnetic orders neither break translation symmetry nor exhibit magnetic orderings in real space. They are multipolar orderings in momentum space, hence, they are difficult to detect via typical experimental methods. Hence, they are natural candidates for hidden orders. In fact, multipolar orderings in real space are also popular candidates for hidden orders in literature.

For example, the well-known system of heavy fermion compound URu_2Si_2 exhibits a mysterious phase transition at 17K by showing a large anomaly in specific heat. It also exhibits a jump in the non-linear magnetic susceptibility at the transition. However, even with efforts after a few decades, the nature of this transition remains elusive.[186,187] Varma proposed an order, which is essentially the p-wave α-phase in our language.[163,164] Calculations for thermodynamic quantities fit in experiment measurements reasonably well. Another hidden order compound $Cd_2Re_2O_7$ exhibits heat capacity anomaly and a kink of DC resistivity around 200K. Recently, it has been discovered that the hidden order phase exhibits inversion symmetry breaking via the optical 2nd harmonic generation measurements.[188,189] Since this is a heavy element compound, Pomeranchuk instabilities of spin-orbit coupled Fermi liquid theory may be a promising candidate.[177,190]

An obstacle to identifying unconventional magnetism is the lack of definitive experimental signatures and detection methods. We know that antiferromagnetism is very common among transition metal oxides, more common than itinerant ferromagnetism. However, the experimental identification of the antiferromagnetic ordering is only possible after the detection method of neutron scattering spectroscopy became available.

Maybe unconventional magnetism already exists somewhere, but we need to think about how to detect them. In addition to the inelastic neutron scattering resonances (Sec. 4.4.3), we outline the following possible methods.

The β phases exhibit effective spin-orbit coupling, hence, standard methods to detect spin-orbit coupling still apply. The distinctive feature is that the spin-orbit coupling effects should turn on and off at a phase transition.

Transport measurements can be used to detect the dynamic generation of spin-orbit coupling. For example, the existence of the anomalous Hall effect (AHE) relies on spin-orbit coupling. Therefore, detecting the AHE signal turning on at a phase transition would be an evidence of the onset of the entanglement of spin and momentum. As for the d-wave α-phase, i.e., spin-$\uparrow$ and spin-$\downarrow$ Fermi surfaces exhibit

opposite quadrupolar distortions. Taking the principal axes of the quadrupolar distortion as x and y-axis, it is straightforward to show that the spin and charge currents satisfy

$$\begin{pmatrix} j_x^{sp} \\ j_y^{sp} \end{pmatrix} \propto \begin{pmatrix} 1 & 0 \\ 0 & -1 \end{pmatrix} \begin{pmatrix} j_x^{c} \\ j_y^{c} \end{pmatrix}. \tag{109}$$

A verification of this transport relation would be a signature of the d-wave α-phase.[100]

Methods that can detect Fermi surface splitting are useful. The angular resolved photon emission spectroscopy (ARPES) can be used to detect the band splitting. In fact, such an experiment has been performed in the system with relativistic spin-orbit coupling. In the unconventional magnetic phases, ARPES in principle can measure temperature-dependent Fermi surface splittings. Fermi surface splitting also shows up in quantum oscillation experiments (e.g. Shubunikov-de Haas (SdH) oscillations) as beat patterns. Hence, a temperature-dependent beat pattern in this kind of experiments would be a signature of the development of unconventional magnetism.

5. Conclusions

We have reviewed a few applications of the symmetry principle in condensed matter and cold atom systems.

First, we reviewed the concept of "space-time" group, which provides a symmetry framework for studying transport and topological properties in a variety of dynamic systems beyond the Floquet framework, such as laser-driven solid state lattices, dynamic photonic crystals, and optical lattices. Various fundamental concepts are generalized, including space-time unit cell, momentum-energy Brillouin zone, Bloch-Floquet theory. Novel nonsymmorphic space-time transformations are identified including time-screw rotation, time-glide reflection, and time-shift rotary reflection. Thirteen space-time groups are classified in 1+1D with 5 of them non-symmorphic, and 275 space-time group are classified in 2+1D. We expect that space-time group will play an important role in studying dynamic systems, in a similar way to space group for static crystals.

Second, we reviewed the progress of studying large-spin ultracold fermions from the perspective of high symmetries. Due to enhanced quantum spin fluctuations from the large number of fermion components, such systems naturally lie in the large-N region instead of the large-S region which is typically studied in solids. A generic Sp(4), or, isomorphically, SO(5) symmetry is proved in spin-$\frac{3}{2}$ systems, which plays a similar role of SU(2) in spin-$\frac{1}{2}$ systems. This symmetry can be upgraded to SO(7) under certain conditions which extends Yang's η-pairing to χ-pairing as its high rank Lie algebra counterpart. The 7D vector and 21D adjoint representations

of SO(7) unify a variety of competing orders in both particle-particle and particle-hole channels. Large-spin systems can exhibit multi-particle clustering orderings or correlations both in the superfluid state with attractions and in the super-exchange physics with repulsions, which is similar to 3-quark baryon (color singlet) formation in high energy physics. The competitions among quartetting superfluidity/density-wave and pairing superfluidity/density-wave are investigated. The SU(4) singlet plaquette states in a 3D cubic lattice can be described by a quantum plaquette model, whose effective description is mapped to a high order gauge theory. We anticipate that research along this direction can bridge cold atom physics, condensed matter, and high energy physics together. Along with the experimental progress, even more exotic strong coupling physics that is not easily accessible in usual solid state systems could be investigated.

At last, we reviewed the unconventional magnetism as a mechanism of "spin from isospin" to generate spin-orbit coupling in non-relativistic Fermi liquids. They are also novel states of itinerant electrons generalizing ferromagnetism to unconventional symmetries based on the Fermi surface instabilities of the Pomeranchuk type. These states include the isotropic β-phase and the anisotropic α-phase, which are the particle-hole channel analogy to the superfluid ^{3}He-B and A phases, respectively. Different from the relativistic spin-orbit coupling, these dynamically generated spin-orbit couplings possess collective excitations of Goldstone modes, whose dynamics couple to spin moment and induce resonances in the inelastic neutron scattering spectroscopy. Possible realizations of "unconventional magnetism" in hidden order systems and experimental detections are discussed.

Acknowledgments

I am grateful to my Ph.D. advisor, S. C. Zhang (deceased), who convinced me of the beauty and the power of symmetry. The last two topics reviewed here were started in my Ph.D. period and were continued with various new developments in my career. I thank Jiangping Hu, E. H. Fradkin, K. Sun, D. Arovas, W. C. Lee, H. H. Hung, Shu Chen, Yupeng Wang, C. K. Xu, Y. Li, D. Wang, S. L. Xu, Z. Q. Gao, Z. M. Pan, C. H. Ke, Z. X. Lin for collaborations on related topics, and J. E. Hirsch, A. L. Fetter, T. L. Ho, S. Das Sarma, S. Kivelson, L. J. Sham for their warm encouragements and appreciations. I also thank Ji Wang for proofreading and polishing. This work is supported by NSFC under the Grants No. 11729402 and No. 12174317.

References

1. T. D. Lee and C. N. Yang, Question of parity conservation in weak interactions, *Phys. Rev.* **104**, 254–258 (Oct, 1956). doi: 10.1103/PhysRev.104.254. URL `https://link.aps.org/doi/10.1103/PhysRev.104.254`.

2. C. N. Yang and R. L. Mills, Conservation of isotopic spin and isotopic gauge invariance, *Phys. Rev.* **96**, 191–195 (Oct, 1954). doi: 10.1103/PhysRev.96.191. URL https://link.aps.org/doi/10.1103/PhysRev.96.191.
3. C. N. Yang, Some exact results for the many-body problem in one dimension with repulsive delta-function interaction, *Phys. Rev. Lett.* **19**, 1312–1315 (Dec, 1967). doi: 10.1103/PhysRevLett.19.1312. URL https://link.aps.org/doi/10.1103/PhysRevLett.19.1312.
4. T. T. Wu and C. N. Yang, Concept of nonintegrable phase factors and global formulation of gauge fields, *Phys. Rev. D.* **12**, 3845–3857 (Dec, 1975). doi: 10.1103/PhysRevD.12.3845. URL https://link.aps.org/doi/10.1103/PhysRevD.12.3845.
5. T. T. Wu and C. N. Yang, Dirac monopole without strings:monopole harmonics, *Nucl. Phys. B.* **107**, 365 (1976).
6. H. Weyl, *Symmetry.* (Princeton University Press; Reprint edition, 2016).
7. D. J. Gross, The role of symmetry in fundamental physics, *Proceedings of the National Academy of Sciences.* **93**(25), 14256–14259 (1996). ISSN 0027-8424. doi: 10.1073/pnas.93.25.14256. URL https://www.pnas.org/content/93/25/14256.
8. C. N. Yang, Symmetry and physics, *Proceedings of the American Philosophical Society.* **140**, 267 (1996).
9. M. Lax, *Symmetry Principles in Solid State and Molecular Physics.* (Dover Publications, 2012).
10. H. Georgi, *Lie Algebras In Particle Physics: from Isospin To Unified Theories.* (CRC Press; 1st edition, 1999).
11. E. Noether, Invariante variationsprobleme, *Nachrichten von der Gesellschaft der Wissenschaften zu Göttingen, Mathematisch-Physikalische Klasse.* **1918**, 235–257 (1918). URL http://eudml.org/doc/59024.
12. E. P. Wigner, *Group Theory and its Application to the Quantum Mechanics of Atomic Spectra.* (Academic Press, New York, 1959).
13. H. Weyl, *The Theory of Groups and Quantum Mechanics.* (Dover, New York, 1950).
14. V. Fock, On the theory of the hydrogen atom, *Z. Phys.* **98**, 145 (1935).
15. J. J. Sakrai and J. J. Napolitano, *Modern Quantum Mechanics.* (Pearson, 2010).
16. S. Glashow, The renormalizability of vector meson interactions, *Nucl. Phys. B.* **10**, 107 (1959).
17. A. Salam and J. C. Ward, Weak and electromagnetic interactions, *Nuovo Cimento.* **11**, 568–577 (1959).
18. S. Weinberg, A model of leptons, *Phys. Rev. Lett.* **19**, 1264–1266 (Nov, 1967). doi: 10.1103/PhysRevLett.19.1264. URL https://link.aps.org/doi/10.1103/PhysRevLett.19.1264.
19. M. Peskin and D. Schroeder, *An Introduction To Quantum Field Theory.* Frontiers in Physics, (Avalon Publishing, 1995). ISBN 9780813345437. URL https://books.google.com.hk/books?id=EVeNNcslvX0C.
20. L. D. Landau, On the theory of phase transition, *Zh. Eksp. Teor. Fiz.* **7**, 19–32 (1937).
21. V. L. Ginzburg and L. D. Landau, *Zh. Eksp. Teor. Fiz.* **20**, 1064 (1950).
22. L. D. Landau and E. Lifshitz, *Statistical Physics.* (Butterworth-Heinemann; 3rd edition, 1980).
23. J. Goldstone, A. Salam, and S. Weinberg, Broken symmetries, *Phys. Rev.* **127**, 965–970 (Aug, 1962). doi: 10.1103/PhysRev.127.965. URL http://link.aps.org/doi/10.1103/PhysRev.127.965.
24. P. W. Anderson, Plasmons, gauge invariance, and mass, *Phys. Rev.* **130**, 439–442 (Apr, 1963). doi: 10.1103/PhysRev.130.439. URL https://link.aps.org/doi/10.1103/PhysRev.130.439.
25. P. W. Higgs, Broken symmetries and the masses of gauge bosons, *Phys. Rev. Lett.* **13**, 508–509 (Oct, 1964). doi: 10.1103/PhysRevLett.13.508. URL https://link.aps.org/doi/10.1103/PhysRevLett.13.508.
26. C. N. Yang, Eta-pairing and off-diagonal long-range order in a hubbard-model, *Phys. Rev. Lett.* **63**(19), 2144–2147 (1989).

27. C. N. Yang and S. Zhang, So4 symmetry in a hubbard model, *Modern Physics Letters B.* **04**(11), 759–766 (1990). doi: 10.1142/S0217984990000933. URL http://www.worldscientific.com/doi/abs/10.1142/S0217984990000933.
28. S. C. Zhang, So-4 symmetry of the hubbard-model and its experimental consequences, *International Journal of Modern Physics B.* **5**(1–2), 153–167 (1991).
29. S. C. Zhang, A unified theory based on so(5) symmetry of superconductivity and antiferromagnetism, *Science.* **275**(5303), 1089–1096 (1997).
30. E. Demler, W. Hanke, and S.-C. Zhang, $SO(5)$ theory of antiferromagnetism and superconductivity, *Rev. Mod. Phys.* **76**, 909–974 (Nov, 2004). doi: 10.1103/RevModPhys.76.909. URL http://link.aps.org/doi/10.1103/RevModPhys.76.909.
31. E. Demler and S. C. Zhang, Theory of the resonant neutron-scattering of high-t-c superconductors, *Phys. Rev. Lett.* **75**(22), 4126–4129 (1995).
32. C. Kittel, *Quantum theory of Solids.* (Wiley, New York, 1987).
33. Y. H. Wang, H. Steinberg, P. Jarillo-Herrero, and N. Gedik, Observation of floquet-bloch states on the surface of a topological insulator, *Science.* **342**, 453 (2013). doi: 10.1126/science.1239834. URL http://dx.doi.org/10.1126/science.1239834.
34. H. Zhu, J. Yi, M.-Y. Li, J. Xiao, L. Zhang, C.-W. Yang, R. A. Kaindl, L.-J. Li, Y. Wang, and X. Zhang, Observation of chiral phonons, *Science.* **359**, 579–582 (2018).
35. C. V. Parker, L.-C. Ha, and C. Chin, Direct observation of effective ferromagnetic domains of cold atoms in a shaken optical lattice, *Nature Physics.* **9**(12):769C774 (Oct, 2013). ISSN 1745-2481. doi: 10.1038/nphys2789. URL http://dx.doi.org/10.1038/nphys2789.
36. B. M. Anderson, L. W. Clark, J. Crawford, A. Glatz, I. S. Aranson, P. Scherpelz, L. Feng, C. Chin, and K. Levin, Direct lattice shaking of bose condensates: Finite momentum superfluids, *Physical Review Letters.* **118**(22) (May, 2017). ISSN 1079-7114. doi: 10.1103/physrevlett.118.220401. URL http://dx.doi.org/10.1103/PhysRevLett.118.220401.
37. M. C. Rechtsman, J. M. Zeuner, Y. Plotnik, Y. Lumer, D. Podolsky, F. Dreisow, S. Nolte, M. Segev, and A. Szameit, Photonic Floquet topological insulators, *Nature.* **496**(7444), 196–200 (Apr, 2013). doi: 10.1038/nature12066. URL http://www.nature.com/doifinder/10.1038/nature12066.
38. M. S. Rudner, N. H. Lindner, E. Berg, and M. Levin, Anomalous Edge States and the Bulk-Edge Correspondence for Periodically Driven Two-Dimensional Systems, *Phys. Rev. X.* **3**(3), 031005 (Jul, 2013). doi: 10.1103/PhysRevX.3.031005. URL http://link.aps.org/doi/10.1103/PhysRevX.3.031005http://arxiv.org/abs/1212.3324.
39. M. Thakurathi, A. A. Patel, D. Sen, and A. Dutta, Floquet generation of Majorana end modes and topological invariants, *Phys. Rev. B - Condens. Matter Mater. Phys.* **88**(15), 155133 (Oct, 2013). doi: 10.1103/PhysRevB.88.155133. URL http://link.aps.org/doi/10.1103/PhysRevB.88.155133.
40. C. W. von Keyserlingk and S. L. Sondhi, Phase structure of one-dimensional interacting Floquet systems. II. Symmetry-broken phases, *Phys. Rev. B.* **93**(24), 245146 (Jun, 2016). doi: 10.1103/PhysRevB.93.245146. URL http://link.aps.org/doi/10.1103/PhysRevB.93.245146http://arxiv.org/abs/1602.06949.
41. Z. Gu, H. A. Fertig, D. P. Arovas, and A. Auerbach, Floquet spectrum and transport through an irradiated graphene ribbon, *Phys. Rev. Lett.* **107**(21), 216601 (Nov, 2011). doi: 10.1103/PhysRevLett.107.216601. URL http://link.aps.org/doi/10.1103/PhysRevLett.107.216601.
42. N. H. Lindner, G. Refael, and V. Galitski, Floquet topological insulator in semiconductor quantum wells, *Nat. Phys.* **7**(6), 490–495 (Jun, 2011). doi: 10.1038/nphys1926. URL http://www.nature.com/doifinder/10.1038/nphys1926http://www.scopus.com/inward/record.url?eid=2-s2.0-79957997633{&}partnerID=40{&}md5=f9e8aa1ba80c5360bd40c535b60b48a4.
43. D. V. Else, B. Bauer, and C. Nayak, Floquet time crystals, *Phys. Rev. Lett.* **117**, 090402 (Aug, 2016). doi: 10.1103/PhysRevLett.117.090402. URL https://link.aps.org/doi/10.1103/PhysRevLett.117.090402.

44. C. W. Von Keyserlingk and S. L. Sondhi, Phase structure of one-dimensional interacting Floquet systems. I. Abelian symmetry-protected topological phases, *Phys. Rev. B - Condens. Matter Mater. Phys.* **93**(24), 245145 (Jun, 2016). doi: 10.1103/PhysRevB.93.245145. URL http://link.aps.org/doi/10.1103/PhysRevB.93.245145.
45. A. C. Potter, T. Morimoto, and A. Vishwanath, Classification of Interacting Topological Floquet Phases in One Dimension, *Phys. Rev. X.* **6**(4), 041001 (Oct, 2016). doi: 10.1103/PhysRevX.6.041001. URL http://arxiv.org/abs/1602.05194{%}5Cnhttp://link.aps.org/doi/10.1103/PhysRevX.6.041001http://arxiv.org/abs/1602.05194http://link.aps.org/doi/10.1103/PhysRevX.6.041001.
46. R. Roy and F. Harper, Periodic Table for Floquet Topological Insulators, *arXiv:1603.06944* (Mar, 2016). URL http://arxiv.org/abs/1603.06944.
47. F. Nathan and M. S. Rudner, Topological singularities and the general classification of Floquet-Bloch systems, *New J. Phys.* **17**(12), 125014 (Dec, 2015). doi: 10.1088/1367-2630/17/12/125014. URL http://stacks.iop.org/1367-2630/17/i=12/a=125014?key=crossref.e03409effca05918e53129bbc45df3d4.
48. N. Fläschner, B. S. Rem, M. Tarnowski, D. Vogel, D.-S. Lühmann, K. Sengstock, and C. Weitenberg, Experimental reconstruction of the Berry curvature in a topological Bloch band, *1509.05763.* **05882**(2015), 1–8 (2015). doi: 10.1126/science.aad4568. URL http://arxiv.org/abs/1509.05763.
49. S. Xu and C. Wu, Space-time crystal and space-time group, *Phys. Rev. Lett.* **120**, 096401 (Feb, 2018). doi: 10.1103/PhysRevLett.120.096401. URL https://link.aps.org/doi/10.1103/PhysRevLett.120.096401.
50. T. Morimoto, H. C. Po, and A. Vishwanath, Floquet topological phases protected by time glide symmetry, *Phys. Rev. B.* **95**, 195155 (May, 2017). doi: 10.1103/PhysRevB.95.195155. URL https://link.aps.org/doi/10.1103/PhysRevB.95.195155.
51. Congjun Wu. Exotic many-body physics with large-spin fermi gases. Physics, 3:92, Nov. 2010. URL https://physics.aps.org/articles/v3/92.
52. I. Affleck, Large-n limit of SU(n) quantum "spin" chains, *Phys. Rev. Lett.* **54**, 966–969 (Mar, 1985). doi: 10.1103/PhysRevLett.54.966. URL http://link.aps.org/doi/10.1103/PhysRevLett.54.966.
53. D. P. Arovas and A. Auerbach, Functional integral theories of low-dimensional quantum heisenberg models, *Phys. Rev. B.* **38**, 16–332 (Jul, 1988). doi: 10.1103/PhysRevB.38.316. URL http://link.aps.org/doi/10.1103/PhysRevB.38.316.
54. I. Affleck and J. B. Marston, Large-n limit of the heisenberg-hubbard model: Implications for high-T_c superconductors, *Phys. Rev. B.* **37**, 3774–3777 (Mar, 1988). doi: 10.1103/PhysRevB.37.3774. URL http://link.aps.org/doi/10.1103/PhysRevB.37.3774.
55. N. Read and S. Sachdev, Spin-peierls, valence-bond solid, and néel ground states of low-dimensional quantum antiferromagnets, *Phys. Rev. B.* **42**, 4568–4589 (Sep, 1990). doi: 10.1103/PhysRevB.42.4568. URL http://link.aps.org/doi/10.1103/PhysRevB.42.4568.
56. C. Wu, J.-P. Hu, and S.-C. Zhang, Exact so(5) symmetry in the spin-3/2 fermionic system, *Phys. Rev. Lett.* **91**, 186402 (Oct, 2003). doi: 10.1103/PhysRevLett.91.186402. URL http://link.aps.org/doi/10.1103/PhysRevLett.91.186402.
57. S. Chen, C. Wu, S.-C. Zhang, and Y. Wang, Exact spontaneous plaquette ground states for high-spin ladder models, *Phys. Rev. B.* **72**, 214428 (Dec, 2005). doi: 10.1103/PhysRevB.72.214428. URL http://link.aps.org/doi/10.1103/PhysRevB.72.214428.
58. C. Wu, Competing orders in one-dimensional spin-3/2 fermionic systems, *Phys. Rev. Lett.* **95**, 266404 (Dec, 2005). doi: 10.1103/PhysRevLett.95.266404. URL http://link.aps.org/doi/10.1103/PhysRevLett.95.266404.
59. C. Wu, Hidden Symmetry and Quantum Phases in SPIN-3/2 Cold Atomic Systems, *Modern Physics Letters B.* **20**, 1707–1738 (2006). doi: 10.1142/S0217984906012213.
60. C. Xu and C. Wu, Resonating plaquette phases in su(4) heisenberg antiferromagnet, *Phys. Rev. B.* **77**, 134449 (Apr, 2008). doi: 10.1103/PhysRevB.77.134449. URL http://link.aps.org/doi/10.1103/PhysRevB.77.134449.

61. C. Wu, J. Hu, and S.-C. Zhang, Quintet pairing and non-abelian vortex string in spin-3/2 cold atomic systems, *International Journal of Modern Physics B.* **24**(03), 311–322 (2010). doi: 10.1142/S0217979210054968. URL http://www.worldscientific.com/doi/abs/10.1142/S0217979210054968.
62. H.-H. Hung, Y. Wang, and C. Wu, Quantum magnetism in ultracold alkali and alkaline-earth fermion systems with symplectic symmetry, *Phys. Rev. B.* **84**, 054406 (Aug, 2011). doi: 10.1103/PhysRevB.84.054406. URL http://link.aps.org/doi/10.1103/PhysRevB.84.054406.
63. Z.-Q. Gao and C. Wu, Exceptional symmetry of g_2 in spin-$\frac{3}{2}$ fermion systems (2020).
64. A. V. Gorshkov, M. Hermele, V. Gurarie, C. Xu, P. S. Julienne, J. Ye, P. Zoller, E. Demler, M. D. Lukin, and A. M. Rey, Two-orbital su(n) magnetism with ultracold alkaline-earth atoms, *Nat. Phys.* **6**(4), 289–295 (Apr, 2010). ISSN 1745-2473. URL http://dx.doi.org/10.1038/nphys1535.
65. M. Hermele, V. Gurarie, and A. M. Rey, Mott insulators of ultracold fermionic alkaline Earth atoms: Underconstrained magnetism and chiral spin liquid, *Phys. Rev. Lett.* **103**(13), 135301 (Sep, 2009). ISSN 0031-9007. doi: 10.1103/PhysRevLett.103.135301. URL http://journals.aps.org/prl/abstract/10.1103/PhysRevLett.103.135301.
66. C. Xu, Liquids in multiorbital SU(n) magnets made up of ultracold alkaline-earth atoms, *Phys. Rev. B.* **81**, 144431 (Apr, 2010). doi: 10.1103/PhysRevB.81.144431. URL http://link.aps.org/doi/10.1103/PhysRevB.81.144431.
67. M. A. Cazalilla, A. F. Ho, and M. Ueda, Ultracold gases of ytterbium: Ferromagnetism and mott states in an su(6) fermi system, *New Journal of Physics.* **11**(10), 103033 (2009). URL http://stacks.iop.org/1367-2630/11/i=10/a=103033.
68. D. Controzzi and A. M. Tsvelik, Exactly solvable model for isospin s = 3/2 fermionic atoms on an optical lattice, *Phys. Rev. Lett.* **96**, 097205 (Mar, 2006). doi: 10.1103/PhysRevLett.96.097205. URL http://link.aps.org/doi/10.1103/PhysRevLett.96.097205.
69. P. Lecheminant, E. Boulat, and P. Azaria, Confinement and superfluidity in one-dimensional degenerate fermionic cold atoms, *Phys. Rev. Lett.* **95**, 240402 (Dec, 2005). doi: 10.1103/PhysRevLett.95.240402. URL http://link.aps.org/doi/10.1103/PhysRevLett.95.240402.
70. K. Hattori, Critical nature of non-fermi liquid in spin 3/2 multipolar kondo model, *Journal of the Physical Society of Japan.* **74**(12), 3135–3138 (2005). doi: 10.1143/JPSJ.74.3135. URL http://jpsj.ipap.jp/link?JPSJ/74/3135/.
71. H.-H. Tu, G.-M. Zhang, and L. Yu, Spin-quadrupole ordering of spin-$\frac{3}{2}$ ultracold fermionic atoms in optical lattices in the one-band hubbard model, *Phys. Rev. B.* **74**, 174404 (Nov, 2006). doi: 10.1103/PhysRevB.74.174404. URL http://link.aps.org/doi/10.1103/PhysRevB.74.174404.
72. H.-H. Tu, G.-M. Zhang, and L. Yu, Mott insulating phases and quantum phase transitions of interacting spin-$\frac{3}{2}$ fermionic cold atoms in optical lattices at half filling, *Phys. Rev. B.* **76**, 014438 (Jul, 2007). doi: 10.1103/PhysRevB.76.014438. URL http://link.aps.org/doi/10.1103/PhysRevB.76.014438.
73. S. Östlund, T. H. Hansson, and A. Karlhede, Properties of the doped spin-$\frac{3}{2}$ mott insulator near half filling, *Phys. Rev. B.* **71**, 165121 (Apr, 2005). doi: 10.1103/PhysRevB.71.165121. URL http://link.aps.org/doi/10.1103/PhysRevB.71.165121.
74. M. Bartenstein, A. Altmeyer, S. Riedl, R. Geursen, S. Jochim, C. Chin, J. H. Denschlag, R. Grimm, A. Simoni, E. Tiesinga, C. J. Williams, and P. S. Julienne, Precise determination of ^{6}Li cold collision parameters by radio-frequency spectroscopy on weakly bound molecules, *Phys. Rev. Lett.* **94**, 103201 (Mar, 2005). doi: 10.1103/PhysRevLett.94.103201. URL http://link.aps.org/doi/10.1103/PhysRevLett.94.103201.
75. A. Rapp, G. Zaránd, C. Honerkamp, and W. Hofstetter, Color superfluidity and "baryon" formation in ultracold fermions, *Phys. Rev. Lett.* **98**, 160405 (Apr, 2007). doi: 10.1103/PhysRevLett.98.160405. URL http://link.aps.org/doi/10.1103/PhysRevLett.98.160405.
76. Á. Rapp, W. Hofstetter, and G. Zaránd, Trionic phase of ultracold fermions in an optical lattice: A variational study, *Phys. Rev. B.* **77**(14):144520 (Apr, 2008). doi: 10.1103/PhysRevB.77.144520.

77. S. Taie, Y. Takasu, S. Sugawa, R. Yamazaki, T. Tsujimoto, R. Murakami, and Y. Takahashi, Realization of a SU(2)×SU(6) system of fermions in a cold atomic gas, *Phys. Rev. Lett.* **105**, 190401 (Nov, 2010). doi: 10.1103/PhysRevLett.105.190401. URL http://link.aps.org/doi/10.1103/PhysRevLett.105.190401.
78. S. Taie, R. Yamazaki, S. Sugawa, and Y. Takahashi, An su(6) mott insulator of an atomic fermi gas realized by large-spin pomeranchuk cooling, *Nat. Phys.* **8**(11), 825–830 (Nov, 2012). ISSN 1745-2473. URL http://dx.doi.org/10.1038/nphys2430.
79. S. Sugawa, K. Inaba, S. Taie, R. Yamazaki, M. Yamashita, and Y. Takahashi, Interaction and filling-induced quantum phases of dual Mott insulators of bosons and fermions, *Nature Physics.* **7**, 642–648 (Aug, 2011). doi: 10.1038/nphys2028.
80. H. Hara, Y. Takasu, Y. Yamaoka, J. M. Doyle, and Y. Takahashi, Quantum degenerate mixtures of alkali and alkaline-earth-like atoms, *Phys. Rev. Lett.* **106**, 205304 (May, 2011). doi: 10.1103/PhysRevLett.106.205304. URL http://link.aps.org/doi/10.1103/PhysRevLett.106.205304.
81. G. Pagano, M. Mancini, G. Cappellini, P. Lombardi, F. Schfer, H. Hu, X.-J. Liu, J. Catani, C. Sias, M. Inguscio, and L. Fallani, A one-dimensional liquid of fermions with tunable spin, *Nature Physics.* **10**(3), 198C201 (Feb, 2014). ISSN 1745-2481. doi: 10.1038/nphys2878. URL http://dx.doi.org/10.1038/nphys2878.
82. B. J. DeSalvo, M. Yan, P. G. Mickelson, Y. N. Martinez de Escobar, and T. C. Killian, Degenerate fermi gas of ^{87}Sr, *Phys. Rev. Lett.* **105**, 030402 (Jul, 2010). doi: 10.1103/PhysRevLett.105.030402. URL http://link.aps.org/doi/10.1103/PhysRevLett.105.030402.
83. P. G. Mickelson, Y. N. Martinez de Escobar, M. Yan, B. J. Desalvo, and T. C. Killian, Bose-Einstein condensation of Sr88 through sympathetic cooling with Sr87, *Phys. Rev. A.* **81**(5):051601 (May, 2010). doi: 10.1103/PhysRevA.81.051601.
84. J. Heinze, J. S. Krauser, N. Fläschner, K. Sengstock, C. Becker, U. Ebling, A. Eckardt, and M. Lewenstein, Engineering spin waves in a high-spin ultracold Fermi gas, *ArXiv e-prints* (Feb, 2013).
85. J. S. Krauser, J. Heinze, N. Flaschner, S. Gotze, O. Jurgensen, D.-S. Luhmann, C. Becker, and K. Sengstock, Coherent multi-flavour spin dynamics in a fermionic quantum gas, *Nat. Phys.* **8**(11), 813–818 (Nov, 2012). ISSN 1745-2473. URL http://dx.doi.org/10.1038/nphys2409.
86. M. Bishof, M. J. Martin, M. D. Swallows, C. Benko, Y. Lin, G. Quéméner, A. M. Rey, and J. Ye, Inelastic collisions and density-dependent excitation suppression in a ^{87}Sr optical lattice clock, *Phys. Rev. A.* 84(5):052716 (Nov, 2011). doi: 10.1103/PhysRevA.84.052716.
87. M. Bishof, Y. Lin, M. D. Swallows, A. V. Gorshkov, J. Ye, and A. M. Rey, Resolved Atomic Interaction Sidebands in an Optical Clock Transition, *Physical Review Letters.* 106(25):250801 (Jun, 2011). doi: 10.1103/PhysRevLett.106.250801.
88. M. J. Martin, M. Bishof, M. D. Swallows, X. Zhang, C. Benko, J. von-Stecher, A. V. Gorshkov, A. M. Rey, and J. Ye, A quantum many-body spin system in an optical lattice clock, *ArXiv e-prints* (Dec, 2012).
89. C. Wu, Exotic many-body physics with large-spin fermi gases, *Physics.* **3**, 92 (Nov, 2010). doi: 10.1103/Physics.3.92. URL http://link.aps.org/doi/10.1103/Physics.3.92.
90. C. Wu, Quantum gases: Mott made easy, *Nat. Phys.* **8**(11), 784–785 (Nov, 2012). ISSN 1745-2473. URL http://dx.doi.org/10.1038/nphys2432.
91. P. Schlottmann, Ground-state and elemental excitations of the one-dimensional multicomponent fermi gas with delta-function interaction, *Journal of Physics: Condensed Matter.* **6**(7), 1359 (1994). URL http://stacks.iop.org/0953-8984/6/i=7/a=008.
92. A. S. Stepanenko and J. M. F. Gunn, 'Baryonic' bound-state instability in trapped fermionic atoms, *eprint arXiv:cond-mat/9901317* (Jan, 1999).
93. D. Wang, Y. Li, Z. Cai, Z. Zhou, Y. Wang, and C. Wu, Competing Orders in the 2D Half-Filled SU(2N) Hubbard Model through the Pinning-Field Quantum Monte Carlo Simulations, *Phys. Rev. Lett.* **112**(15), 156403 (Apr, 2014). ISSN 0031-9007. doi: 10.1103/PhysRevLett.112.156403. URL http://www.ncbi.nlm.nih.gov/pubmed/24785061https://link.aps.org/doi/10.1103/PhysRevLett.112.156403.

94. D. Wang, L. Wang, and C. Wu, Slater and mott insulating states in the su(6) hubbard model, *Phys. Rev. B.* **100**, 115155 (Sep, 2019). doi: 10.1103/PhysRevB.100.115155. URL https://link.aps.org/doi/10.1103/PhysRevB.100.115155.
95. Z. Zhou, D. Wang, Z. Y. Meng, Y. Wang, and C. Wu, Mott insulating states and quantum phase transitions of correlated SU($2n$) dirac fermions, *Phys. Rev. B.* **93**, 245157 (Jun, 2016). doi: 10.1103/PhysRevB.93.245157. URL https://link.aps.org/doi/10.1103/PhysRevB.93.245157.
96. H. Xu, Y. Wang, Z. Zhou, and C. Wu, Mott insulating states of the anisotropic su(4) dirac fermions (2019).
97. S. Xu, J. T. Barreiro, Y. Wang, and C. Wu, Interaction effects with varying n in SU(n) symmetric fermion lattice systems, *Phys. Rev. Lett.* **121**, 167205 (Oct, 2018). doi: 10.1103/PhysRevLett.121.167205. URL https://link.aps.org/doi/10.1103/PhysRevLett.121.167205.
98. I. I. Pomeranchuk, On the stability of a fermi liquid, *Soviet Physics Jetp-Ussr.* **8**(2), 361–362 (1959).
99. C. Wu and S. C. Zhang, Dynamic generation of spin orbit coupling, *Physical Review Letters.* **93**, 36403 (2004). URL doi:10.1103/PhysRevLett.93.036403.
100. C. Wu, K. Sun, E. Fradkin, and S.-C. Zhang, Fermi liquid instabilities in the spin channel, *Phys. Rev. B.* **75**, 115103 (Mar, 2007). doi: 10.1103/PhysRevB.75.115103. URL http://link.aps.org/doi/10.1103/PhysRevB.75.115103.
101. T. Xiang and C. Wu, *D-Wave Superconductivity.* (Peking University Press and Cambridge University Press, 2022).
102. A. J. Leggett, Theoretical description of new phases of liquid-he-3, *Rev. Mod. Phys.* **47**(2), 331–414 (1975).
103. M. Sigrist and K. Ueda, Phenomenological theory of unconventional superconductivity, *Rev. Mod. Phys.* **63**, 239–311 (Apr, 1991). doi: 10.1103/RevModPhys.63.239. URL https://link.aps.org/doi/10.1103/RevModPhys.63.239.
104. E. Fradkin, S. A. Kivelson, M. J. Lawler, J. P. Eisenstein, and A. P. Mackenzie, Nematic fermi fluids in condensed matter physics, *Annual Review of Condensed Matter Physics.* **1**(1), 153C178 (Aug, 2010). ISSN 1947-5462. doi: 10.1146/annurev-conmatphys-070909-103925. URL http://dx.doi.org/10.1146/annurev-conmatphys-070909-103925.
105. L. Fu, Topological Crystalline Insulators, *Phys. Rev. Lett.* **106**(10), 106802 (Mar, 2011). ISSN 0031-9007. doi: 10.1103/PhysRevLett.106.106802. URL http://link.aps.org/doi/10.1103/PhysRevLett.106.106802.
106. S. A. Parameswaran, A. M. Turner, D. P. Arovas, and A. Vishwanath, Topological order and absence of band insulators at integer filling in non-symmorphic crystals, *Nat. Phys.* **9**(5), 299–303 (Apr, 2013). ISSN 1745-2473. doi: 10.1038/nphys2600. URL http://www.nature.com/doifinder/10.1038/nphys2600.
107. S. M. Young and C. L. Kane, Dirac Semimetals in Two Dimensions, *Phys. Rev. Lett.* **115**(12), 126803 (Sep, 2015). ISSN 0031-9007. doi: 10.1103/PhysRevLett.115.126803. URL http://link.aps.org/doi/10.1103/PhysRevLett.115.126803.
108. Z. Wang, A. Alexandradinata, R. J. Cava, and B. A. Bernevig, Hourglass fermions, *Nature.* **532**, 189 (2016). doi: 10.1038/nature17410.
109. H. Watanabe, H. C. Po, M. P. Zaletel, and A. Vishwanath, Filling-Enforced Gaplessness in Band Structures of the 230 Space Groups, *Phys. Rev. Lett.* **117**(9), 096404 (Aug, 2016). ISSN 0031-9007. doi: 10.1103/PhysRevLett.117.096404. URL http://link.aps.org/doi/10.1103/PhysRevLett.117.096404.
110. G. Kadic, M. Milton, M. van Hecke, and M. Wegener, 3d metamaterials, *Nature Reviews Physics.* **1**, 198 (2019). doi: doi.org/10.1038/s42254-018-0018-y.
111. M. S. Rudner and N. H. Linder, Band structure engineering and non-equilibrium dynamics in floquet topological insulators, *Nature Reviews Physics.* **2**, 229 (2020). doi: doi.org/10.1038/s42254-020-0170-z.

112. F. Harper, R. Roy, M. S. Rudner, and S. Sondhi, Topology and broken symmetry in floquet systems, *Annual Review of Condensed Matter Physics.* **11**(1), 345–368 (2020). doi: 10.1146/annurev-conmatphys-031218-013721. URL `https://doi.org/10.1146/annurev-conmatphys-031218-013721`.
113. L. Guo and P. Liang, Condensed matter physics in time crystals, *New. J. Phys.* **22**, 075003 (2021).
114. J. Yu, R. X. Zhang, and Z. D. Song, Dynamical symmetry indicators for floquet crystals, *Nat. Comm.* **12**, 5985 (2021).
115. K. Giergiel, M. Dauphin, A. Lewenstein, J. Zakrzewski, and K. Sacha, Topologial time crystals, *New. J. Phys.* **21**, 052003 (2019).
116. Y. Peng and G. Refael, Floquet second-order topological insulators from nonsymmorphic space-time symmetries, *Phys. Rev. Lett.* **123**, 016806 (Jul, 2019). doi: 10.1103/PhysRevLett.123.016806. URL `https://link.aps.org/doi/10.1103/PhysRevLett.123.016806`.
117. R. Kleiner, X. Zhou, E. Dorsch, X. Zhang, D. Koelle, and D. Jin, Space-time crystalline order of a high-critical-temperature superconductor with intrinsic Josephson junctions, *Nature Communications.* **12**(1) (Oct 15, 2021). doi: {10.1038/s41467-021-26132-y}.
118. Q. Gao and Q. Niu, Floquet-bloch oscillations and intraband zener tunneling in an oblique spacetime crystal, *Phys. Rev. Lett.* **127**, 036401 (Jul, 2021). doi: 10.1103/PhysRevLett.127.036401. URL `https://link.aps.org/doi/10.1103/PhysRevLett.127.036401`.
119. A. Muenchinger, V. Hahn, D. Beutel, S. Woska, J. Monti, C. Rockstuhl, E. Blasco, and M. Wegener, Multi-Photon 4D Printing of Complex Liquid Crystalline Microstructures by In Situ Alignment Using Electric Fields, *Advanced Materials Technologies.* **7**(1) (Jan, 2022). ISSN 2365-709X. doi: {10.1002/admt.202100944}.
120. L. Zhang and Q. Niu, Chiral phonons at high-symmetry points in monolayer hexagonal lattices, *Phys. Rev. Lett.* **115**, 115502 (Sep, 2015). doi: 10.1103/PhysRevLett.115.115502. URL `https://link.aps.org/doi/10.1103/PhysRevLett.115.115502`.
121. D. Xiao, M.-C. Chang, and Q. Niu, Berry phase effects on electronic properties, *Rev. Mod. Phys.* **82**, 1959–2007 (Jul, 2010). doi: 10.1103/RevModPhys.82.1959. URL `https://link.aps.org/doi/10.1103/RevModPhys.82.1959`.
122. C. K. Chiu, J. C. Y. Teo, A. P. Schnyder, and S. Ryu, Classification of topological quantum matter with symmetries, *Rev. Mod. Phys.* **88**(3), 1–63 (2016). ISSN 15390756. doi: 10.1103/RevModPhys.88.035005.
123. A. Kyprianidis, F. Machado, W. Morong, P. Becker, K. S. Collins, D. V. Else, L. Feng, P. W. Hess, C. Nayak, G. Pagano, N. Y. Yao, and C. Monroe, Observation of a prethermal discrete time crystal, *Science.* **372**(6547), 1192C1196 (Jun, 2021).
124. A. Shapere and F. Wilczek, Classical time crystals, *Phys. Rev. Lett.* **109**, 160402 (Oct, 2012). doi: 10.1103/PhysRevLett.109.160402. URL `https://link.aps.org/doi/10.1103/PhysRevLett.109.160402`.
125. F. Wilczek, Quantum time crystals, *Phys. Rev. Lett.* **109**, 160401 (Oct, 2012). doi: 10.1103/PhysRevLett.109.160401. URL `https://link.aps.org/doi/10.1103/PhysRevLett.109.160401`.
126. P. Bruno, Impossibility of spontaneously rotating time crystals: A no-go theorem, *Phys. Rev. Lett.* **111**, 070402 (Aug, 2013). doi: 10.1103/PhysRevLett.111.070402. URL `https://link.aps.org/doi/10.1103/PhysRevLett.111.070402`.
127. H. Watanabe and M. Oshikawa, Absence of quantum time crystals, *Phys. Rev. Lett.* **114**, 251603 (Jun, 2015). doi: 10.1103/PhysRevLett.114.251603. URL `https://link.aps.org/doi/10.1103/PhysRevLett.114.251603`.
128. K. Sacha, Modeling spontaneous breaking of time-translation symmetry, *Phys. Rev. A.* **91**, 033617 (Mar, 2015). doi: 10.1103/PhysRevA.91.033617. URL `https://link.aps.org/doi/10.1103/PhysRevA.91.033617`.
129. N. Y. Yao, A. C. Potter, I.-D. Potirniche, and A. Vishwanath, Discrete time crystals: Rigidity, criticality, and realizations, *Phys. Rev. Lett.* **118**, 030401 (Jan, 2017). doi:

10.1103/PhysRevLett.118.030401. URL https://link.aps.org/doi/10.1103/PhysRevLett.118.030401.

130. V. Khemani, A. Lazarides, R. Moessner, and S. L. Sondhi, Phase structure of driven quantum systems, *Phys. Rev. Lett.* **116**, 250401 (Jun, 2016). doi: 10.1103/PhysRevLett.116.250401. URL https://link.aps.org/doi/10.1103/PhysRevLett.116.250401.
131. G. Q. AI and collaborations, Observation of time-crystalline eigenstate order on a quantum processor (2021).
132. J. Randall, C. E. Bradley, F. V. van der Gronden, A. Galicia, M. H. Abobeih, M. Markham, D. J. Twitchen, F. Machado, N. Y. Yao, and T. H. Taminiau, Many-body localized discrete time crystal with a programmable spin-based quantum simulator, *Science.* **374**(6574), 1474C1478 (Dec, 2021). ISSN 1095-9203. doi: 10.1126/science.abk0603. URL http://dx.doi.org/10.1126/science.abk0603.
133. T.-L. Ho and S. Yip, Pairing of fermions with arbitrary spin, *Phys. Rev. Lett.* **82**, 247–250 (Jan, 1999). doi: 10.1103/PhysRevLett.82.247. URL http://link.aps.org/doi/10.1103/PhysRevLett.82.247.
134. S.-K. Yip and T.-L. Ho, Zero sound modes of dilute fermi gases with arbitrary spin, *Phys. Rev. A.* **59**, 4653–4656 (Jun, 1999). doi: 10.1103/PhysRevA.59.4653. URL http://link.aps.org/doi/10.1103/PhysRevA.59.4653.
135. C. Wu, B. A. Bernevig, and S.-C. Zhang, Helical liquid and the edge of quantum spin hall systems, *Phys. Rev. Lett.* **96**, 106401 (Mar, 2006). doi: 10.1103/PhysRevLett.96.106401. URL http://link.aps.org/doi/10.1103/PhysRevLett.96.106401.
136. H.-H. Lin, L. Balents, and M. P. A. Fisher, Exact so(8) symmetry in the weakly-interacting two-leg ladder, *Phys. Rev. B.* **58**, 1794–1825 (Jul, 1998). doi: 10.1103/PhysRevB.58.1794. URL http://link.aps.org/doi/10.1103/PhysRevB.58.1794.
137. E. Berg, E. Fradkin, and S. A. Kivelson, Charge-4e superconductivity from pair-density-wave order in certain high-temperature superconductors, *Nature Physics.* **5**(11), 830C833 (Sep, 2009). ISSN 1745-2481. doi: 10.1038/nphys1389. URL http://dx.doi.org/10.1038/nphys1389.
138. D. F. Agterberg, J. S. Davis, S. D. Edkins, E. Fradkin, D. J. Van Harlingen, S. A. Kivelson, P. A. Lee, L. Radzihovsky, J. M. Tranquada, and Y. Wang, The physics of pair-density waves: Cuprate superconductors and beyond, *Annual Review of Condensed Matter Physics.* **11**(1), 231C270 (Mar, 2020). ISSN 1947-5462. doi: 10.1146/annurev-conmatphys-031119-050711. URL http://dx.doi.org/10.1146/annurev-conmatphys-031119-050711.
139. S.-K. Jian, Y. Huang, and H. Yao, Charge-4e superconductivity from nematic superconductors in two and three dimensions, *Phys. Rev. Lett.* **127**, 227001 (Nov, 2021). doi: 10.1103/PhysRevLett.127.227001. URL https://link.aps.org/doi/10.1103/PhysRevLett.127.227001.
140. R. M. Fernandes and L. Fu, Charge-4e superconductivity from multicomponent nematic pairing: Application to twisted bilayer graphene, *Phys. Rev. Lett.* **127**, 047001 (Jul, 2021). doi: 10.1103/PhysRevLett.127.047001. URL https://link.aps.org/doi/10.1103/PhysRevLett.127.047001.
141. M. Zeng, L.-H. Hu, H.-Y. Hu, Y.-Z. You, and C. Wu, Phase-fluctuation induced time-reversal symmetry breaking normal state, (arXiv:2102.06158).
142. J. Ge, P. Wang, Y. Xing, Q. Yin, H. Lei, Z. Wang, and J. Wang, Discovery of charge-4e and charge-6e superconductivity in kagome superconductor csv3sb5, (arXiv:2201.10352).
143. M. van den Bossche, F.-C. Zhang, and F. Mila, Plaquette ground state in the two-dimensional su(4) spin-orbital model, *The European Physical Journal B - Condensed Matter and Complex Systems.* **17**(3), 367–370 (2000). ISSN 1434-6028. doi: 10.1007/PL00011085. URL http://dx.doi.org/10.1007/PL00011085.
144. S. Pankov, R. Moessner, and S. L. Sondhi, Resonating singlet valence plaquettes, *Phys. Rev. B.* **76**, 104436 (Sep, 2007). doi: 10.1103/PhysRevB.76.104436. URL http://link.aps.org/doi/10.1103/PhysRevB.76.104436.

145. D. S. Rokhsar and S. A. Kivelson, Superconductivity and the quantum hard-core dimer gas, *Phys. Rev. Lett.* **61**, 2376–2379 (Nov, 1988). doi: 10.1103/PhysRevLett.61.2376. URL `http://link.aps.org/doi/10.1103/PhysRevLett.61.2376`.
146. R. M. Nandkishore and M. Hermele, Fractons, *Annual Review of Condensed Matter Physics.* **10**(1), 295–313 (2019). doi: 10.1146/annurev-conmatphys-031218-013604. URL `https://doi.org/10.1146/annurev-conmatphys-031218-013604`.
147. J. E. Hirsch, Discrete hubbard-stratonovich transformation for fermion lattice models, *Phys. Rev. B.* **28**, 4059–4061 (Oct, 1983). doi: 10.1103/PhysRevB.28.4059. URL `http://link.aps.org/doi/10.1103/PhysRevB.28.4059`.
148. J. E. Hirsch, Two-dimensional hubbard model: Numerical simulation study, *Phys. Rev. B.* **31**, 4403–4419 (Apr, 1985). doi: 10.1103/PhysRevB.31.4403. URL `https://link.aps.org/doi/10.1103/PhysRevB.31.4403`.
149. J. E. Hirsch and S. Tang, Antiferromagnetism in the two-dimensional hubbard model, *Phys. Rev. Lett.* **62**, 591–594 (Jan, 1989). doi: 10.1103/PhysRevLett.62.591. URL `http://link.aps.org/doi/10.1103/PhysRevLett.62.591`.
150. N. Read and S. Sachdev, Large-N expansion for frustrated quantum antiferromagnets, *Phys. Rev. Lett.* **66**, 1773–1776 (Apr, 1991). doi: 10.1103/PhysRevLett.66.1773. URL `http://link.aps.org/doi/10.1103/PhysRevLett.66.1773`.
151. R. Jackiw and C. Rebbi, Spin from isospin in a gauge theory, *Phys. Rev. Lett.* **36**, 1116–1119 (May, 1976). doi: 10.1103/PhysRevLett.36.1116. URL `https://link.aps.org/doi/10.1103/PhysRevLett.36.1116`.
152. C. Wu, H.-D. Chen, J.-P. Hu, and S.-C. Zhang, Vortex configurations of bosons in an optical lattice, *Phys. Rev. A.* **69**, 043609 (Apr, 2004). doi: 10.1103/PhysRevA.69.043609. URL `http://link.aps.org/doi/10.1103/PhysRevA.69.043609`.
153. G. Baym and C. Pethick, *Landau Fermi-liquid theory.* (John Wiley & Sons, Inc., 1984).
154. J. E. Hirsch, Spin-split states in metals, *Phys. Rev. B.* **41**, 6820–6827 (Apr, 1990). doi: 10.1103/PhysRevB.41.6820. URL `http://link.aps.org/doi/10.1103/PhysRevB.41.6820`.
155. J. E. Hirsch, Chromium: A possible spin-split metal, *Phys. Rev. B.* **41**, 6828–6835 (Apr, 1990). doi: 10.1103/PhysRevB.41.6828. URL `http://link.aps.org/doi/10.1103/PhysRevB.41.6828`.
156. D. G. Barci and L. E. Oxman, Strongly correlated fermions with nonlinear energy dispersion and spontaneous generation of anisotropic phases, *Phys. Rev. B.* **67**, 205108 (May, 2003). doi: 10.1103/PhysRevB.67.205108. URL `http://link.aps.org/doi/10.1103/PhysRevB.67.205108`.
157. M. J. Lawler, D. G. Barci, V. Fernandez, E. Fradkin, and L. Oxman, Nonperturbative behavior of the quantum phase transition to a nematic fermi fluid, *Phys. Rev. B.* **73**, 085101 (2006).
158. C. J. Halboth and W. Metzner, d-wave superconductivity and pomeranchuk instability in the two-dimensional hubbard model, *Phys. Rev. Lett.* **85**, 5162–5165 (Dec, 2000). doi: 10.1103/PhysRevLett.85.5162. URL `http://link.aps.org/doi/10.1103/PhysRevLett.85.5162`.
159. L. Dell'Anna and W. Metzner, Fermi surface fluctuations and single electron excitations near pomeranchuk instability in two dimensions, *Phys. Rev. B.* **73**, 045127 (2006).
160. H.-Y. Kee, Sound propagation in a nematic fermi liquid, *Phys. Rev. B.* **67**, 073105 (Feb, 2003). doi: 10.1103/PhysRevB.67.073105. URL `http://link.aps.org/doi/10.1103/PhysRevB.67.073105`.
161. S. A. Kivelson, I. P. Bindloss, E. Fradkin, V. Oganesyan, J. M. Tranquada, A. Kapitulnik, and C. Howald, How to detect fluctuating stripes in the high-temperature superconductors, *Rev. Mod. Phys.* **75**, 1201–1241 (Oct, 2003). doi: 10.1103/RevModPhys.75.1201. URL `http://link.aps.org/doi/10.1103/RevModPhys.75.1201`.
162. L. P. Gorkov and A. Sokol, Fermi surface fluctuations and single electron excitations near pomeranchuk instability in two dimensions, *Phys. Rev. Lett.* **69**, 2586 (1999).
163. C. Varma, Cure to the landau–pomeranchuk and associated long-wavelength fermi-surface instabilities on the lattice, *Philosophical Magazine.* **85**(15), 1657–1666 (2005).

164. C. M. Varma and L. J. Zhu, Helicity order: Hidden order parameter in uru2si2, *Phys. Rev. Lett.* **96**, 036405 (2006).
165. H. Y. Kee and E. H. Kim, Itinerant metamagnetism induced by electronic nematic order, *Phys. Rev. B.* **71**, 184402 (2005).
166. C. Honerkamp, Charge instabilities at the metamagnetic transition, *Physical Review B.* **72**, 115103 (2005). URL doi:10.1103/PhysRevB.72.115103.
167. V. Oganesyan, S. A. Kivelson, and E. Fradkin, Quantum theory of a nematic fermi fluid, *Phys. Rev. B.* **64**, 195109 (Oct, 2001). doi: 10.1103/PhysRevB.64.195109. URL http://link.aps.org/doi/10.1103/PhysRevB.64.195109.
168. S. A. Kivelson, E. Fradkin, and V. J. Emery, Electronic liquid crystal phases of a doped mott insulator, *Nature.* **393**, 550 (1998).
169. M. P. Lilly, K. B. Cooper, J. P. Eisenstein, L. N. Pfeiffer, and K. W. West, Evidence for an anisotropic state of two-dimensional electrons in high landau levels, *Phy. Rev. Lett.* **82**, 394 (1999).
170. R. R. Du, D. C. Tsui, H. L. Stormer, L. N. Pfeiffer, K. W. Baldwin, and K. W. West, *Sol. Stat. Comm.* **109**, 389 (1999).
171. S. A. Grigera, R. S. Perry, A. J. Schofield, M. Chiao, S. R. Julian, G. G. Lonzarich, S. I. Ikeda, Y. Maeno, A. J. Millis, and A. P. Mackenzie, Magnetic field-tuned quantum criticality in the metallic ruthenate sr3ru2o7, *Science.* **294**, 329 (2001).
172. S. A. Grigera, P. Gegenwart, R. A. Borzi, F. Weickert, A. J. Schofield, R. S. Perry, T. Tayama, T. Sakakibara, Y. Maeno, A. G. Green, and A. P. Mackenzie, Disorder-sensitive phase formation linked to metamagnetic quantum criticality, *Science.* **306**, 1154 (2004).
173. R. A. Borzi, S. A. Grigera, J. Farrell, R. S. Perry, S. J. S. Lister, S. L. Lee, D. A. Tennant, Y. Maeno, and A. P. Mackenzie, Formation of a nematic fluid at high fields in sr3ru2o7, *Science.* **315**, 214 (2007).
174. A. V. Chubukov and D. L. Maslov, Spin conservation and fermi liquid near a ferromagnetic quantum critical point, *Phys. Rev. Lett.* **103**, 216401 (Nov, 2009). doi: 10.1103/PhysRevLett.103.216401. URL https://link.aps.org/doi/10.1103/PhysRevLett.103.216401.
175. J. A. Hertz, Quantum critical phenomena, *Phys. Rev. B.* **14**(3), 1165–1184 (Aug, 1976). doi: 10.1103/PhysRevB.14.1165.
176. A. J. Millis, Effect of a nonzero temperature on quantum critical points in itinerant fermion systems, *Phys. Rev. B.* **48**(10), 7183–7196 (Sep, 1993). doi: 10.1103/PhysRevB.48.7183.
177. L. Fu, Parity-breaking phases of spin-orbit-coupled metals with gyrotropic, ferroelectric, and multipolar orders, *Phys. Rev. Lett.* **115**, 026401 (Jul, 2015). doi: 10.1103/PhysRevLett.115.026401. URL https://link.aps.org/doi/10.1103/PhysRevLett.115.026401.
178. D. Vollhardt and P. Wolfle, *The superfluid phases of helium 3.* (Taylor & Francis, London, 1990).
179. P. G. de Gennes and J. Prost, *The Physics of Liquid Crystals.* (Clarendon Press; 2nd edition, 1995).
180. Y. Li and C. Wu, Spin-orbit coupled fermi liquid theory of ultracold magnetic dipolar fermions, *Phys. Rev. B.* **85**, 205126 (May, 2012). doi: 10.1103/PhysRevB.85.205126. URL https://link.aps.org/doi/10.1103/PhysRevB.85.205126.
181. W.-C. Lee and C. Wu, Theory of unconventional metamagnetic electron states in orbital band systems, *Phys. Rev. B.* **80**, 104438 (Sep, 2009). doi: 10.1103/PhysRevB.80.104438. URL https://link.aps.org/doi/10.1103/PhysRevB.80.104438.
182. A. J. Leggett, Spin diffusion and spin echoes in liquid 3 he at low temperature, *Journal of Physics C: Solid State Physics.* **3**(2), 448 (1970). URL http://stacks.iop.org/0022-3719/3/i=2/a=027.
183. L. R. Corruccini, D. D. Osheroff, D. M. Lee, and R. C. Richardson, Spin diffusion in liquid ^{3}He: The effect of leggett and rice, *Phys. Rev. Lett.* **27**, 650–653 (Sep, 1971). doi: 10.1103/PhysRevLett.27.650. URL http://link.aps.org/doi/10.1103/PhysRevLett.27.650.
184. D. Osheroff, Textural spin waves in 3heb, *Physica B+C.* **90**(1), 20–34 (1977). ISSN 0378-4363.

doi: http://dx.doi.org/10.1016/0378-4363(77)90005-5. URL http://www.sciencedirect.com/science/article/pii/0378436377900055.

185. D. S. Greywall, Specific heat of normal liquid ^{3}He, *Phys. Rev. B.* **27**, 2747–2766 (Mar, 1983). doi: 10.1103/PhysRevB.27.2747. URL http://link.aps.org/doi/10.1103/PhysRevB.27.2747.
186. J. A. Mydosh, P. M. Oppeneer, and P. S. Riseborough, Hidden order and beyond: An experimental theoretical overview of the multifaceted behavior of uru2si2, *Journal of Physics: Condensed Matter.* **32**(14), 143002 (Jan, 2020). ISSN 1361-648X. doi: 10.1088/1361-648x/ab5eba. URL http://dx.doi.org/10.1088/1361-648X/ab5eba.
187. C. T. Wolowiec, N. Kanchanavatee, K. Huang, S. Ran, A. J. Breindel, N. Pouse, K. Sasmal, R. E. Baumbach, G. Chappell, P. S. Riseborough, and M. B. Maple, Isoelectronic perturbations to f-d-electron hybridization and the enhancement of hidden order in uru2si2, *Proceedings of the National Academy of Sciences.* **118**(20), (2021). ISSN 0027-8424. doi: 10.1073/pnas.2026591118. URL https://www.pnas.org/content/118/20/e2026591118.
188. J. W. Harter, Z. Y. Zhao, J.-Q. Yan, D. G. Mandrus, and D. Hsieh, A parity-breaking electronic nematic phase transition in the spin-orbit coupled metal cd2re2o7, *Science.* **356**(6335), 295C299 (Apr, 2017). ISSN 1095-9203. doi: 10.1126/science.aad1188. URL http://dx.doi.org/10.1126/science.aad1188.
189. J. W. Harter, D. M. Kennes, H. Chu, A. de la Torre, Z. Y. Zhao, J.-Q. Yan, D. G. Mandrus, A. J. Millis, and D. Hsieh, Evidence of an improper displacive phase transition in $cd_2re_2o_7$ via time-resolved coherent phonon spectroscopy, *Phys. Rev. Lett.* **120**, 047601 (Jan, 2018). doi: 10.1103/PhysRevLett.120.047601. URL https://link.aps.org/doi/10.1103/PhysRevLett.120.047601.
190. M. R. Norman, Crystal structure of the inversion-breaking metal $cd_2re_2o_7$, *Phys. Rev. B.* **101**, 045117 (Jan, 2020). doi: 10.1103/PhysRevB.101.045117. URL https://link.aps.org/doi/10.1103/PhysRevB.101.045117.